Renaissance Robotics: Novel applications of Multipurpose Robotic Arms spanning Design Fabrication, Utility, and Art

by

Steven J. Keating

Bachelor of Science in Mechanical and Materials Engineering, 2010
Bachelor of Arts in Film and Media, 2010
Queen's University, Canada

Submitted to the Department of Mechanical Engineering in partial fulfillment of the requirements for the degree of

Master of Science in Mechanical Engineering
at the
Massachusetts Institute of Technology

September 2012

Signature of Author: _____
Department of Mechanical Engineering
August 10, 2012

Certified by: _____
Neri Oxman
Assistant Professor of Media Arts and Science
Thesis Co-Supervisor

Certified by: _____
David R. Wallace
Professor of Mechanical Engineering
Thesis Co-Supervisor

Accepted by: _____
David E. Hardt
Professor of Mechanical Engineering
Chairman, Department Committee on Graduate Students

Renaissance Robotics: Novel Applications of Multipurpose Robotic Arms spanning Design Fabrication, Utility, and Art

by

Steven J. Keating

Submitted to the Department of Mechanical Engineering on
August 10th, 2012 in partial fulfillment of the requirements for the degree of
Master of Science in Mechanical Engineering

Abstract

This work investigates, defines, and expands on the use of robotic arms in digital fabrication, design, and art through methods including 3D printing, milling, sculpting, functionally graded fabrication, construction-scale additive manufacturing, jammable granular system design, light painting, and volumetric sensing. While most current applications of robotics in manufacturing rely on repetitive automation and assembly tasks, the flexibility, dexterity, and precision of industrial robotic arms provide for design opportunities of multi-functionary roles. Through exploration and demonstration, a multipurpose fabrication platform was developed using a KUKA KR5 sixx R850 robotic arm. The platform is capable of conventional manufacturing techniques spanning the three traditional fabrication categories: additive, subtractive, and formative. Case studies and digital design fabrication protocols were developed as part of the robotic platform to demonstrate these three types of fabrication including 3D printing, multi-axis milling, and clay sculpting, respectively. Compound processes, such as combining 3D printing and milling, were developed that offer product-, and process-based improvements over standalone techniques. The benefits and drawbacks of a multi-fabrication platform are discussed, including cost, physical footprint, resolution, and flexibility.

In addition to replicating conventional manufacturing techniques with a single robotic platform, several novel applications were developed which take advantage of the flexibility of an arm system. First, functionally graded 3D printing was explored using concrete through which density gradients were shown to achieve higher structural efficiency. A novel construction-scale additive manufacturing process capable of 3D printing building components was developed. Secondly, direct recycling 3D printing was developed where waste thermoplastic products are transformed into feedstock and printed into new components within a single operation. Work conducted on jammed granular structures, where external pressure controls system stiffness and strength, resulted in several new formative fabrication possibilities. Combined with robotics, waste-free digital casting using jammable materials was enabled along with a variety of design projects including the design of robotic arms themselves.

Finally, the use of robotic arms for fabrication of material and environmental properties without mechanical force transfer was explored. Coined *immaterial fabrication*, this fabrication category captures methods that do not fall within the definitions of additive, subtractive, or formative processes. Work produced in this area includes a volumetric sensing technique and robotic light paintings that reveal thermal, electromagnetic, and optical fields.

Thesis Supervisors: Neri Oxman, Assistant Professor of Media Arts and Science
David Wallace, Professor of Mechanical Engineering

Acknowledgements

"I have no special talent. I am only passionately curious."

Albert Einstein

I would first like to thank my co-advisors, Prof. Neri Oxman and Prof. David Wallace, for their unwavering support and guidance. Neri, thank you for inspiring me to dream and for providing the opportunity to do so. I am in awe of your contagious enthusiasm, powerful ideas, and amazing ability to hold the world on your shoulders with such character and poise. Thank you for taking a chance on me and for always putting your students first. David, thank you for being an incredible teacher and role model. Thinking back, it is impossible to list the wide range of lessons you have taught me. From technical skills, to life skills, to even teaching me how to teach, you have defined my MIT experience in such a wonderful and outstanding manner.

Thank you to my colleagues and friends in both Mediated Matter and CADLAB: Ben, Liz, Yoav, Michal, and Sarah; Ilan, James, Sangmok, Ari, Ming, Jeff, Sue, Lauren, Josh, Taylor, Lindy, and Alison (CADLAB by association). Special thanks to Geoff for all the amazing times teaching Toy Lab together, to Nadia for all the jamming collaborations, and to the Boston Metro Club for all the crazy workouts. Thank you to my network of friends back home and here at MIT. You guys keep me sane and smiling!

There have been several companies and institutions that have generously supported my thesis work through funding, materials, and technical guidance including the National Science Foundation (Award Number: 115250), Elastizell, and KUKA Robotics. As well, support through the Steven R. Holtzman Fellowship program is gratefully acknowledged.

Thank you to the Media Lab and the Mechanical Engineering departments. Cynthia Wilkes and Leslie Regan, thank you for always having all the answers to my many questions!

I have had the privilege of working with many undergraduate students through UROP positions. Thank you to Ali AlShehab, Hannah Barrett, Louis DeScioli, Keren Gu, Shaymus Hudson, Banks Hunter, Atif Javed, Robert Johnson, Julian Merrick, Nathan Spielberg, Timothy Robertson, and Anne Warren for all your help on the various projects.

It is hard to put into words the amazing support and unconditional love from Eliza. Thank you so much for putting up with me throughout the many midnight science experiments and all the rounds of edits.

And finally, and most importantly, thank you to my family. Mom and Dad, thank you for encouraging my never-ending questions and fostering my curiosity. Your resolute belief in me is humbling and a constant source of happiness. And to Laura, thank you for being the best role model a younger brother could ever ask for.

Table of Contents

List of Figures

List of Tables

Chapter 1: Introduction and Overview

> *"To me, the universe is simply a great machine which never came into being and never will end. The human being is no exception to the natural order. Man, like the universe, is a machine. Nothing enters our minds or determines our actions which is not directly or indirectly a response to stimuli beating upon our sense organs from without."*
>
> **— Nikola Tesla**

The definition of a robot – "a machine capable of carrying out a complex series of actions automatically" is extremely broad in its interpretation (Oxford Dictionaries, 2010). Under this definition, an inkjet printer, cellphone, and even organisms can be considered robots. Still, the typical cultural vision of a robot is an anthropomorphic electromechanical machine as reinforced by movies ranging from *Metropolis* to *The Terminator* (Lang, 1927; Cameron, 1984). While cinematic and cultural norms reinforce the idea of a robotic humanoid form capable of serving one's every need, the true picture of modern robotics is vastly different. Instead of custom, unconstrained, and diverse tasks as imagined by generations of science fiction novelists, most industrial robots are used to automate repetitive tasks. The car assembly line, the current largest use of industrial robotics worldwide, is a perfect example (International Federation of Robotics, 2011). Many robotic arms will each complete a single task, such as spot welding a body panel on, and repeat this singular task for every car produced by the assembly line. In the last several decades, robotic arms have been used in thousands of factories around the world to perform complex, repetitive tasks ranging the spectrum of manufacturing techniques. From silicon wafer handling to slaughterhouses, robotic arms have transformed mass manufacturing and yet the traditional image of a robot being able to perform a multitude of custom, non-repetitive, and informed procedures from the cinemas does not exist.

Rather, industrial robotics has excelled in the antithesis to that image: singular, repetitive, and precise tasks. This failure of robotics to inhabit varying, custom, and complex tasks is primarily due to programming difficulty rather than mechanical, financial, or

integration problems (Pires J. N., 2006). An unconstrained environment requiring robust system behaviour is a very challenging computational problem. Though in the last decade, a new rising of repurposing industrial robotics for complex fabrication projects has been occurring in research institutions and commercial firms around the world. Applications ranging from surgery, to art, to custom amusement park rides have been new fields for industrial robots (da Vinci Surgery, 2012; Walker, 2012; Robocoaster, 2012). Digital fabrication is part of the evolution; recent literature on industrial robotic arms feature arms being repurposed for customized manufacturing roles such as 3D printing processes, metal folding operations, multi-axis milling, foam cutting systems, and even brick-laying (Vander Kooij, 2011; RoboFold, 2012; Bechthold, The Return of the Future: A Second Go at Robotic Construction, 2010; Brooks & Aitchison, 2010; Gramazio & Kohler, 2008) In this thesis, the use of robotics – specifically robotic arms – for design fabrication, utility and art outside the traditional confines of the repetitive assembly line is explored, defined, and demonstrated.

In this work a theoretical exploration of fabrication concepts alongside in-depth physical fabrication experiments is conducted within the context of a robotic arm. The methodology used in this thesis is structured into two main categories: replicating conventional manufacturing techniques using a robotic arm and exploring novel fabrication techniques and design applications enabled by a robotic arm. A brief introduction of the different project work presented in this thesis, along with their respective chapter locations in this document, follows.

In the first category, a multipurpose fabrication platform capable of additive, subtractive, and formative manufacturing techniques was developed based on a six axis robotic arm. The designed system explores how a single manipulator can be used in a flexible manufacturing application to perform operations typically done with standalone machines. Processes from each of the traditional fabrication categories (additive, subtractive, and formative) were demonstrated by the system to explore potential benefits and drawbacks of an integrated manufacturing platform. Example processes developed include 3D printing (additive), multi-axis milling (subtractive), and sculpting (formative).

The use of various end effectors enables the single arm to perform many types of operations while maintaining part orientation and calibration. By combining processes, such as 3D printing and milling, hybrid operations are developed to offer advantages and new possibilities. Finally, a multipurpose fabrication platform reduces the cost and physical machine footprint as opposed to multiple traditional standalone counterparts. The approach, system, and discussion on the multi-functional fabrication platform for conventional manufacturing methods are found in Chapter 4.

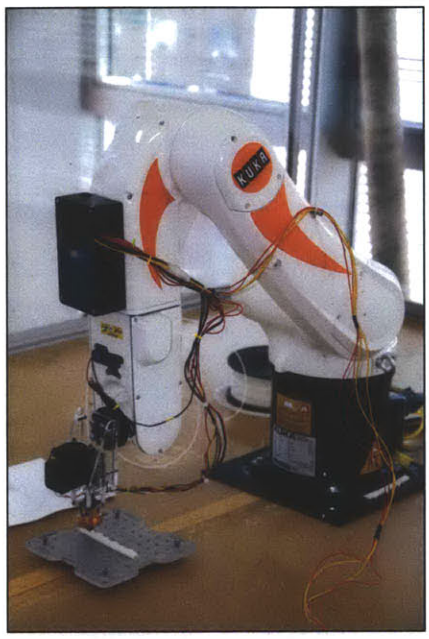

Figure 1. The development of a robotic multipurpose fabrication platform capable of processes like 3D printing (as seen here), milling, and sculpting is discussed in Chapter 4.

The second facet of work involves novel fabrication, art, and design applications enabled by robotic arm. As introduced in Chapter 5, the potential for industrial robotic arms beyond the assemble line is immense. The following methods of fabrication using a robotic arm were explored: functional gradient 3D printing (additive process), construction-scale 3D printing (additive process), direct recycling (additive process), and jammable design and fabrication (formative process). Artistic applications were investigated through the development of robotic light painting techniques. Finally, sensing applications using a robotic arm for volumetric scanning were explored using electromagnetic and thermal sensing.

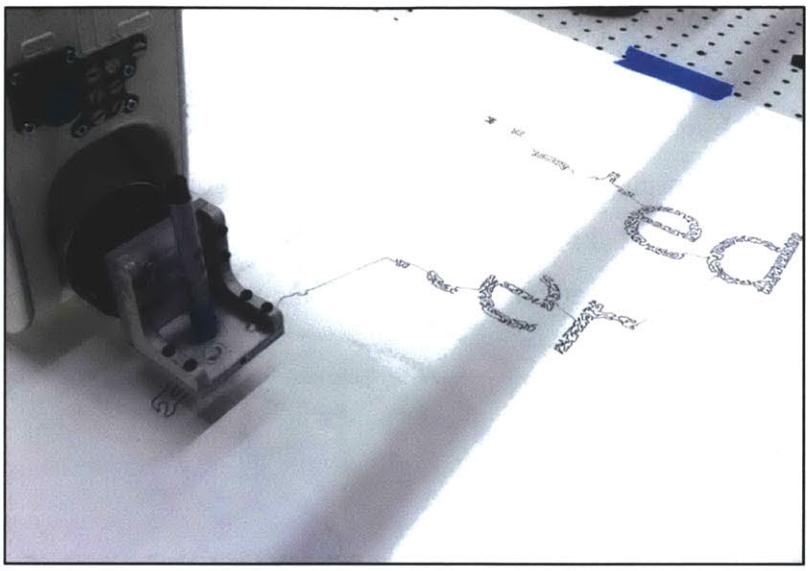

Figure 2. Applications beyond the assembly line for industrial robotic arms, such as this artistic drawing configuration, are introduced in Chapter 5.

Functionally graded materials are materials with spatially varying properties. A common example of a functional graded material is surface annealing of metals. When a piece of metal is annealed, the crystal structure changes locally and creates a material that has different hardness values depending on where the annealing heat was applied. By having graded properties, structures can have new functionalities, enhanced efficacy, and monolithic integration instead of joined parts. Functional gradients are commonly found in natural materials, such as trees and bones (Gibson, Ashby, & Harley, 2010). As a case study, the radial density gradients in bones inspired a project focused on concrete density gradients. By replicating density gradients within monolithic concrete structures, stronger and lighter structures can be produced. To facilitate a production process of designed gradient structures, the robotic arm platform was used. The robotic arm is an ideal platform for additive manufacturing of concrete systems, as typical concrete structures are much larger than a tabletop gantry configuration could provide. Chapter 6 focuses on the experimentation, analysis, and results on printed gradient concrete structures.

Figure 3. Chapter 6 explores 3D printing of functional density gradients in concrete objects using a robotic arm platform for extrusion purposes.

Taking concrete printing to construction-scale printed objects, such as buildings, was investigated with the development of the Print-in-Place process. The Print-in-Place construction method uses a robotic arm to additively manufacture large structures through an in-situ printing approach. The novel approach utilizes a polyurethane mould structure that is printed on-site using a robotic arm and can be subsequently poured with structural materials like concrete. The Print-in-Place technique was developed, tested, and several large wall sections were printed. Benefits, drawbacks, and a comparison to traditional construction methods are discussed alongside the developed method in Chapter 7.

Figure 4. The development of a construction-scale additive manufacturing process based on a robotic arm 3D printing system is discussed in Chapter 7.

Continuing with the robotic arm additive manufacturing work, the concept of recycling objects using additive processes was explored. The project explored the idea of de-centralizing recycling and allowing users to recycle their own thermoplastic waste into new goods. Using the robotic arm as a plastic 3D printer, a system was constructed where scrap plastic from waste beverage containers was used as feedstock for additive manufacturing. This resulted in a single machine capable of transforming scrap plastic bottles into printed objects, termed a direct recycling machine. Chapter 8 investigates at the concept and implications of direct recycling.

Figure 5. Chapter 8 explores a prototype direct recycling system based on a robotic 3D printer that prints with recycled plastic.

New formative processes were explored through the investigation of jammed granular structures. Jammed granular structures are systems comprised of a granular media, like sand or coffee, that can be compressed using air or mechanical pressure to create different system stiffness. An everyday example of a jammed granular system is a vacuum-packed bag of coffee. The vacuum-packed bag is very stiff as the air pressure

compresses the coffee grains together, increases friction and locks the grains in place. Once the seal is broken, the coffee bag becomes much more flexible as the jamming pressure is reduced. Looking at the overall system, the stiffness of the coffee bag is dependent on the vacuum pressure. Using this jamming principle, structures can be developed which are capable of changing shape and stiffness. Like clay that can be digitally manipulated, jammable materials offer interesting new avenues for formative processes as the shape can be altered and locked in place. Robotics can be used to set this initial position for fabrication processes like digital casting. In addition, robotic arms themselves and other structural devices can be manufactured using jammable joints instead of traditional rotary joints. Several prototypes structures were created and evaluated. The design space of jammable materials, along with material system characteristics of different jammed granular media, is detailed in Chapter 9.

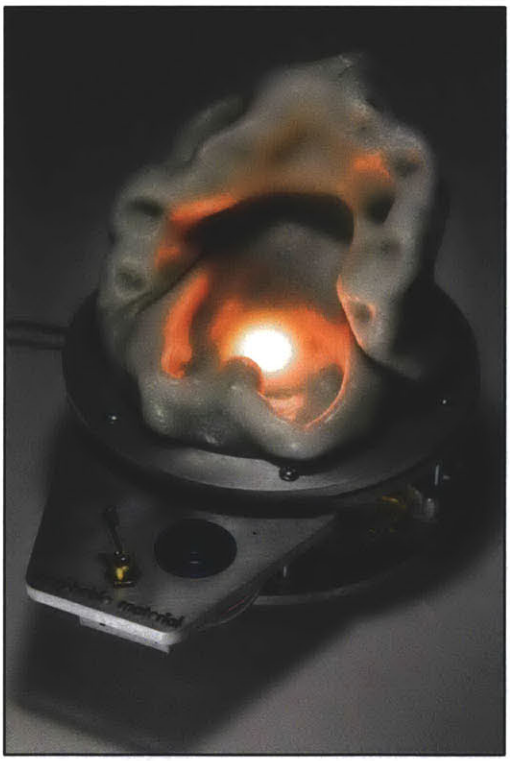

Figure 6. Jammed granular systems, like the prototype seen here, are investigated in design, fabrication, and robotic applications in Chapter 9.

In addition to the developed methods that fall within conventional categories of manufacturing, two new categories of fabrication were explored and defined. Robotic arms have the benefits of speed, agility, and flexibility, and can be used as both inputs (sensing) and outputs (modifying the physical environment). In addition to mechanical outputs, elements of an environment can be transformed as an output without the movement of physical material. Instead of physical matter, properties and fields can be made into spatial outputs of the system, such as light, sound, heat, radiation, and radio waves. Heat, for example, can be applied to a metallic object in varying quantities to impart an annealing pattern. While a digital fabrication method is implemented here, the medium has altered from relocating physical matter in a specific design to repositioning a heat source in an intended design. The design process is still a process constructed from parts (in this case it is the alteration of altering crystal structure), but not by manipulating material with direct mechanical force, as is characteristic of additive, subtractive, and formative processes. To facilitate the characterization of this type of environmental fabrication and distinguish it from physical construction, the term *immaterial fabrication* was developed. In Chapter 10 this definition is explored and demonstrated using different examples of immaterial robotic fabrication distinct from conventional additive, subtractive, and formative processes.

As mentioned, robotic arms can be used as input or output devices. When implemented as an input device, sensors are coupled with the arm to allow spatial measurements of the environment. For example, an optical scanning system can be combined with the robotic arm to automatically generate 3D data of objects in an environment. As an output device, end effectors are coupled with the arm to allow the robot to modify its own environment. Such environmental modification can be made useful for a variety of digital and physical automation purposes such as fabrication, entertainment, or organization. For example: one robot cuts foam to create a sculpture, another splashes paint across a canvas to create artwork, and a third robot organizes a mess during a cleaning process.

The coupling of input and output fabrication capabilities of a robotic arm allows for a system capable of producing objects that incorporate environmental data. This use of

environmental feedback to directly inform and influence fabrication holds many potential new avenues for design and manufacturing which will be discussed in this paper. The term *informed fabrication* is used to refer to combinations of environmental sensing and fabrication and is also discussed in Chapter 10.

Figure 7. Robotic light painting, shown here using long-exposure photography, and volumetric sensing applications are explored in Chapter 10.

Finally, appendices with sample code, raw experimental data, and a list of suppliers of materials and software used can be found at the end of this thesis.

Chapter 2: Context and Motivation

"I can't define a robot, but I know one when I see one."

— Joseph Engelberger

This thesis investigates the use of robotic arms for multipurpose fabrication, design, and utility. To provide context for this work, the evolution of the robotic arm is discussed along with the current state of industrial robotics. The motivations behind this work are detailed and discussed in context of the current state of industrial robotics.

History of the Robot Arm

The term *robot* is derived from the Czech word *robota,* which refers to "forced labour" and was first introduced in a play by Karel Capek in the 1920s (Zunt, 2004). In his play, machines with emotional capabilities overtake humans – a storyline oft repeated throughout popular modern culture. However, robots were around much earlier than 1920. In fact, under the Oxford dictionary definition of a robot being "a machine capable of carrying out a complex series of actions automatically", examples of early robots are referenced in text from Ancient China, Greece, and Egypt dating earlier than the 1st century A.D (Currie, 1999). These early machines consisted of mechanical statutes and automatons of figures and animals.

The first digitally operated and reprogrammable industrial robot was invented by George Devol in 1954 (Nof, 1999). Together with Joseph Engelberger, Devol started the world's first industrial robotics company, Unimation (derived from the term *Universal Automation*). Unimation's first production line robot was the Unimate, which was used for materials handling tasks in factories (Figure 8).

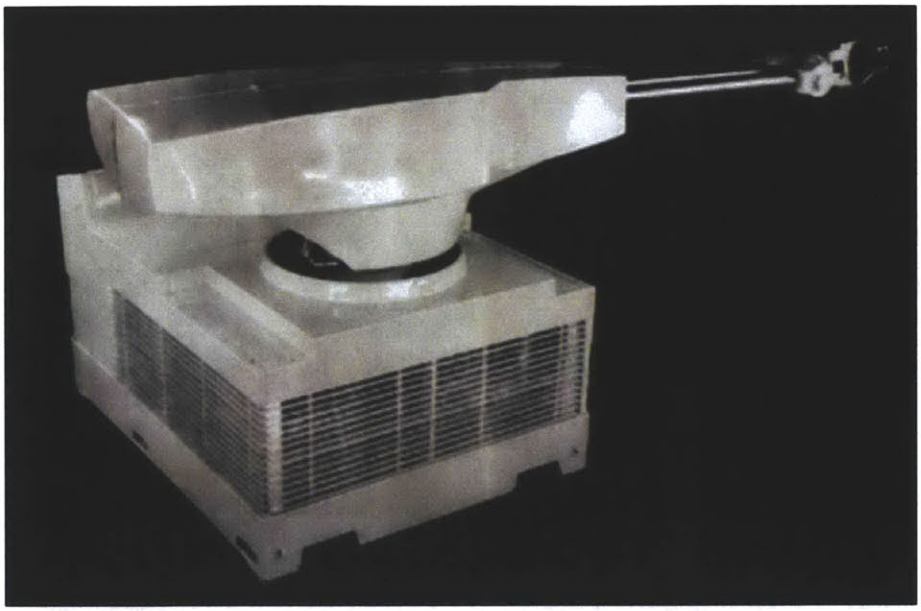

Figure 8. The Unimate robot was the first modern industrial robot and was used for material handling in factories. Image source: University of Coloardo, Correll Lab

Since the introduction of the Unimate, the field of robotics has developed at an incredibly fast pace and continues to do so with advances in computer science, mechanical engineering, and material science.

Today, modern robotics falls into two main categories as defined by the ISO 8373 standard on the vocabulary of robotics: industrial robots and service robots (International Standards Organization, 1996). An industrial robot is defined as "an automatically controlled, reprogrammable, multipurpose manipulator programmable in three or more axes, which may be either fixed in place or mobile for use in industrial automation applications". On the other hand, a service robot "operates semi- or fully autonomously to perform services useful to the well-being of humans and equipment, excluding manufacturing operations" (International Federation of Robotics, 2012). Service robots are a very broad category, covering most robotic applications other than robots for manufacturing and fabrication purposes. Within the service robotics category, there are both professional service robots and domestic service robots. Professional service robots are used in industries like defense, medicine, and logistics, while domestic robots are

used for household tasks, entertainment, and education (International Federation of Robotics, 2011).

The vast majority of robotic units sold each year are domestic robots, which had annual sales of over 2.2 million units in 2010 totaling US$538 million. However, the sales of industrial robots comprise the bulk market of the robotics industry due to the higher unit price per robot. In 2010, annual sales of industrial robots totaled US$5.7 billion with 118,000 units sold. Factoring in peripherals, software, and systems engineering, the worldwide market for industrial robotic systems was estimated at US$17.5 billion per year in 2010 (International Federation of Robotics, 2011). The current market for industrial robotics is driven by many different industries as shown in Figure 9.

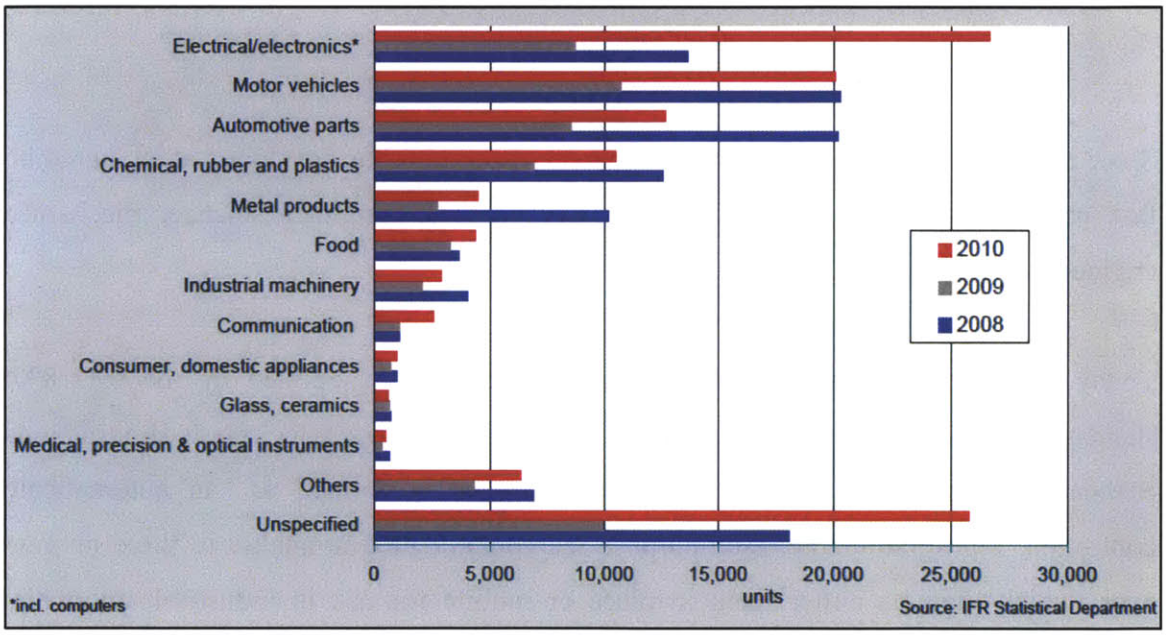

Figure 9. The estimated worldwide annual supply of industrial robots at year-end by industries. Image source: International Federation of Robotics

Motivation

The motivation of this work is to develop industrial robotics as adaptable, reconfigurable, multipurpose platforms for design fabrication, utility, and art beyond the current

repetitive, single purpose tasks on assembly lines. This motivation to push industrial robots into more flexible roles is rooted in the definition of robotics and machines.

The definition of a robot is a debatable topic due to the broad scope of most classifications. For example, under the Oxford definition, any type of machine capable of complex, automatic actions is termed a robot. However, most people would not consider their inkjet printer or their kitchen blender a robot. Instead, people consider these objects as machines, as they are built for a specific purpose. Even though kitchen appliances and inkjet printers have complex, reprogrammable microcontrollers and electromagnetic actuators, they are not referred to as robots. Looking again at the ISO 8373 standard, the definition of an industrial robot as a "reprogrammable, multipurpose manipulator" sets out an important distinction between robots and machines: *multipurpose*. The standard defines "multipurpose" as the capacity to be "adapted to a different application with physical alterations".

In this context, the categorization of an inkjet printer as a machine and not a robot now makes sense. It is difficult to repurpose a desktop printer for anything other than its designed purpose of printing. On the other hand, industrial robotic arm systems are purchased by radically different industries and adapted to a multitude of tasks like welding, gluing, painting, assembly and much more. This requirement of multipurpose adaptability is a key idea and motivation of this thesis.

The vast majority of industrial robots are being used as machines rather than as robots. Instead of continually taking advantage of the multipurpose capability that defines an industrial robot, most robotic arms are only physically modified once and given a specific, repetitive task on an assembly line. In this sense, industrial robot arms are used to serve the role of a machine after being customized for the initial desired task. To clarify this argument, take the example of a computer numerically controlled (CNC) milling machine. A CNC mill is a common machine used to subtractively manufacture objects according to a digital design. CNC mills have many of the qualities of a robot – reprogrammable, electromechanical actuators, and complex automation. Still, a CNC mill

is referred to as a machine rather than a robot. In contrast, an industrial robotic arm in an assembly line with a mounted milling effector does the same task as a CNC mill, but is referred to as a robot. Is there a difference, other than the geometry of the positioning system (arm vs. gantry)? The difference is that the robotic arm could easily be adapted to a variety of other tasks, however most industrial robotic installations do not take advantage of this multipurpose reconfigurability. Most industrial robots have specific, singular purpose roles that emulate the capabilities of a custom machine designed for that purpose.

The motivation behind this work is based on using a robotic arm system to its full potential as a multipurpose fabrication platform. The incredible mechanical capabilities of modern industrial robotic arms seem limitless for a variety of new applications beyond simple repetitive tasks. Instead of multiple machines and robots performing single tasks in an assembly line, can a single system fulfill multiple tasks? If so, what are the benefits and novel possibilities enabled by such a flexible system?

The drive towards developing these robotic fabrication systems is based on a worldwide movement towards digital fabrication techniques, flexible automation systems, and customized manufacturing. By integrating digital fabrication, environmental sensing, and robotic arms, the possibilities for multipurpose fabrication platforms extend far beyond assembly lines and into the realm of the Renaissance robot, capable of novel fabrication techniques, custom artistic applications, and even design itself.

Chapter 3: Setup and Equipment

"What I cannot create, I do not understand."

— Richard P. Feynman

Approach

To explore the use of a robotic arm in digital fabrication, a flexible, multi-functional system was developed. This system, built around a robotic arm, was used in various experiments to evaluate the possibilities and effectiveness of its use in both conventional and novel fabrication methods. The detailed design and methodology for each fabrication technique are described in more depth in subsequent chapters, along with the specific methods. Chapter 4 focuses on replicating conventional fabrication techniques from each traditional fabrication category (additive, subtractive, and formative). Chapters 5 through 9 discussed novel fabrication techniques developed in this work that conform to the traditional fabrication categories. Last, Chapter 10 introduces fabrication concepts outside of the traditional categories and introduces the definitions of *immaterial fabrication* and *informed fabrication.* Immaterial fabrication relates to manufacturing methods where material properties are manipulated without direct mechanical forces or mass transfer. Informed fabrication is a concept defined by the use of environmental sensing to inform fabrication – allowing the robot arm to both input, interpret, and output data with the physical world.

Robotic Arm System

Details common to all experiments are centered upon the robotic arm. The robotic system used in all experiments is a KUKA KR5 sixx R850 (Figure 10) (KUKA Robot Group, 2007). The KUKA arm is a tabletop industrial arm with six axes, allowing for full manipulation in both the Cartesian and angular domain. The arm is lightweight (29 kg), fast (maximum speed of 2 m/s), and has a reach of 850 mm with a repeatability of +/-

0.03mm. A KUKA KR C2 sr controller was used for communication with the robotic arm along with the included teach pendant. The arm was purchased for this work and related projects using funds from a National Science Foundation EAGER grant (Award Number: 115250). A custom aluminum and polycarbonate safety cage was designed and built for the arm and the experiments (Figure 11).

Figure 10. The KUKA KR5 sixx R850 is a 6 axis lightweight robotic arm. Image source: KUKA Robot Group

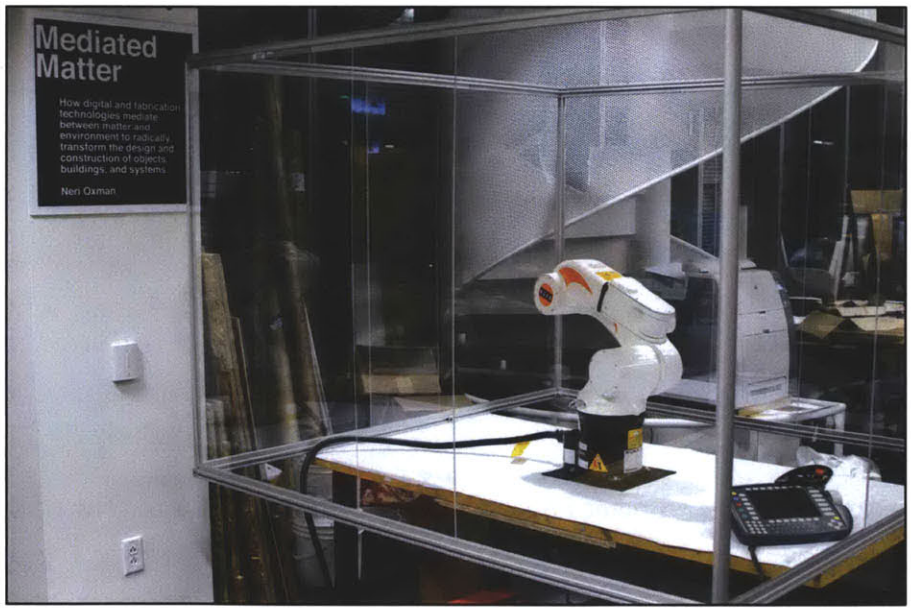

Figure 11. The robotic arm during its installation in the Mediated Matter lab space along with its constructed aluminum and polycarbonate enclosure.

Programming the Arm

The interface to controlling the arm is through KUKA Robot Language (KRL), which is a propriety programming language used by all KUKA robotic products. The use of proprietary programming languages in the commercial industrial robotics field is widespread and often poses problems for applications outside of traditional automation applications. Additionally, interfacing to more common programming languages for real-time control is difficult. For these reasons, all programming for the various experiments utilized offline programming. Depending on the experiment, code was either written directly in KRL and uploaded to the robotic controller, or KRL was produced as an output of another programming language and uploaded to the controller. Python was the primarily scripting language to output more complex KRL codes for various digital fabrication experiments. Sample code of both KRL and Python generation scripts can be found in Appendix A. These include some useful scripts including a G-CODE (a common machining programming language) to KRL generator and light painting programs. Specific code workflows, such as 3D printing tool path generation, for different projects are discussed in more detail alongside their project chapters.

End Effectors

To enable different functionalities, various end effectors were designed, constructed, and evaluated. Example end effectors include 3D printing extruders, end mills, sculpting tools, cameras, lights, and other sensors. These end effectors attach easily to the wrist faceplate of the robotic arm using four bolts and a circular locating feature. Switching between end effectors was done manually, but could easily be automated using a tool changer. Specific end effectors are described with their respective applications in further chapters.

Chapter 4: The Multi-Functional Fabrication Platform

"I am putting myself to the fullest possible use, which is all I think that any conscious entity can ever hope to do."

—Hal, 2001: A Space Odyssey

Introduction

Though robotic arms have the inherent advantages of workspace flexibility and adaptability over conventional gantry systems, they are not being fully utilized. More than just a positioning system for a single process, robotic arms offers unparalleled possibilities through end effectors that can transform arms into fabricators, sensors, manipulators, and designers. Typically, separate and dedicated gantry-style computer numerical control (CNC) machines are used for these purposes. But what if a single machine could serve all these functions?

The concept of a multi-functional machine tool has been studied before, but the mentioned CNC multi-functional machines are based on a gantry milling setup with a tool changer, limiting their operations to subtractive processes (Moriwaki, 2008). One notable setup relevant to this paper is the MultiFab project, which uses a robotic arm, combined with a conventional 5-axis milling machine, to make a machining cell capable of laser-based additive manufacturing and milling (Research Center for Advanced Manufacturing, 2012). Still, no single machine has demonstrated representative processes from each of the traditional fabrication categories. In this chapter, a multi-functional robotic arm platform capable of all three of the major fabrication categories (additive, formative, and subtractive manufacturing) is demonstrated and explored. As well, combinations of manufacturing processes, like 3D printing and multi-axis milling, were demonstrated and discussed in terms of integrated performance.

Methodology

To investigate the idea of a multi-functional robotic arm digital fabrication system, an industrial robotic arm was utilized in the three conventional categories of fabrication: additive, formative, and subtractive. While numerous types of manufacturing exist within these three broad categories, a single representative fabrication process for each category was selected to explore the capabilities. To evaluate additive processes, 3D printing was selected as the fabrication technique. More specifically, extrusion-based 3D printing systems were selected, where the deposited material either solidifies due to thermal changes (fused deposition) or chemical changes (cured deposition). In the formative category, sculpting was chosen. Sculpting uses a pliable material, like clay, and can produce moulds for cast part. Last, for subtractive fabrication, milling was selected.

In addition to replicating conventional fabrication techniques, the flexibility of a robotic arm offers new possibilities for manufacturing. With a minimal physical footprint, the workspace can accommodate parts larger than the arm itself and access interior regions that are not possible for a gantry-based machine. As well, the added degrees of freedom over conventional 3-axis CNC machines can be utilized for multi-axis machining, assembly purposes, and novel processes like multi-axis 3D printing. By using four or more axes to print 3D structures, multi-axis printing offers several benefits compared to the XYZ positioning systems of conventional 3D printers. First, complex 3D structures with sharp overhangs can be printed without support material by rotating the build platform in respect to a stationary extruder. This novel process eliminates support material that reduces waste, print time, and removes post-processing chemical steps. Furthermore, material can be deposited on complex 3D surfaces instead of solely on planar build platforms. This allows for objects to be placed into the printer and printed upon, instead of printing as a standalone process starting from a blank build platform. While multi-axis additive processes have been previously demonstrated with laser-based systems, it is believed that this work is novel in its application to plastic deposition printers (Research Center for Advanced Manufacturing, 2012).

Software

The arm was programmed using Python scripts written to generate the KRL files from coordinate tool paths. For the 3D printing control files that used a conventional XYZ extruder movement, the open-source ReplicatorG program generated the tool paths from input 3D part files. For 3D printing utilizing five axes (with a fixed extruder and a moving build platform), the tool paths were written directly in KRL with the use of fixed tool frames to simplify the math. In this setup, the build platform is rotated about the fixed extruder to allow for complex structures without support material. For milling control files, HSMWorks was used to generate the KRL tool paths directly from within the CAD program SolidWorks through a custom post-processor script. For sculpting, light painting, and volumetric scanning, Python scripts were used to output the tool paths and KRL files directly. All KRL files were tested using KUKA SimPro to ensure no path singularities or work envelopes were exceeded.

End Effectors

To enable the various functionalities, different end effectors were constructed. These effectors connect easily to the wrist faceplate of the robotic arm and can also be used in a fixed tool configuration.

For additive fabrication, a print head that extrudes acrylonitrile butadiene styrene (ABS) plastic was built based on a MakerBot MK6 Extruder. This extruder utilizes a stepper motor to feed an ABS filament through a heated 0.3 mm nozzle. The nozzle is heated with a Nichrome wire element and a thermocouple to provide a feedback loop. The build platform is an electrically heated aluminum plate maintained at a temperature of 170°C to reduce thermal warping of the printed structures. The build platform is wrapped with tape (3M ScotchBlue Painter's Tape) to provide surface texture for the first printed layer to adhere to. The setup for ABS 3D printing is seen in Figure 12.

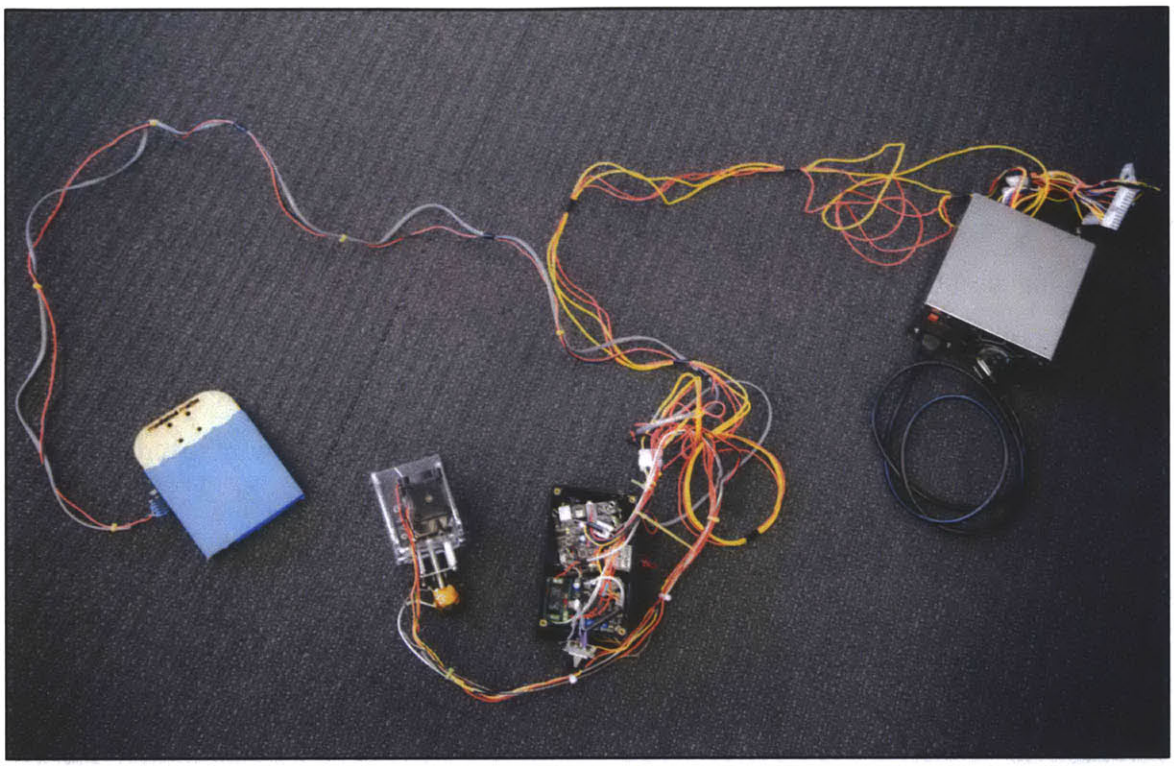

Figure 12. The ABS 3D printing setup used with the robotic arm included (from left to right) a heated build platform with temperature control, an ABS extruder, a control board, and a power supply.

To explore formative fabrication techniques, a simple holder for various sculpting tools was made. Different sculpting tool heads can be quickly changed with a screw tightening adjustment. Modeling clay (Plasticine) was used as the sculpting medium and objects cast using the sculpted clay moulds were made with urethane plastic (Smooth-On Smooth-Cast 45D).

For subtractive fabrication, a rotary tool attachment was converted to serve as a milling effector. A rotary tool (Dremel 4000) with an adjustable chuck was used along with various milling bits. Several materials were milled, including polyurethane foam, ABS, medium-density fiberboard, and modeling wax.

Results

Additive

The use of an industrial robot arm as a 3D print platform was successful for both the ABS and HDPE materials. Using the ABS print head in a conventional XYZ extruder positioning system (Figure 13), the achieved layer resolution was 0.3 mm produced useable parts from a 3D input file. Vibrations and rigidity were not found to restrict printing capabilities and the resolution was only limited by the nozzle extrusion size. Improvements were found by optimizing the path speed and extrusion speed, applying approximate motion control to smooth the tool path, and by utilizing a heated print surface to reduce thermal stresses. As support material was not used, parts were limited to geometries without large overhangs (over 45 degrees) or interior cavities. Example printed parts are seen in Figures 14 - 17. The printed parts demonstrated good layer adhesion and were of equal quality to a commercial MakerBot 3D printer. The tolerances on the extruder positioning via the arm did not limit the printer; the printer was run at a speed of 0.05 m/s without any printing errors due to vibrations or instabilities. The use of an ABS filament feed was robust and allow the machine to print for hours at a time without user interaction.

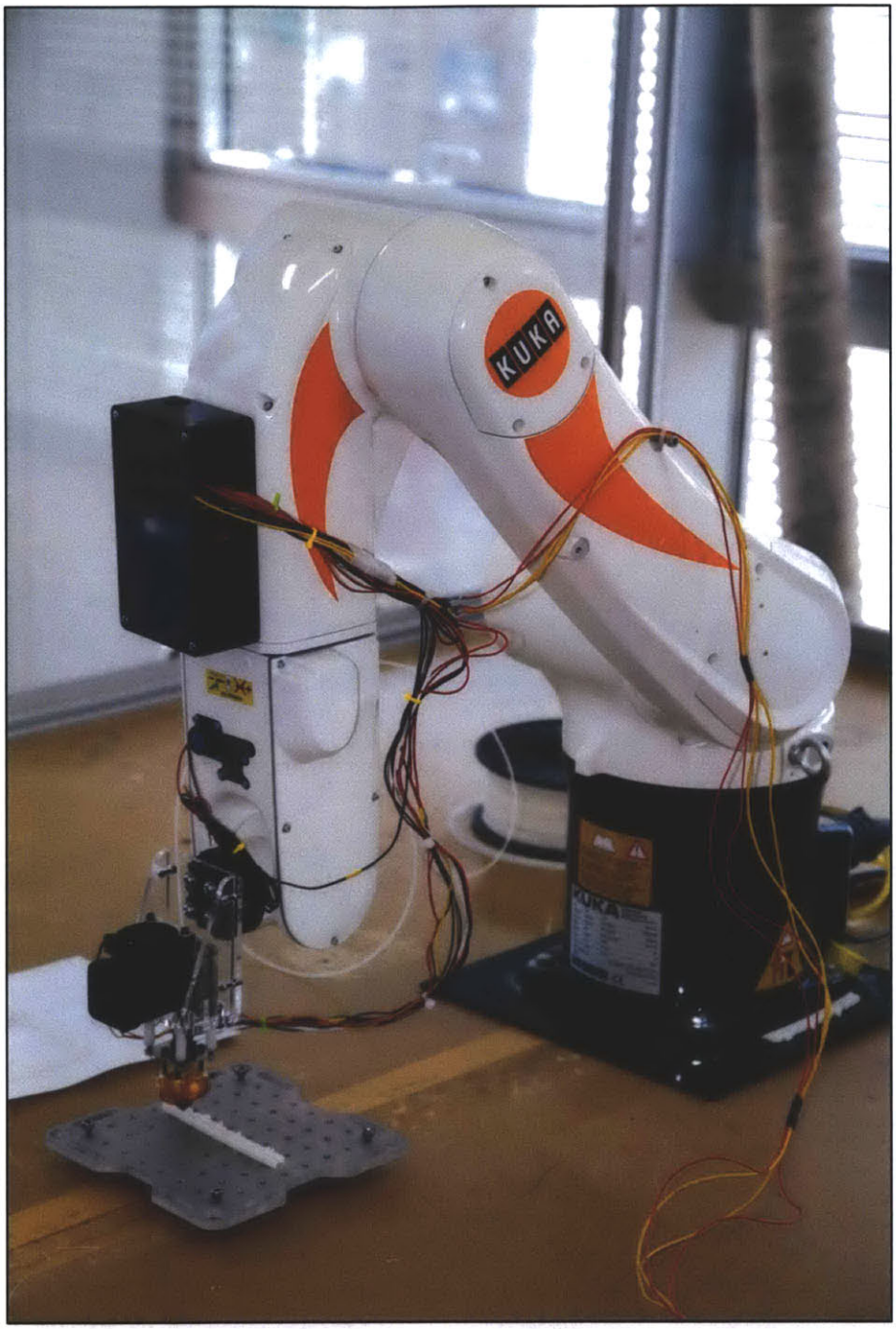

Figure 13. The arm configured with the ABS print head end effector. The thermal control system is mounted to the arm above the wrist section. Note that in this image, the heated build platform is not being used.

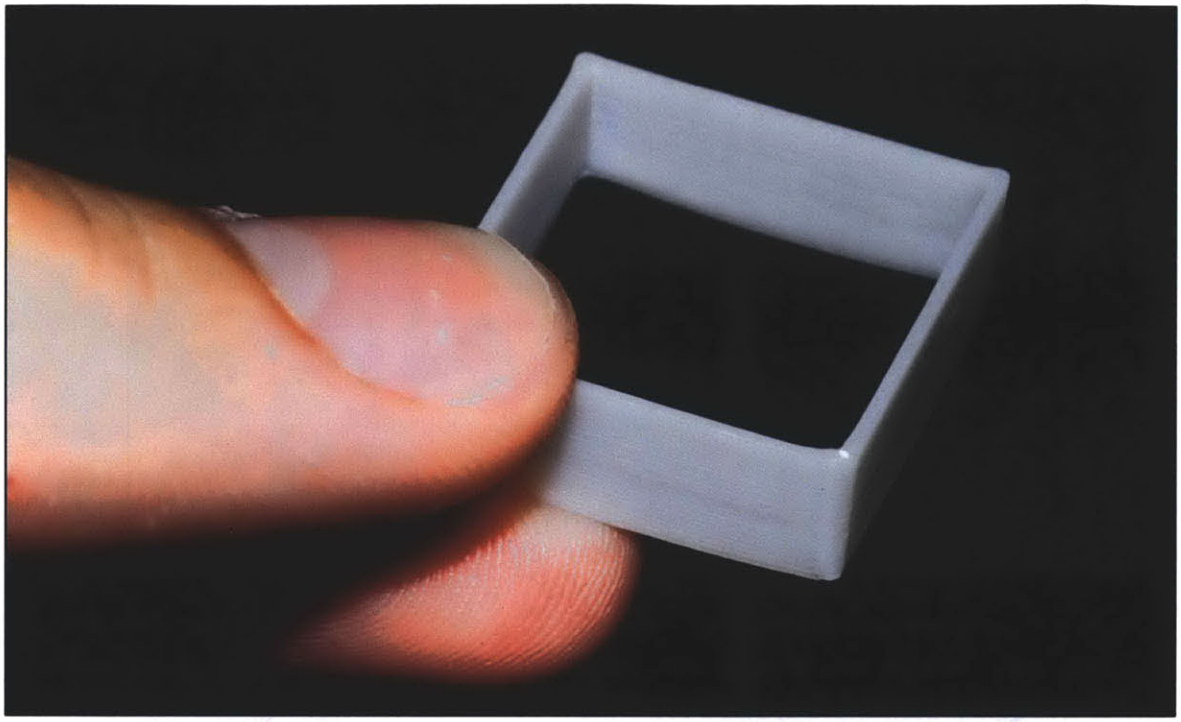

Figure 14. A 3D printed square form shows the layer size of 0.3 mm.

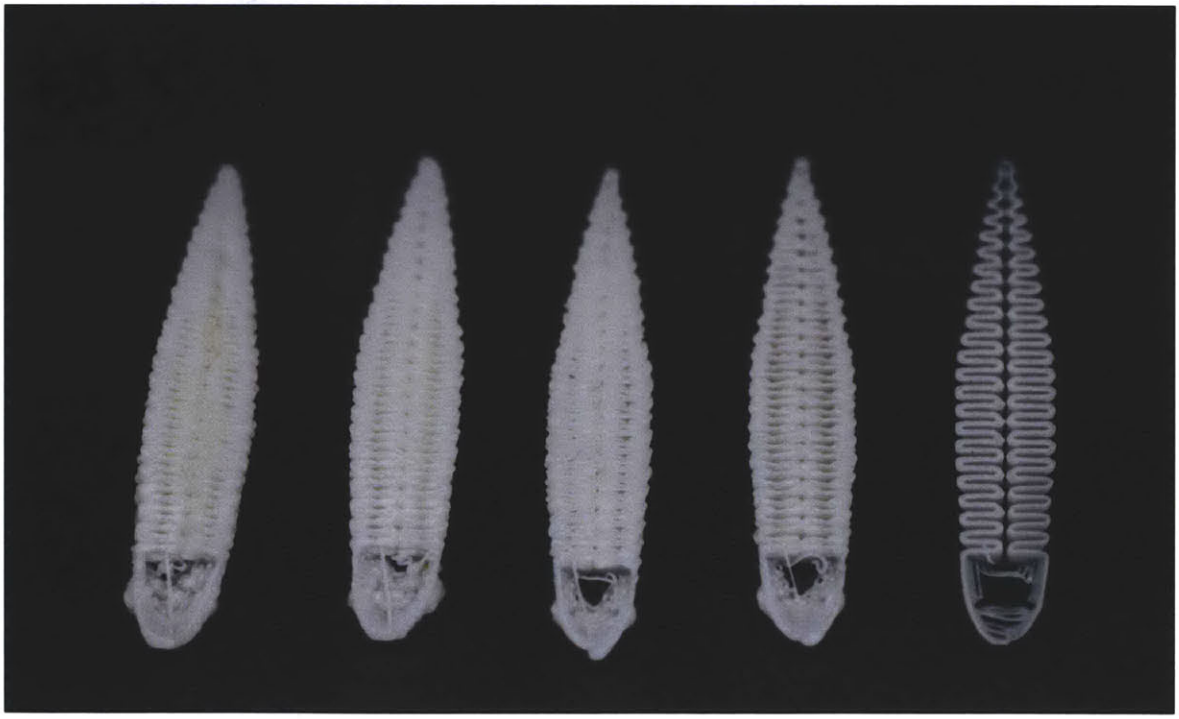

Figure 15. The improvements of using approximate path control to keep speed consistent are shown here as the same object is printed with different configurations of approximate motion control.

Figure 16. A 3D printed sign shows the level of detail and thin wall capabilities of the system.

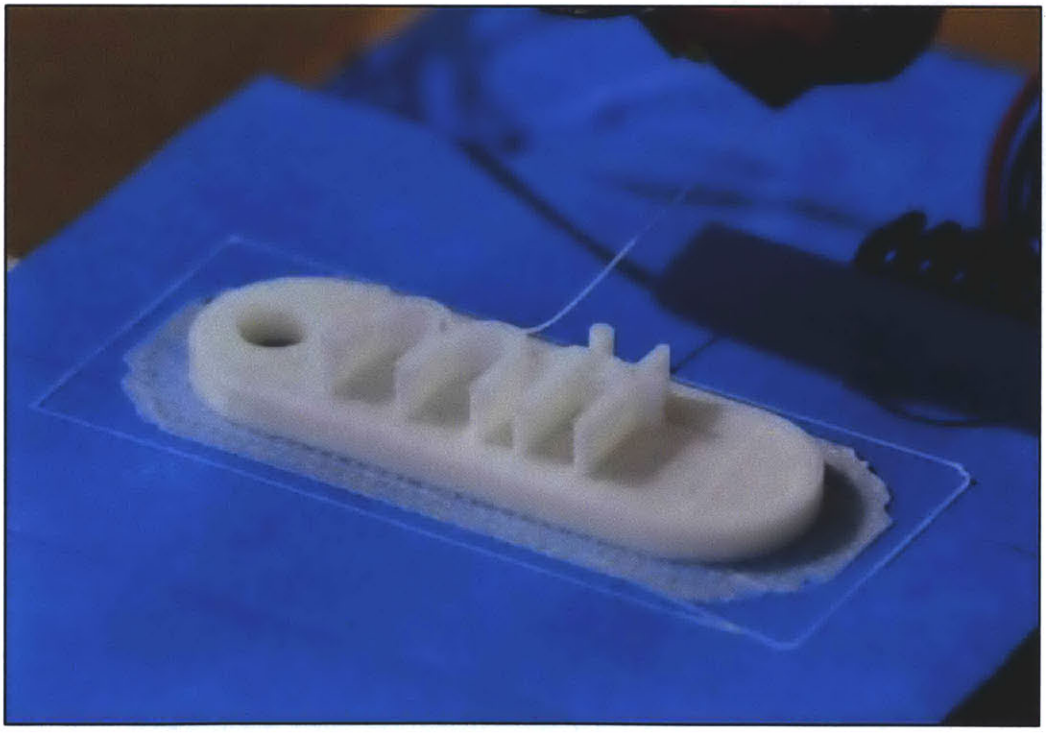

Figure 17. A 3D printed key chain on the heated build platform after printing. The interior fill structure uses a honeycomb pattern to reduce density of the part.

Utilizing the ABS print head in a novel multi-axis system was achieved by moving the build platform about the ABS extruder held in an external fixed tool position (Figure 18). The robotic arm controlled the critical angle between the nozzle and the previous printed layer. By rotating the platform, the angle between the extruder and printed structure was kept under 45 degrees, allowing for sharp overhangs to be printed without support material (Figure 19). As an example, a 20 mm hollow cube was printed with a one-layer wall thickness of 0.3 mm (Figure 20).

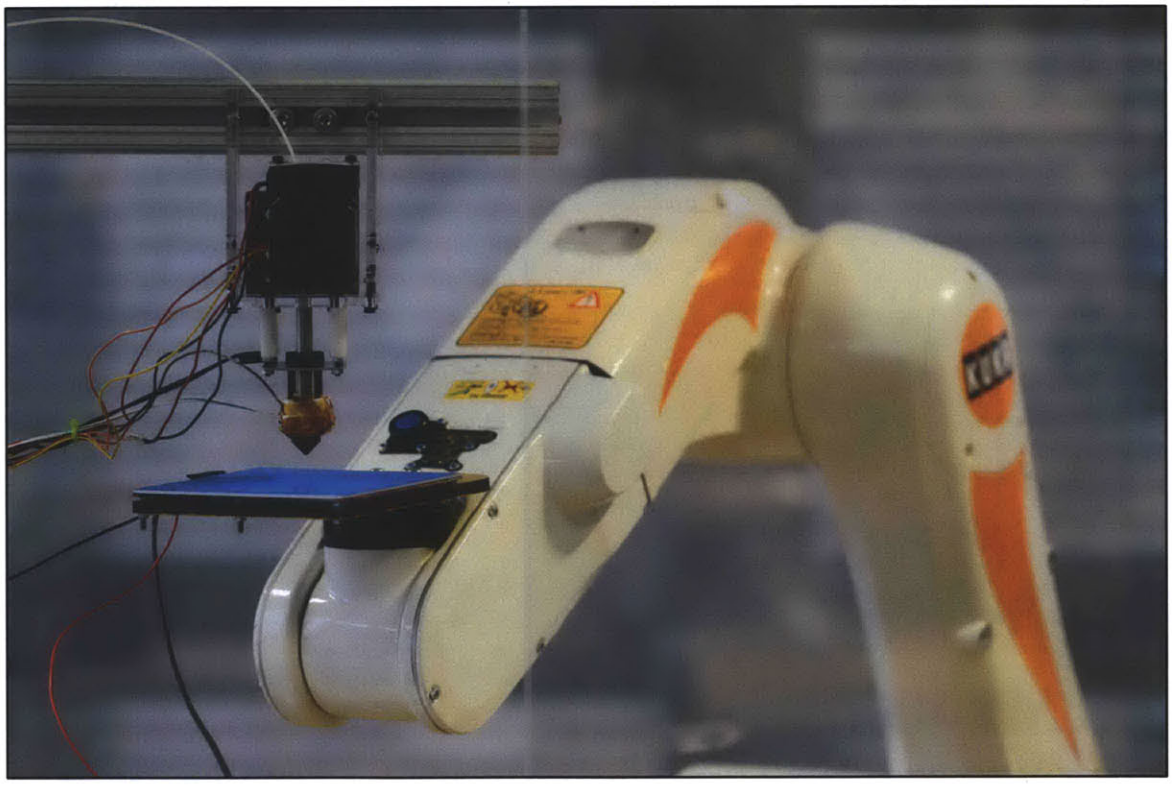

Figure 18. The 3D printing configuration using an external fixed extruder. The robotic arm manipulates the heated build platform around the fixed extruder to construct structures through multi-axis printing.

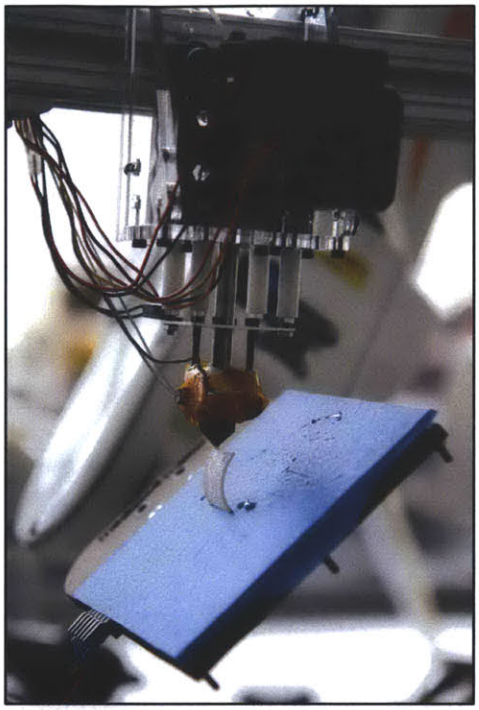

Figure 19. The rotation of the build platform during a print allows multi-axis printing, as seen here. By keeping the angle between the nozzle and the previously printed layer at 90°, overhang structures can be printed without support material.

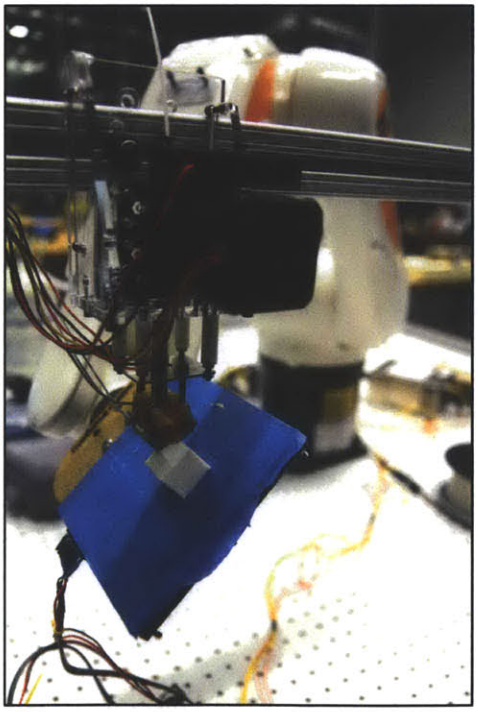

Figure 20. A hollow cube is printed using the multi-axis printing technique developed. The roof of the cube is printed at an angle to remove the need for support material.

This multi-axis configuration proved to be very flexible, which allows for complex structures made without support material and opens the possibility to printing directly onto existing objects if their surface structure is known (through scanning or measurement). In addition, the lack of support material facilitates printing around objects and embedded printing. For instance, a hollow cube was printed and a loose screw was inserted into the center of the cube before printing the roof, leaving the captive screw within the closed structure (Figure 21).

Figure 21. The 3D printed hollow cube printed using the multi-axis technique with the captive screw inside.

Formative

The formative clay sculpting utilized an indentation method where the depth of each indentation was informed by thickness of the desired final object at that point. This resulted in a 2.5D mould being formed in the clay (Figure 22) that was used to cast the

final object in urethane plastic (Figure 23). The indentation method was simple, fast, and effective, though the resolution was limited by the sculpting tool footprint, the step size, and the physical clay properties. The clay properties, especially the adhesion and viscosity, affected the sculpting tool and the desired material distribution. To limit the adhesion, a fast return stroke from each indentation was used to separate the tool from the clay. Secondary passes and smoothing runs were investigated to further improve the sculpting resolution and showed significant improvements.

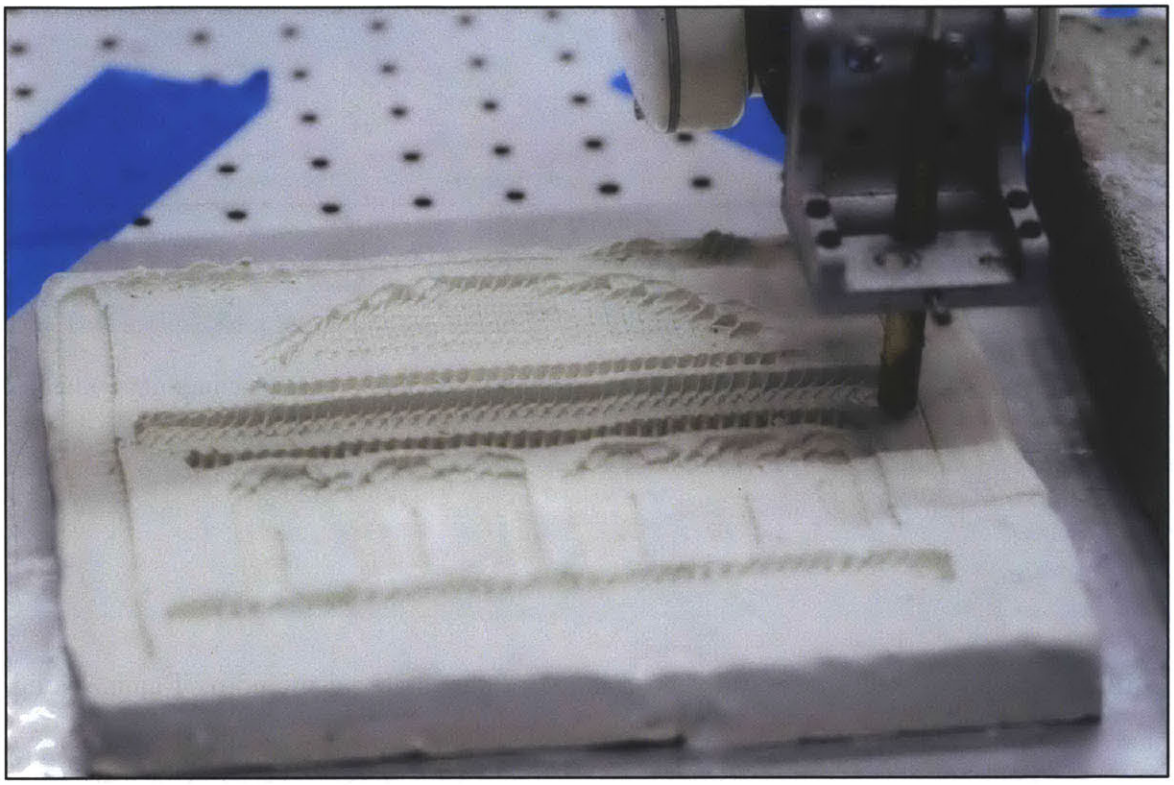

Figure 22. The formative clay sculpting process uses a depressing technique to create a mould.

Figure 23. The produced clay mould was used to cast a urethane object (a rough image of a columned building from MIT's Killian Court).

Subtractive

Milling was completed successfully on a range of soft material including foams, wood, and wax. For example, urethane foam signs milled using a 3 mm end mill bit are shown in Figure 24. Using long exposure photography and a light source attached to the milling end effector, Figure 25 was captured with details the tool path of the effector. In addition to 3-axis milling, multi-axis milling was explored to produce shapes with overhangs.

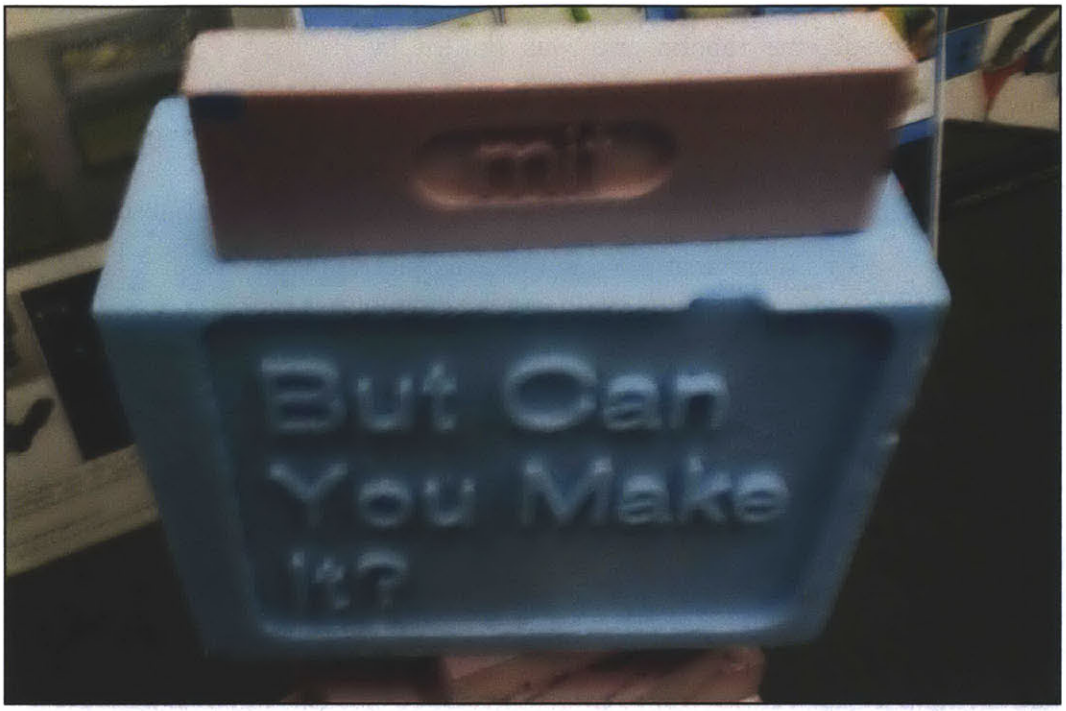

Figure 24. Polystyrene foam signs milled using the robotic arm platform.

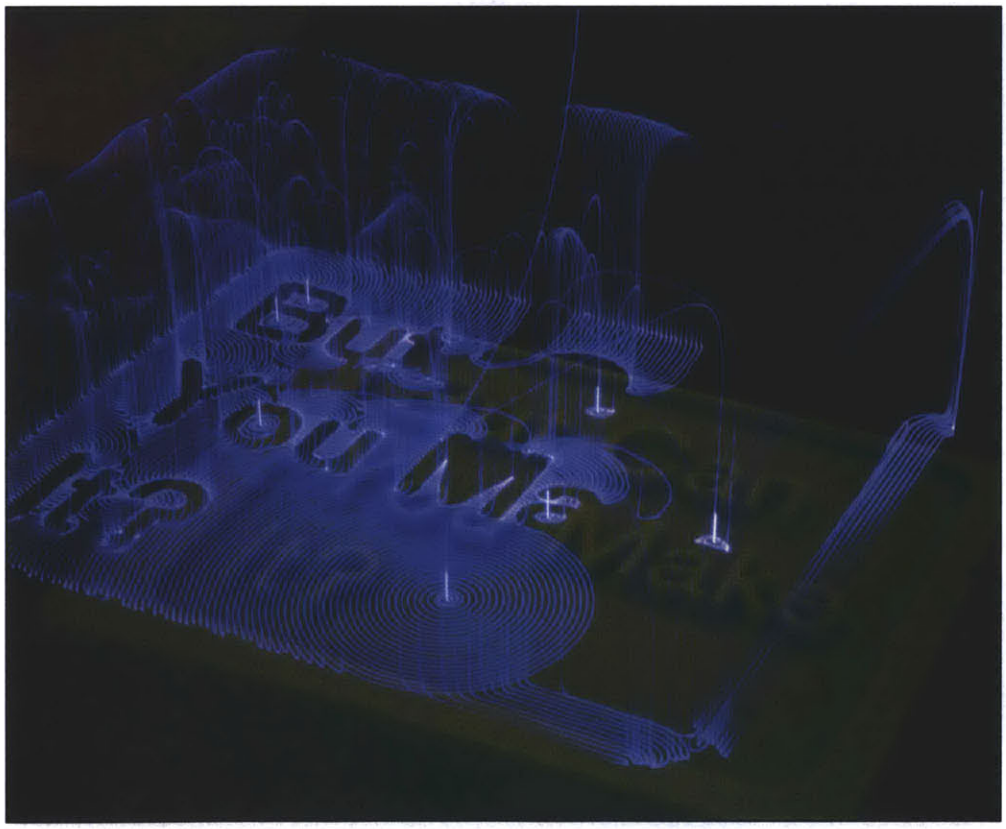

Figure 25. The foam milling tool paths were imaged using long-exposure photography and a light source attached to the milling effector. The milled foam sign is seen below.

In the milling mode, the robotic arm was limited by its rigidity in comparison to conventional CNC milling machines. This reduced the material selection to softer materials and slower cutting speeds. Vibrations, causing chatter in the milled parts, was reduced by optimizing the position of the work piece. Based on visual observations and experimentation, it was found that moving the work piece towards the arm base reduced the system vibrations. This improvement can be attributed to reducing the moment arm and increasing the system stiffness.

Milling completed with the robotic arm platform was very versatile due to the range of motion, ease of access to the work piece, and large working space. For example, a pumpkin was milled to demonstrate the flexibility of the system (Figures 26 and 27). The milling setup was particularly simple to configure, due to the integration of programming through a single CAD/CAM system (SolidWorks/HSMWorks). Using a base coordinate system referenced from the work piece surface allowed for quick calibration to each new stock material work piece.

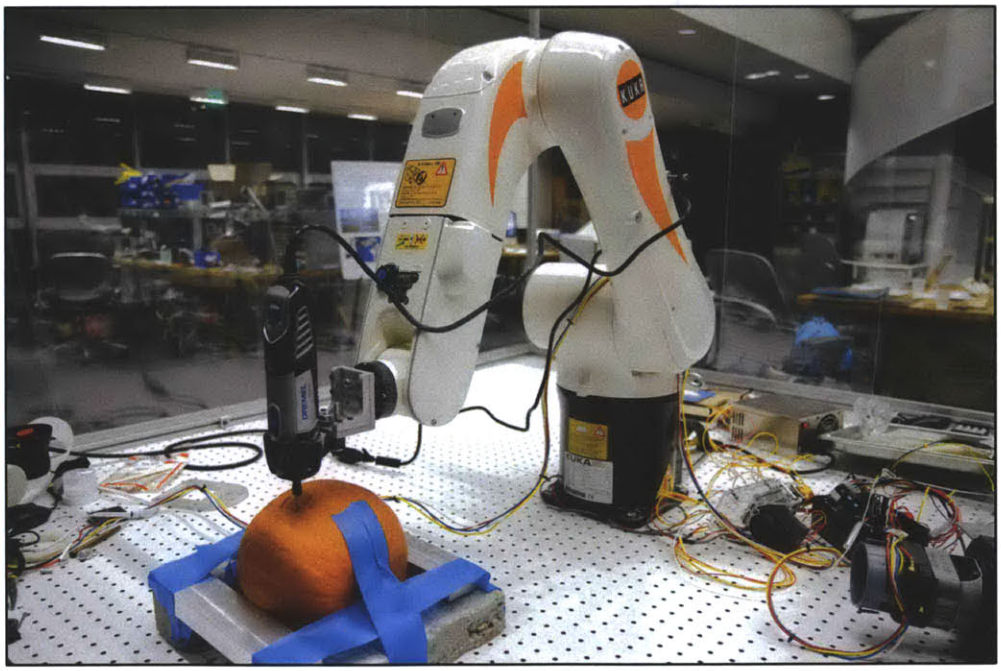

Figure 26. A pumpkin was milled using the robotic arm platform for Halloween festivities.

Figure 27. The milled pumpkin produced using the robotic arm platform.

Compound Processes

To explore the effectiveness in combining processes with a single platform, 3D printing and milling operations were automatically sequenced to generate an object and apply finishing cuts to obtain superior surface finishes and cutouts. This combination technique using a single system is referred to as a compound process. Rather than switch end effectors on the arm, as was done with the other experiments, fixed tool mounts in the workspace held the effectors and the arm manipulated the work piece (Figure 28). This configuration allowed seamless transitions between the processes and the work piece coordinates were maintained throughout the operations without recalibration.

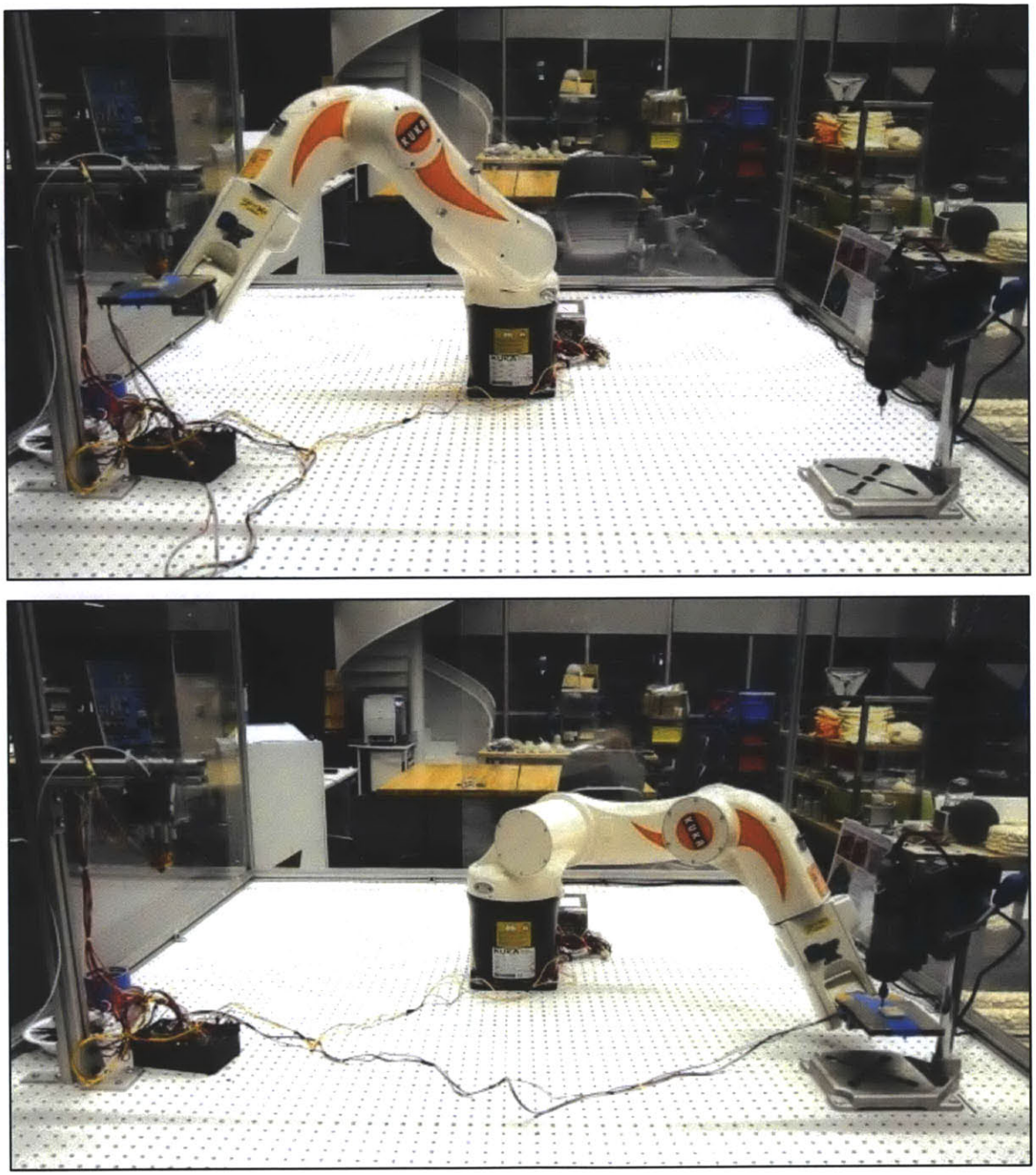

Figure 28. The compound fabrication process of 3D printing and milling is seen here using the external fixed tool configuration. The top image shows an object being printed and the bottom image shows the printed object undergoing surface milling to achieve a better surface finish.

The ABS extruder was used to print a solid 2 cm cube that was then milled by a 3 mm end mill bit. The surface finish of the part was significantly improved by milling, as the 3D printed layered texture was removed (Figure 29). The adhesion between the 3D

printed ABS and the build platform provided sufficient fixturing of the cube for milling to proceed directly following the printing process. The heated build platform was turned off at the end of the printing process to facilitate cooling in order to provide a stronger fixture for milling.

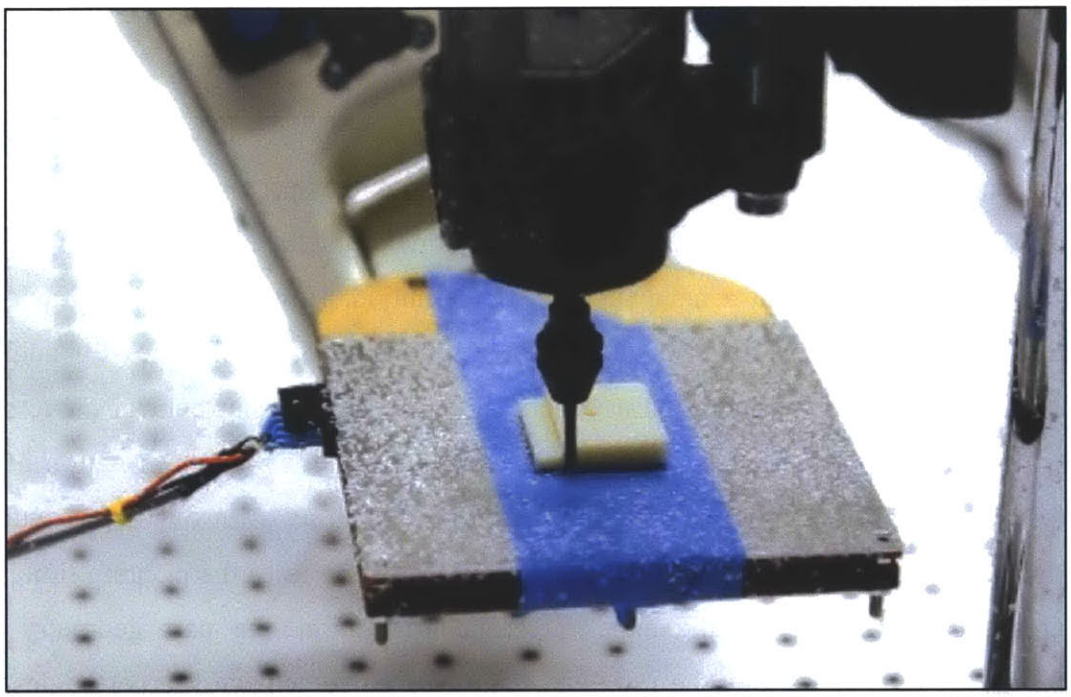

Figure 29. The milling process allows a 3D printed object to have a better finish and tighter tolerances. With the combination configuration, the 3D printed object is already fixtured and calibrated on the build platform to enable milling without re-alignment.

Discussion

Demonstrated techniques

Additive

The use of a robotic arm platform for additive manufacturing techniques is promising and offers several advantages compared to current technologies. First, the printable workspace area is significantly larger, especially when compared to the footprint of the machine, when compared to conventional printers. Secondly, robotic arms can easily be

reconfigured for different printer heads and systems (laser sintering, deposition-based systems, powder/binder systems), making them very attractive for additive manufacturing research. For example, the described system was able to easily switch between an ABS printer, a urethane foam printer (Chapter 7), and a direct recycling HDPE printer (Chapter 8). Finally, the extra axes of robotic arms can be utilized for multi-axis 3D printing, enabling novel benefits.

While multi-axis milling has been commonly used for decades, for all current methods of deposition-based 3D printing, only the XYZ positioning space is utilized. At first thought, there is no apparent use for multi-axis printing as the material nozzle is ideally a single spatial point without a need for angular definition. However, the multi-axis 3D printing explored in these experiments offers a new realm of possibilities for additive manufacturing. While the single point argument stands, the angular control matters for deposition construction due to gravity. Multi-axis control allows for the rotation of the platform to use gravity as an advantage for printing structures with overhangs without support material. Support material is costly, significantly increases the printing time, and requires post-processing. In the experimental configuration, the part geometry and overhangs are only limited by the nozzle size and shape. To achieve sharper angles, the nozzle and extruder could also be positioned to accommodate sharper angles than would be permitted by a solely vertical nozzle. The proof-of-concept shapes printed with the multiple axes were generated with custom tool paths. An algorithmic approach to generating multi-axis tool paths can be developed by maintaining an angle under 45 degrees between the previous layer and the current nozzle position while avoiding a collision with previously printed features.

This concept of rotating the build platform to allow for printed overhangs without support material can be applied to standard gantry XYZ printers with the addition of a variable angle platform. This idea, useful for fused deposition printers without support material, could take the form of a tight tolerance pivot point, actuated by a small motor. An even simpler modification could be done with a manually-operated pivot joint, set to fixed

angle intervals, which could be rotated at pre-programmed intervals calculated by the tool path generation to allow for structures with overhangs.

Formative

The robotic clay sculpting experiments demonstrated an environmentally friendly method of manufacturing given the lack of input material and low input energy. Once a mould is sculpted and a part cast, the clay media can be re-used to make new moulds. To reset the Plasticine clay, heat is applied and the clay is allowed to soften and re-form into a planar solid form. The lack of waste material allows for a cost-effective process where multiple mould designs can be cheaply tested and evaluate.

Formative processes, like the clay sculpting, are well suited for robotic arm platforms due to the required degrees of freedom for manipulating material. Akin to a human sculptor, a robotic sculptor needs complex spatial abilities to position tools and avoid colliding with the work piece. However, while the robotic arm can mimic the mechanics of a human arm sufficiently for sculpting, emulating the human feedback system is a challenge. In the experiment conducted, this was noticed in the form of the clay's variable physical behavior as it was sculpted. For instance, variability in the adhesion to the tool and the direction of the material flow during compression hindered the process. The human sculptor inherently knows to vary their movements and pressure in response to dynamic behavior of the material being sculpted, but for a robotic system the physics must be explicitly modeled and evaluated in real-time. One way to avoid the complex behavior of non-Newtonian fluids (like clay) is to use a granular material, though this substantially limits the geometrical range of produced designs (where the angle of repose controls the geometrical limits). This approach was recently implemented by a group who is using a robotic arm to form sand moulds for custom cast concrete panels (Kohler, Gramzio, Oesterle, & Vansteenkiste, 2011).

Subtractive

Of the various functionalities explored in this experiment (3D printing, sculpting, milling, and immaterial), robotic arm milling was the most researched in existing literature (Pandremenos, Doukas, Stavropoulos, & Chryssolouris, 2011; Tse & Chen, 1997). While not yet a commonplace fixture in industry, robotic arm milling packages are now commercially available and offer many benefits over CNC milling, such as a large workspace and flexible multi-axis options (Robotic Solutions Inc., 2012). As robotic milling is covered in the literature, a detailed analysis will not be covered here. The material and precision limitations are acknowledged due to lack of system rigidity, though improvements could be made through optimizations in cutting parameters and work piece position (Vosniakos & Matsas, 2010).

Integrated performance

Using a single machine for multiple processes allows for integrated performance and novel compound manufacturing techniques. The main benefit is derived from the ability to process a single work piece with many different effectors, without having to re-fixture, re-calibrate, or require human operation in a relatively small space. Conventional CNC mills regularly employ this benefit by switching milling heads for different operations. A multi-functional robotic arm platform takes the concept one further with the ability to switch processes entirely. For instance, 3D printed parts can be immediately milled to achieve the desired tolerance and surface finish. By compounding the two operations, the benefits of additive manufacturing (internal features, material usage) are mixed with the benefits of subtractive manufacturing (higher precision, better surface finishes). A multitude of process combinations can yield hybrid advantages and offer a truly flexible manufacturing machine.

Multi-axis printing combined with assembly also facilitates the avenues of embedded printing and object printing. Current 3D printing technologies work from a blank canvas

where the entire structure is printed and the outputted object is constrained to the limited materials available to 3D printing. The concept of embedded printing combines 3D printing with pick-and-place assembly techniques to merge 3D printed features with pre-fabricated objects like electronics, hardware, and fabrics. Utilizing a digital scanner, an object complex surface can be integrated into a design and 3D printed on or around. With the spatial flexibility of multi-axis printing, these complex surfaces can be reached and undercuts can be printed into. Of all the 3D printing techniques, only lithographic methods based on curing photopolymers have allowed for 3D printed structures around physical inserts (Kataria & Rosen, 2001; Chen, Zhou, & Lao, 2011). These lithographic techniques are limited to photopolymer materials and suffer from difficulties like laser shadowing from the inserted object (Kataria & Rosen, 2001). The use of multi-axis 3D printing for embedded printing and assembly operations opens a realm of new possibilities for additive manufacturing.

One of the benefits of a robotic arm system for integrated performance is the open access to the workspace by the effector. Unlike a gantry system, a robotic arm can navigate around several fixed tools, offering an alternative approach to switching end effectors. Mounting the work piece on the arm, several fixed tools (print heads, milling stations, grinding stations, etc.) can be used without re-fixturing or swapping effectors. This efficient approach was demonstrated successfully with the combined 3D printing and milling.

Limitations

The avenues explored in these experiments are excitingly diverse and a promising argument for future development into multi-function robotic fabrication systems. However, there are limitations with robotic arm systems that need to be addressed to advance their use. These limitations include the programming environment, performance issues, and economic considerations.

Software limitations are the primary reason for the lack of robotic arms in non-cyclic tasks. Generally speaking, the current hardware on industrial arms is more than capable for numerous fabrication tasks. While the issue is generally improving due to growth in programming languages and interest in digital fabrication, several issues complicate the process.

First, the programming architectures of industrial robotic arms are not easily compatible with digital fabrication. Issues relating to singularity avoidance are not sufficiently solved in the programming architecture to enable the needed smooth, complex, and long tool paths required for digital fabrication. This problem arose many times during these experiments, where a tool path would be halted in-progress due to a singularity issue. To avoid this, all tool paths were digitally checked using a simulator (KUKA SimPro) and minor movements were added to bypass problem zones.

Physical constraints of a robotic arm system for digital fabrication relate to the maximum accuracy, strength, and stiffness. Given the configuration of a conventional robotic arm, the system's mechanical properties are orders of magnitude lower than a similarly sized gantry system. As seen in the effects of system stiffness on milling, the lack of stiffness in a robotic arm limits the material choice to softer work pieces and slow cutting rates. This is also true for accuracy and strength. There are significant improvements that can be implemented to improve arm rigidity for milling operations, for instance in work piece position and in tool path optimization (Vosniakos & Matsas, 2010). However, robotic arm milling operations will not be able to replicate the precision, material capabilities, and speed of gantry-style machines for processes that require high forces (likely types of subtractive and formative fabrication).

Compared to conventional gantry platform, robotic arms are more expensive due to the additional complexity. For individual conventional fabrication processes, it will be difficult for robotic arm system to complete economically with gantry-style machines. However, the added capabilities and multi-functionality of a robotic arm platform justify the added cost. As shown by these experiments, a single platform can be quickly

reconfigured to function in all of the major fabrication categories. Furthermore, the integration of multiple distinct machines into a single unit enticing possibilities of compound processes, such as 3D printing and milling as demonstrated. Such a combination could offer the benefits of both processes: allowing complex internal structures, reduced material usage, and precise surface finishes and tolerances. Assembly tasks can also be integrated directly into the digital fabrication workflow, for instance with pick-and-place functionality and embedded object 3D printing. With the flexibility of a multi-functional robotic arm fabrication platform, a truly integrated manufacturing machine is achievable.

Conclusions

The uses for robotic arm systems in digital fabrication are growing and will continue to grow due to their flexibility and size advantages over gantry-style positioning systems. While the inherent lack of rigidity and higher cost prevents direct replacement for many gantry-style CNC systems, new manufacturing avenues suitable for arms are appearing rapidly. As opposed to gantry systems that are large, heavy, and constrained to their internal workspace, robotic arms can be easily moved and tracks can be added for enormous workspace capabilities. These benefits, along with the multi-functionality demonstrated, provide a strong argument for the future growth of robotic arm platform for digital fabrication.

The true flexibility of industrial robotic arms is currently underutilized due to their relegation to primarily cyclic tasks. As demonstrated in this chapter, a single robotic arm system can serve as an additive, subtractive, and formative fabricator. By serving as a multi-functional fabrication platform, the benefits range from integrated performance capabilities, large workspace performance, a minimized physical footprint, and cost. While barriers still exists for robotic arm digital fabrication, such as the complexity of generating tool paths, the evolution of proprietary industrial control systems, and the

issues of system rigidity, progress in all categories provides an optimistic outlook for robotic arms in digital fabrication.

Chapter 5: Moving Beyond Conventional Fabrication

"The future masters of technology will have to be light-hearted and intelligent. The machine easily masters the grim and the dumb."

-Marshall McLuhan

As demonstrated in Chapter 4, a single robotic arm system can be utilized and reconfigured to perform conventional fabrication techniques spanning the three traditional categories of additive, subtractive, and formative processes. This ability to serve as a multifunctional machine tool very important and could reduce the cost and footprint of a traditional machine shop extensively. However, looking forward, the remainder of this thesis asks a more exploratory question: What new fabrication techniques are possible?

With the amazing mechanical capabilities in speed, precision, and strength, today's industrial robotic arms are only confined in applications by programming technology and imagination. While the vast majority of industrial arms are relegated to repetitive tasks on the manufacturing line, a new era of repurposed robotic arms is emerging with applications ranging from digital fabrication, to entertainment, to art. As the cost of industrial arms continues to decrease, this burgeoning expansion of industrial robotics to non-traditional fields can only be expected to grow. In addition to cost, another important consideration for new growth fields for industrial robotics is the ease of programming and interface.

Currently, the barrier for entry to industrial robotics is far too high in terms of programming complexity, flexibility, and ease of access. All of the major robotic arm manufacturers use proprietary programming languages that impede the use of third party software and open-source platforms. While the competitive nature of industry dictated the evolution of the various proprietary industrial robotic control solutions, the introduction of easy interfaces to open-source control systems would allow for the rapid advancement

in new growth areas, such as digital fabrication. Several groups around the world have made promising progress in this area, such as the open-source MATLAB KUKA Control Toolbox and the Parametric Robot Control plug-in for Grasshopper (Siena Robotics and Systems Lab, 2011; Robots in Architecture, 2012). The industry is beginning to take notice as well, with KUKA's recent foray into arms specifically designed for research use, namely the Lightweight Robotic Arm and the YouBot (KUKA Robot Group, 2012). These robotic systems both have new control structures that facilitate open-source programming. The next few years will be an exciting time for industrial robotic arms due to a renewed interest in domestic manufacturing, open-source control, and digital fabrication. New creative growth areas for industrial robots will grow exponentially if cost and proprietary programming are improved. The do-it-yourself (DIY) community has proven extremely effective in adapting new technologies for novel purposes once these cost and complexity barriers are overcome. Examples such as the Arduino platform, Microsoft's Kinect, and MakerBot demonstrate the power, growth, and rise of the result of breaking the cost and complexity barriers (Arduino, 2012; OpenKinect, 2012; Industries, 2012).

As a further example, the use of the robotic arm installed in the Mediated Matter space is evidence of the community interest for new applications. Upon installing the KUKA arm, a significant number of people from around the Media Lab were proposing projects and showing interest in using the arm for a variety of purposes. Once the cost barrier was reduced (by having the arm in the lab) and the programming barrier was avoided (by discussing the projects with the author), the amount of ideas was only limited by the collective imagination. However, as the programming barrier was still a very real issue and lab members did not want to invest time to learn a new programming language, the majority of these suggestions were left as just that and nothing more. If the arm had an interface to a common programming language, many more projects and users would have been enabled. A few are mentioned as proof of the range and flexibility of the arm:

A cricket ball test experiment was conducted using the arm to study the heat signature of a ball contacting a bat. The motivation behind the experiment was that current cricket

technology uses a thermal infrared camera to image the heat signature of a ball striking a bat. This technology allows the umpire to determine if a ball came in contact with a bat or if the ball was completely missed. The experiment was based around whether various materials, like Vaseline or silicone, could cover up the heat signature, preventing the umpire from knowing if the ball was struck. The robotic arm was used to simulate a thrown ball tipping a bat. Using the setup shown in Figure 30, a cricket ball was moved across a stationary bat and various speeds, angles, and with different materials applied to the bat to test the heat signature masking effect (Khullar, Joshi, Lawson, Keating, & Raskar, 2012).

Figure 30. The robotic arm was used to move a cricket ball into contact with a cricket bat at various speeds and angles to test material heat signatures of the collisions.

Another request of the robotic arm was for precise angular photography for a view-dependent screen. Students from the Camera Culture lab invented a display consisting of stacked liquid crystal screens capable of generating 3D images by showing view-dependent images. In order to demonstrate and evaluate their display, the robotic arm was used to precisely move a camera in an angular sweep with the display as the focal point (Figure 31). A series of long exposure images were taken in this precise manner to account for the low brightness of the display due to the stacked polarizers. Stacking the photographs into a video sequence allowed their technology to be evaluated and demonstrate with a repeatability camera movement for their paper (Wetzstein, Lanman, Hirsch, & Raskar, 2012).

Figure 31. The robotic arm was used to create a fluid video of an angular display prototype for colleagues in the Camera Culture Group at the Media Lab.

Various other small side projects involving the robotic arm have included a robotic artist that draws images without lifting its pen (Figure 32) and a robotic laser projector capable of drawing on objects with a red laser (Figure 33).

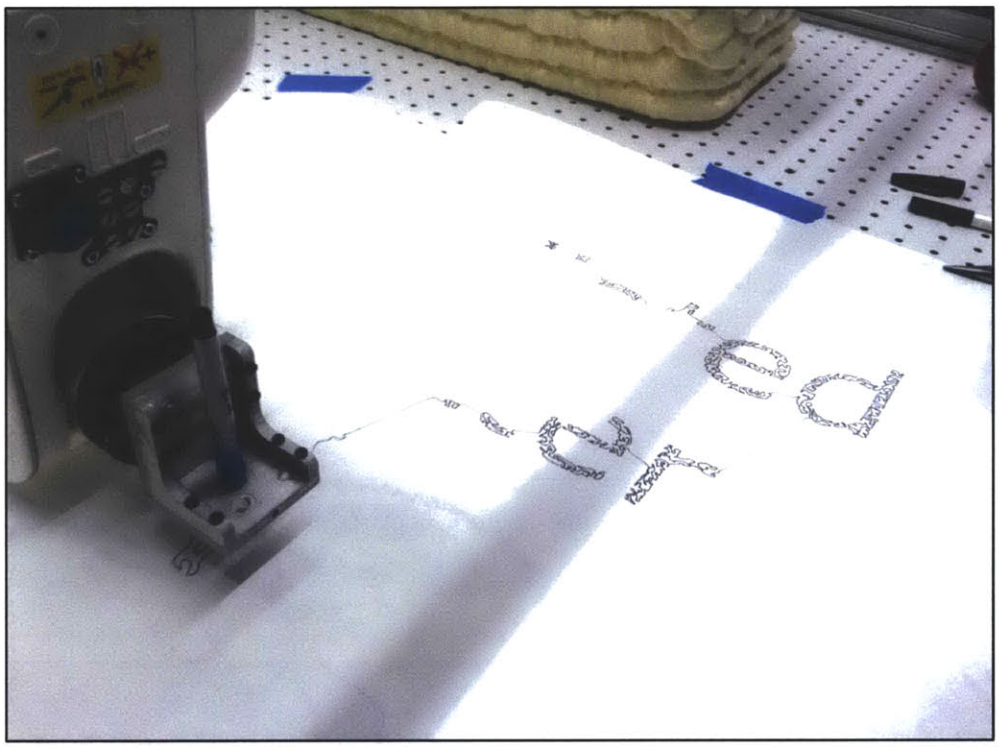

Figure 32. The robotic arm was used to draw images using a single line without lifting the pen from the paper. Here it is drawing a Mediated Matter sign with a robot figure below.

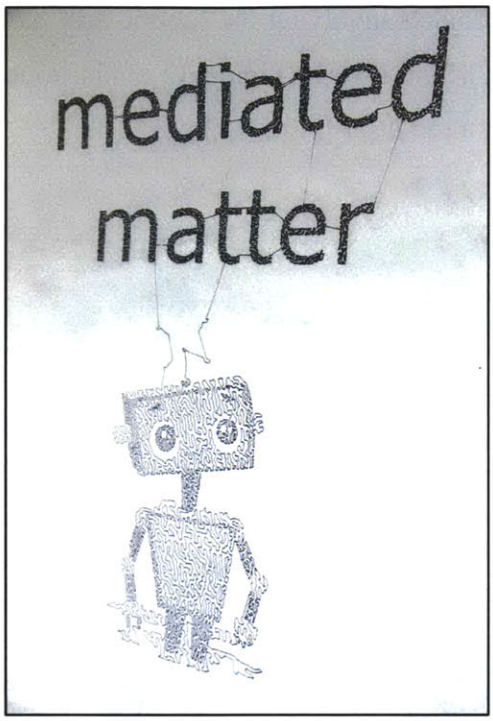

Figure 33. A drawing completed by the robotic arm platform using a single pen stroke.

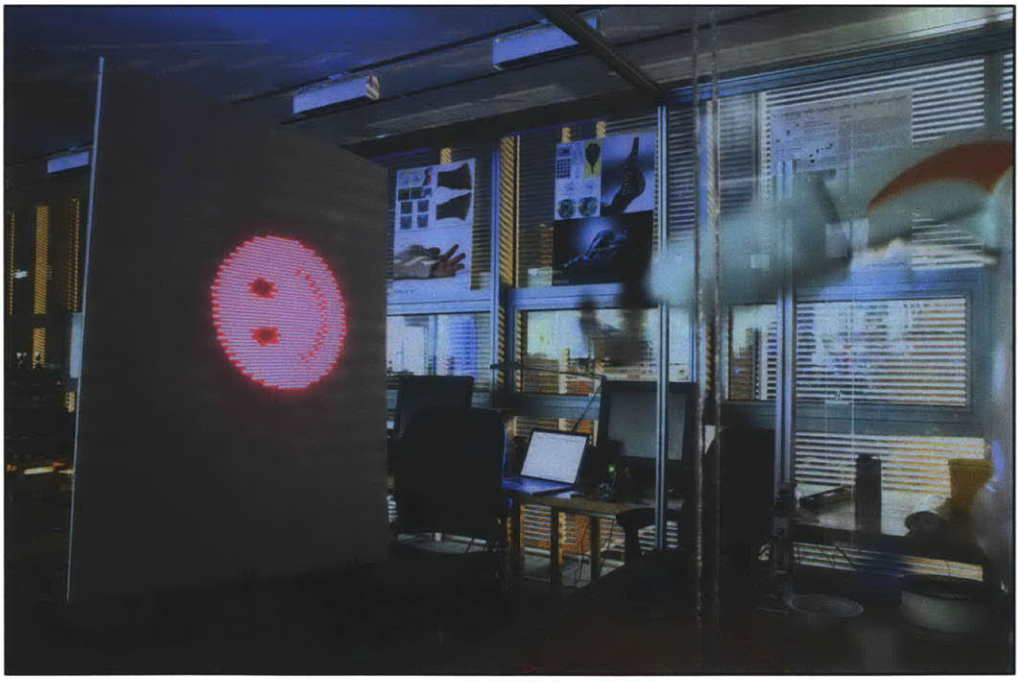

Figure 34. A red laser mounted to the robotic arm created a slow laser projector system. Here an image is captured through a long-exposure photograph.

The following chapters detail projects that investigate new ideas in fabrication relating back to robotic arms. First, the theory and practicality of functionally graded additive manufacturing is explored using cement foams and density gradients in Chapter 6. Functional gradients are a new frontier in 3D printing, which has traditionally produced single-material, homogenous objects. Continuing with additive cement manufacturing, Chapter 7 discusses the development and testing of a large-scale method for 3D printing large structures and buildings. The developed technique, termed *Print-in-Place* construction, uses a 3D printed mould structure akin to insulated concrete forms. Chapter 8 looks at incorporating recycled materials into additive manufacturing through the prototyping of a direct recycling system. Chapter 9 details a project focusing on a type of formative fabrication process using jammable granular systems. By altering the pressure applied to granular systems, the material system exhibits tunable material properties such as stiffness and strength. The characterization of such systems and design possibilities are explored. Chapter 10 focuses on expanding the definition of fabrication to include immaterial-based fabrication, where altered material properties define a design. Chapter 10 also discusses the concept of informed fabrication, where direct environmental feedback is used to inform the fabrication process.

Chapter 6: Functionally Graded Cement Fabrication

"I believe in God, only I spell it Nature."

— Frank Lloyd Wright

Introduction

The reach, flexibility, and dexterity of robotic arms can be useful for large-scale 3D printing operations in contrast to modern gantry-based systems. Current limitations on 3D printing include product size and material selection. Focusing on these areas, this chapter introduces the concept of functionally graded 3D printing of cement structures using a robotic extrusion technique.

Most manufactured parts are constrained to a single type of material with homogenous properties. To achieve different material functionalities, multiple separate parts made of dissimilar materials are typically connected or assembled using some form of fastener or adhesive. This method of assembling parts from different materials to form an overall structure is required due to the current manufacturing limitations on producing complex functional gradients within monolithic parts. In contrast, natural systems consistently produce functionally graded structures such as gradients of elasticity in human skin, gradients of translucency and colour in fish scales, and gradients of density in bones. This ability to produce monolithic gradient structures results in higher material efficiency, enhanced functionality, and a more integrated system.

The current limitations of manufacturing techniques for functional gradients is due to both a lack of fabrication processes and CAD tools required to design and produce variations of properties within solids (Oxman, Variable property rapid prototyping, 2011). Functional gradients are used in manufacturing, such as heat annealing metals to achieve a hard surface finish, but complex designs of functional gradients are difficult to produce. Additive manufacturing techniques hold promise in this area of fabrication as

the material is distributed with a precise position. If the material extruded, or cured, at various positions could be varied to produce controllable material properties, 3D printers could be used to fabricate complex functionally graded objects. The vast majority of current 3D printing technology is based on a single material output, due to simplicity, difficulty in material compatibility, and design challenges around multiple materials. However, this concept is beginning to emerge in industry and a 3D printer by Objet offers multiple material printing capable of outputting preset combinations of resins (Objet, 2012). This allows the formation of composite-like materials with preset values of elasticity and tensile strength. The Objet Connex line of printers offers the ability to have fourteen different materials within a printed part, offering a glimpse into the future of 3D printers capable of functional gradients. The Connex line uses an optical curing process to form parts, requiring expensive feed resin that is limited to certain plastics with limited stability and lifespan. Thermoplastic gradient printing is also feasible, though the various melting temperatures of the component plastics would complicate dynamic mixing of the molten plastic before extrusion.

In terms of structural materials, most man-made materials are completely homogenous and uniform in their properties. Concrete, the world's most widely used construction material, is typically poured into moulds to achieve uniform properties (Aïtcin, 2000). In contrast, natural structure materials, like wood and bone, exhibit density gradients and anisotropic properties (Gibson, Ashby, & Harley, 2010). These functional density gradients in natural structural elements provide benefits of strength and functionality. If these gradient structures could be replicated in man-made objects, materials and structures could be designed for specific loads. Benefits of improved strength and lower material usage are possible. In this chapter, the used of additive manufacturing techniques with cement and concrete is explored in terms of functional density gradients.

The work conducted on functional density gradients in cement can be broken down into answering two key questions: i) Would density gradients in cement be useful in terms of structural and material efficiency?; and ii) How can these density gradients be reliably produced according to a design?

Focusing initially on the first question, a theoretical investigation into the ideal density gradient structure for a column was conducted. Using experimental data obtained from compression testing of chemically foamed samples, the benefits of structural and material efficiency were demonstrated. The qualitative observations from the chemical foam tests were compared to cement foam produced using mechanical foaming techniques for suitability in additive manufacturing.

Second, with the supporting theoretical work in hand, methods of additive manufacturing cement structures were explored. Using the robotic arm as a test platform, several printing tests were conducted. Different methods, such as direct extrusion, negative mould printing, and perimeter mould printing were investigated.

Background

Natural Structural Density Gradients

The idea of a density gradient is naturally inspired by density gradients in the stems of arborescent palm trees. As palm tree stems do not have the ability to increase their diameter over time to combat loads, they instead thicken their cell walls, producing a density gradient. The density is highest at the peripheries and lowest in the center, and ranges from 100-1000 kg/m^3 in a single stem (Gibson, Ashby, & Harley, 2010). The radial density varies with position as given by:

$$\frac{\varrho}{\varrho_{\max}} = \left(\frac{r}{r_0}\right)^n \qquad \text{Eq. (1)}$$

where r is the radial position, r_0 is the outer radius, and n is a constant that is determined experimentally (Gibson, Ashby, & Harley, 2010).

Cement Foams

Concrete is the most widely used construction material in the world because of its low price, readily available materials, and structural properties. Concrete is composed of cement and aggregates. Concrete is made from common materials: sand, lime, water, and stone. It does not require expensive equipment or processing techniques, thus making it cheap to produce. Its hydraulicity, or insolubility under water, allows it to function effectively as a structural material. Although concrete's properties secure its importance as a construction material, concrete production creates large amounts of emissions and is responsible for approximately 5% of global CO2 production (Worrell, Price, Martin, Hendriks, & Meida, 2001).

Cement foams are produced by incorporating gas into a cement paste matrix. In these experiments, cement foams were analyzed instead of concrete foams to reduce the number of manipulated variables and to allow for comparisons to the cement literature. By adding aggregates like fly ash or sand to cement foams, concrete foams can be made at a lower expense. Concrete foams are currently used for building construction applications because of their low thermal conductivity, high stiffness per unit cost, energy efficiency, easy processing, and fire resistance (Tonyan, 1991). The motivation for this project comes from the idea that density gradients in concrete beams may increase the strength of the beam while reducing material waste, and thus be less harmful to the environment.

Cement foams are commonly produced using one of two methods: chemical foaming or mechanical foaming. In chemical foaming a metal powder, such as aluminum, is added to the cement-lime slurry. The reaction of the aluminum with lime produces hydrogen gas, producing concrete foams of densities ranging from 15-60 pcf (Short & Kinniburgh, 1978; Taylor W. H., 1974). The other cement foam production method is called mechanical foaming. In this method a preformed foam or foaming agent is added to the slurry. The use of an autoclave for curing purposes can be used in chemical foaming. This type of foamed cement is called pre-castable autoclaved lightweight ceramic, or

PALC. The advantages of the autoclaving process are better mechanical properties for a given density and shorter curing times relative to the mechanical process. The disadvantages are high cost and complex processing (Tonyan, 1991).

Mechanical Model of Cement Foams

Scanning Electron Microscopy (SEM) imaging reveals the structure of the cement foam matrix follows the closed cell model in which a significant amount of material is found in the faces in addition to the struts of the cell (Tonyan, 1991). The mechanical behavior of these foams can be described using the brittle closed cell foam model and empirical models of porous ceramics, depending on the relative density of the foam. The compressive strength of brittle closed cell foams with relative densities below 0.3 is given by Equation 2, assuming bending stresses dominate and axial deformation is negligible (Gibson & Ashby, 1988).

$$\frac{\sigma}{\sigma_{fs}} = C\left(\frac{\varrho}{\varrho_s}\right)^2 \qquad \text{Eq. (2)}$$

When the macroscopic porosity contribution is introduced to the foam matrix, a ceramic model is used to describe the mechanical behavior. The compressive strength of a ceramic is given by the equation:

$$\sigma = \sigma_0 e^{-qp} \qquad \text{Eq. (3)}$$

where σ is the compressive strength of the porous material, σ_0 is the compressive strength of the solid material, p is porosity, and q is a constant. Rice (1976) and Roy and Gouda (1973) empirically find an average q of 7 and a high porosity q equal to 3.

Chemically Foamed Cement

Methods

Five different ratios of dry mix were used to create cement foam samples of with varying densities. As detailed in Table 1, the variable that was manipulated was the amount of aluminum powder. Type III Portland cement was used for of its fast strength maturity. Slaked lime and aluminum powder were added to the dry Portland cement and mixed by hand. Water was added using a ratio of 45% (by weight) water to dry mix for the pure cement sample (sample group a). For all of the remaining samples groups (b – e), a water ratio was 50% was used as the foam mixtures required additional water than expected. From each of the five sample groups, four standard compression cylinder samples (4" diameter by 8" height) were poured. The samples were poured into mould cylinders using WD40 as a releasing agent. The poured samples were vibrated for several minutes and left to set. Smaller samples for each mixture group were made for pore size analysis. After 2 hours, the foamed samples had risen due to gas generation and excess material was troweled off of the top before capping the samples to retain moisture and cure. After a week of curing, the samples were removed from the moulds and placed in a water bath for three days to ensure the full cured strength (Figure 35). Finally, the samples were air-dried and the ends were sanded flat before any measurements were taken. Samples were made and tested in collaboration with Leah Nation from materials engineering and Timothy Cooke from the Building Technology program at MIT.

Figure 35. Samples of cast foamed cement used in compression testing.

Table 1. Details of the cement foam samples made using varying amounts of aluminum powder.

	Sample group a)	Sample group b)	Sample group c)	Sample group d)	Sample group e)
Total dry mix weight (kg)	10.00	7.53	7.53	7.53	7.53
Type III Portland Cement (kg)	10.00	7.00	7.00	7.00	7.00
Slaked Lime (kg)	0.00	0.53	0.53	0.53	0.53
Fine Aluminum Powder (g)	0.00	3.00	6.00	9.00	12.00
Ratio of Aluminum powder to dry mix (g/kg)	0.00	0.40	0.80	1.20	1.60

Density measurements were taken by recording the weight and dimensions of each sample. Porosity and pore size measurements were made through image analysis of cross-sections cut from representative samples for each group. The software analysis program ImageJ was used to threshold the image and perform a particle analysis to determine the dimensions of each pore recognized by the software (Rasband, 2011). Standard uniaxial ASTM compression samples were conducted for each set of samples. All foam samples (sample groups b – e) were tested in compression to failure using a 10,000 lb-capacity Instron Model 1321. Testing was conducted with a displacement rate of 0.5mm/min. The fully dense cement samples required the use of a 100,000 lb-capacity Instron machine and tests were conducted at a displacement rate of 0.05mm/min. The compressive strengths were determined by dividing the maximum load by the area.

To qualitatively investigate how cement foams with functional density gradients could be produced, two methods were explored. First, samples were made using segmented moulds with barriers that could be removed after the cement foams had been poured. Cement mixes containing varying amounts of aluminum powder were poured into the different sections and the barriers were then removed to allow the sections to coalesce

and diffuse to create a blended gradient. Both linearly and radially graded density samples were produced in this manner. As these were qualitative investigations, fly ash was used as an aggregate to produce concrete foams that are more economical and practical than cement foams.

The use of gravity was another method of production that was explored, which was suggested by Timothy Cooke. Cement mix with aluminum powder was poured in a tall vertical mould to determine the effects of the pressure gradient generated by gravity on the porosity of the sample. The spatial pore size distribution of the gravity-produced sample was analyzed using the image processing technique mentioned earlier.

Results

All samples containing aluminum powder (sample groups b – e) showed foamed structures, seen in Figure 36. Conducting image analysis of the pore structure, as detailed in Figure 37, yielded the average pore size and porosity values reported in Table 2 and Figure 38. Porosity measurements agreed well with density measurements calculated through traditional mass and volume measurement.

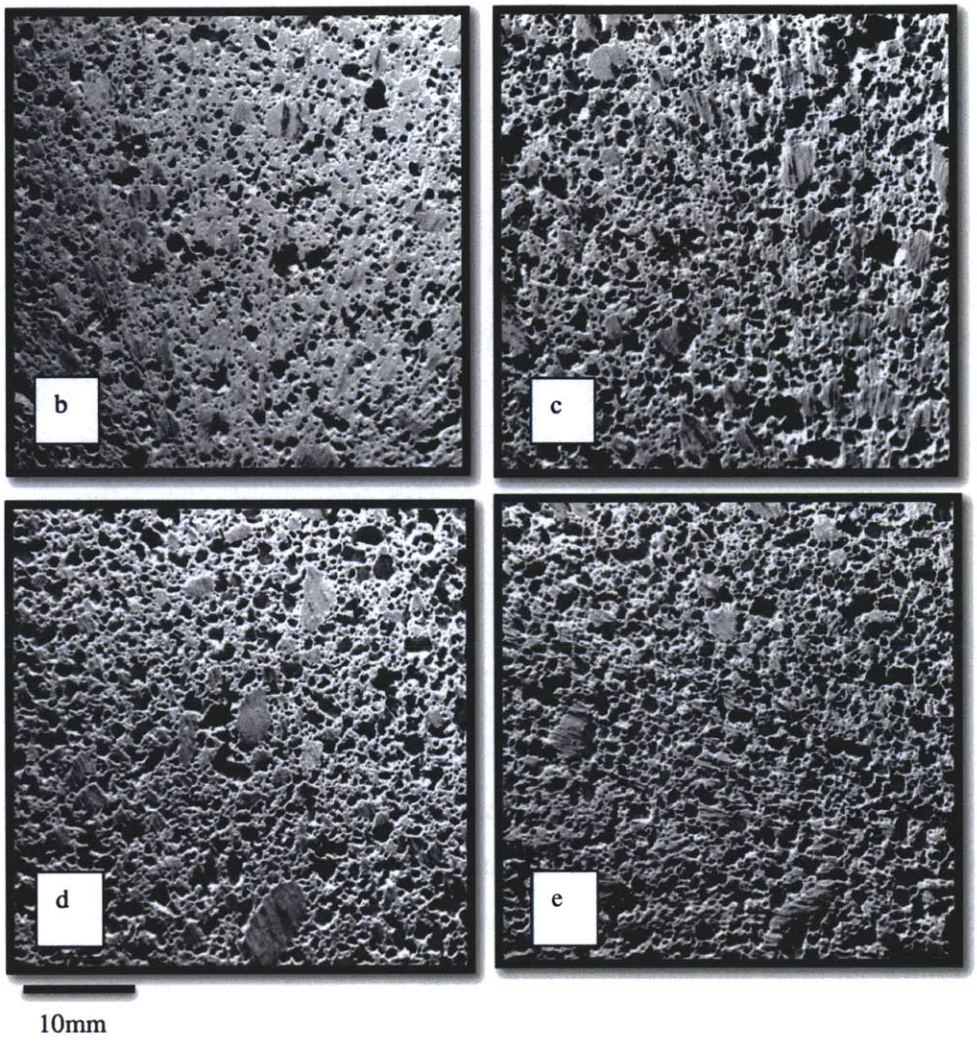

Figure 36. Images of the foam microstructure for each sample group. Sample group a) is omitted as it is the fully dense cement and does not show any macroscopic porosity. As expected due to the increasing aluminum/lime ratios, the porosity increases from samples b) through e).

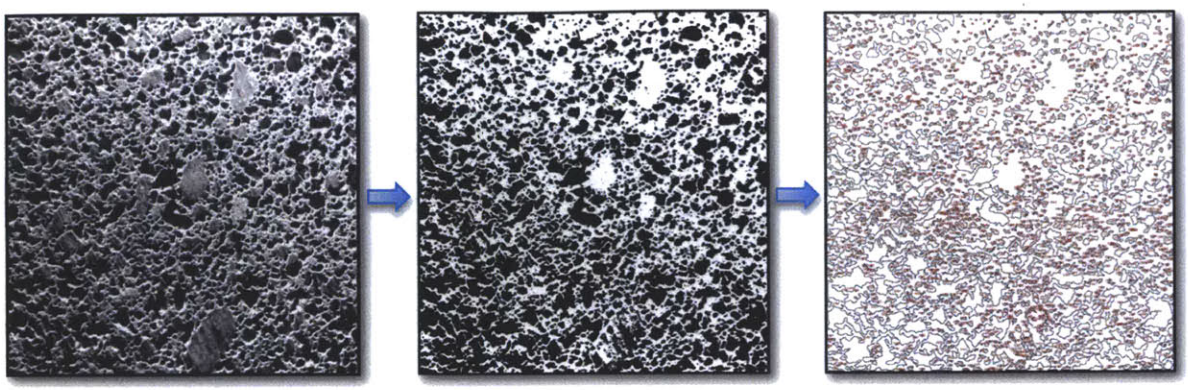

Figure 37. The pore size analysis was done using image analysis software (ImageJ). An image from sample group d (left) is first thresholded to create a binary image (middle). A particle analysis (left) gives the sizes and distribution of pores.

Table 2. Porosity and density results from both weight measurements and image analysis of pore structure.

Sample group	Ratio of Aluminum Powder to Dry Mix (g/kg)	Average Density (kg/m^3)	Relative Density (weight measurement)	Relative density (Pore size visual analysis)	Average Pore Size (mm)
a	0.0	1905.4	1.000	1.000	0.000
b	0.4	1367.3	0.718	0.703	0.265
c	0.8	1220.1	0.640	0.661	0.373
d	1.2	1133.8	0.595	0.592	0.441
e	1.6	1208.3	0.634	0.602	0.480

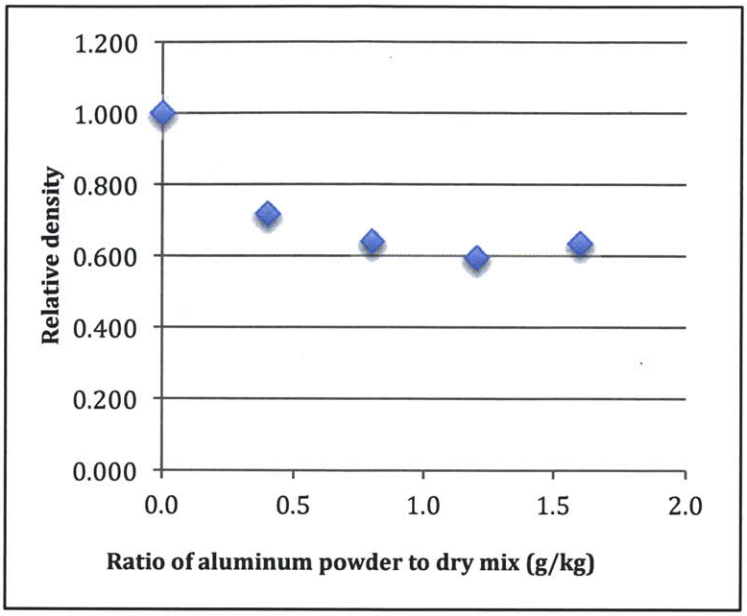

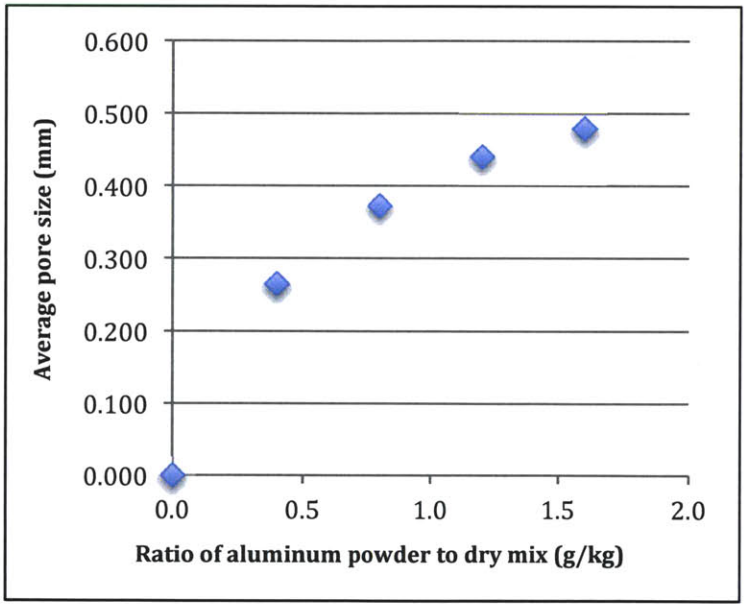

Figure 38. The porosity is dependent on the ratio of aluminum power to dry cement mix and the relations are seen in the density change (top) and the average pore size (bottom).

The samples were tested in compression to failure (Figure 39) and the average compressive strength for each sample group is shown in Figure 40. These data strongly agree with the exponential ceramic strength equation, with q = 5.4.

Figure 39. Instron setup (left) and a sample after compression testing (left).

Using the strength relation found in the experiment and standard beam theory equations, a solid cylindrical beam was compared to a cylindrical beam with a radial density gradient. The optimal distribution of density was determined by setting the tensile strength to the calculated bending stress at a given radial location, based on a consistent bending load. The tensile strength of the cement foam was approximated as 15% of the compressive strength. Keeping the diameter constant between the two cylinders, the calculations show that a 9% difference in mass exists between the solid and graded structure, with both structures loaded to the same maximum bending load. To use real numbers in the calculation, take, for example, a simply supported 0.3 m diameter cylinder of 2 m length, with a 4000 kg point load in the middle. The optimal radial density gradient for this configuration is shown in Figure 41. To ensure that the shear stress in the graded structure does not cause failure, the shear stress distribution was also calculated (see Figure 41) and the maximum shear stress falls far below the predicted shear strength. The predicted shear stress of the foams is found by taking ~0.6 of the modulus of rupture of the cement foam, as found by Toyan (1991).

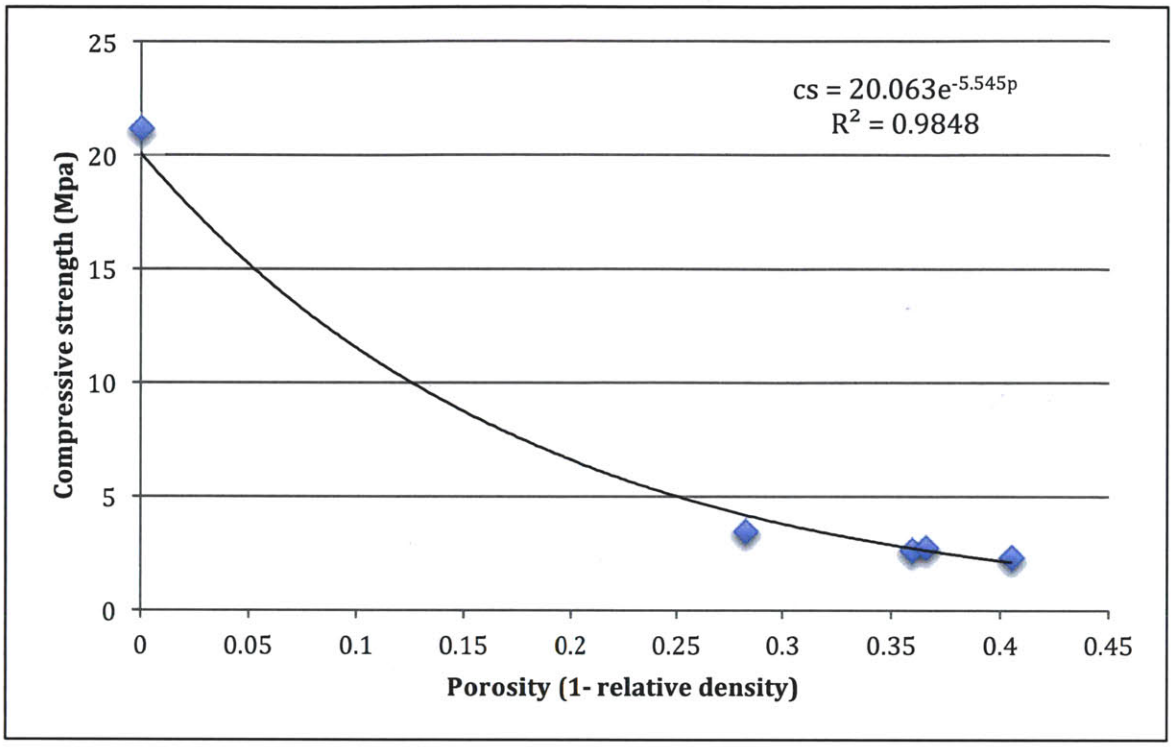

Figure 40. Compressive strength vs porosity. The data is well represented by the ceramic strength relationship, with the q constant = 5.545 as seen in the fitted equation and corresponding R^2 value.

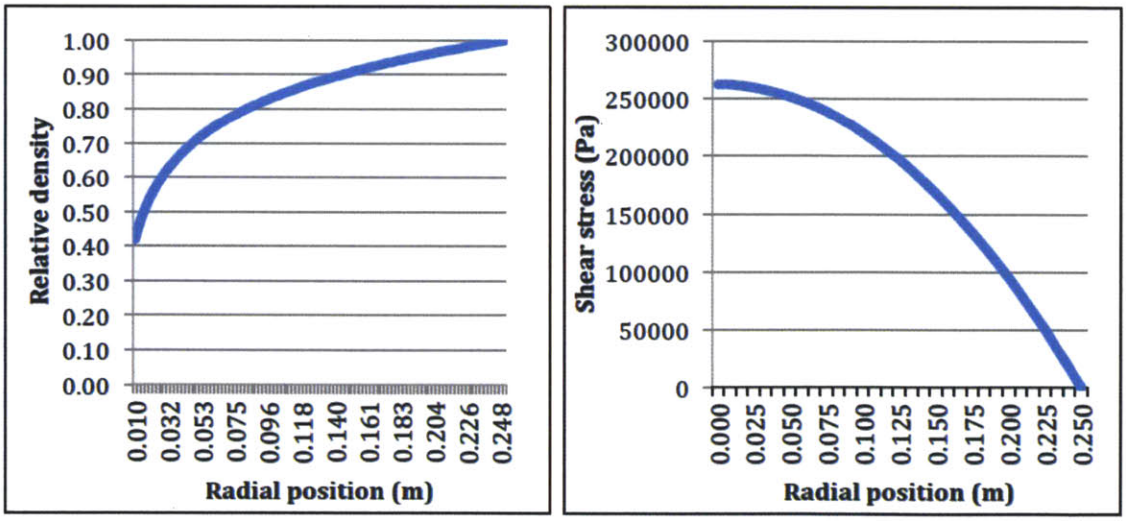

Figure 41. The optimal density distribution for a simply supported 0.3m diameter beam under a 4000 kg point load is shown on the left (a). The corresponding shear stress distribution on the left (b) falls below the predicted shear strength, meaning that the beam will fail due to bending stress.

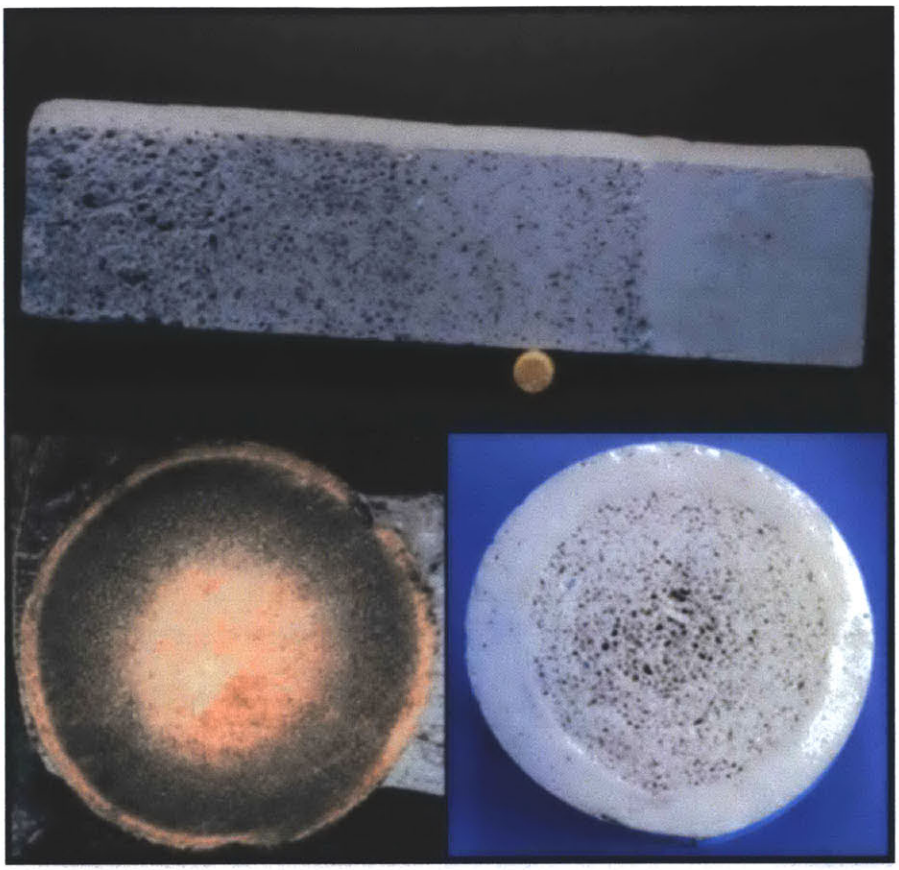

Figure 42. Samples with density gradients were made using moulds with segmented regions. A linearly-graded sample (top) was made with four distinct regions of density and the resulting density gradient is visually demonstrated by the sample's center of gravity. A radially graded sample was also produced (bottom right) which shares a similar structure to the natural density gradients found in palm trees (bottom right). Samples produced in collaboration with Leah Nation and Timothy Cooke. Palm tree image source: Food and Agriculture Organization of the United Nations

The two methods explored for producing density gradients in a monolithic piece both produced successful test samples. The segmented moulding technique was used to make both linear and radial gradients, as seen in Figure 42. The distinct regions of different densities can be seen in both samples, but the radial sample showed a smoother transition between regions compared to the linear sample. The vertical mould which tested effect of gravity produced a density gradient, though not as distinct as the segmented sample (Figure 43). The gravity-produced gradient was quantified through image analysis and the porosity as a function of axial position shows a density gradient that is rough and covers a small range of porosities (Figure 44).

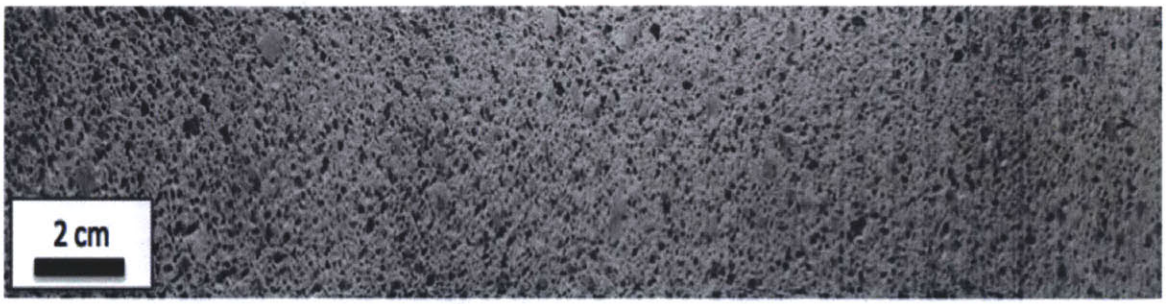

Figure 43. The foam sample with a gravity-dependent porosity gradient. Note that the left end of this image was at the top of the vertical pour. Sample produced in collaboration with Timothy Cooke.

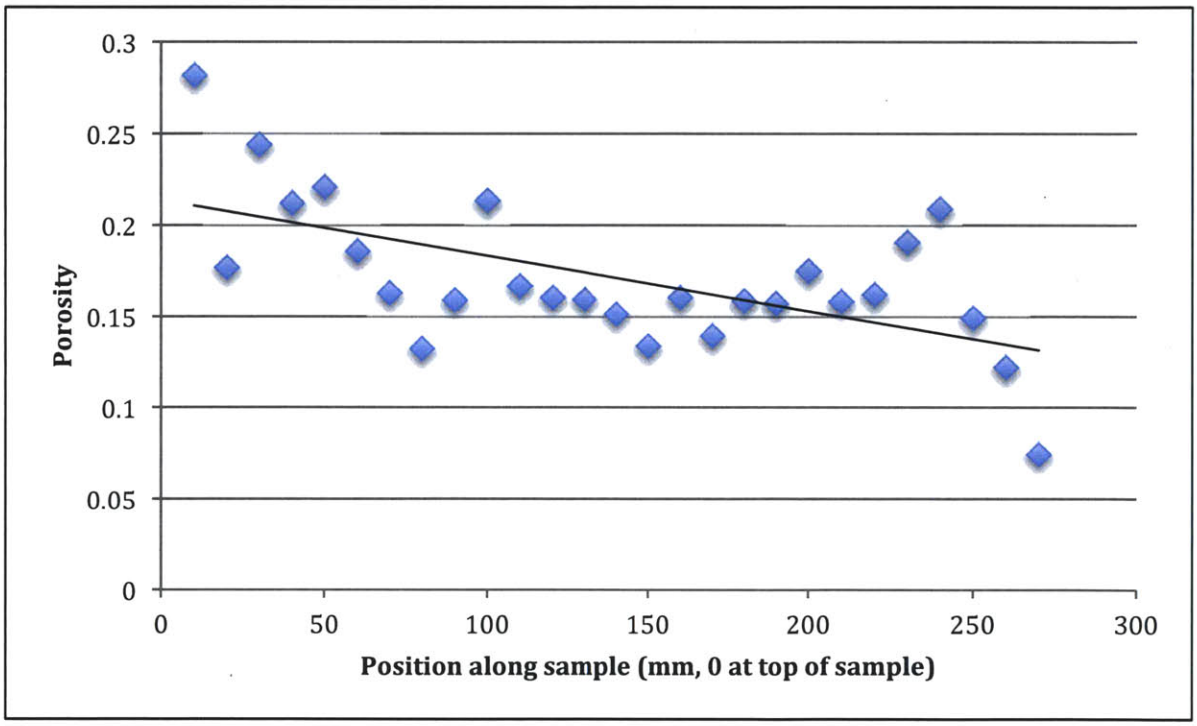

Figure 44. The porosity as a function of axial position for the gravity-dependent porosity gradient sample as determined using image analysis.

Discussion of Chemically Foamed Cement Tests

Component mixtures and resulting porosity

As expected, the results show that cement foam porosity can be controlled by the ratio of aluminum powder to dry cement mix. With increased amounts of aluminum powder, more hydrogen gas is produced, causing the porosity to increase in the final structure. This non-linear relationship is clearly seen in Figure 38. The data suggest that an optimal amount of aluminum can be added to increase the porosity, and if this amount is exceeded, the porosity will actually decrease from the optimum result. In this foam experiment, 1.2 g/kg of aluminum powder to dry mix produced the lowest density foam. Exceeding this value reduced the porosity, but continued the trend of increasing the average pore size. This behavior can be explained by the surface tension of the gas bubbles during the foaming process. If excess aluminum powder is added, the amount of hydrogen gas causes the bubbles to break, collapse, and coalesce during the foaming process. This theory explains the reduction in porosity past a certain amount of aluminum powder, whereas average pore size continues to increase with added aluminum. Looking at the average pore size, the data seems to fit a quadratic curve, which suggests that a peak average pore size will result if even higher amounts of aluminum powder are used. This fits with the theory of surface tension being able to only maintain gas bubbles of a certain maximum size before collapsing or breaking due to the weight of the surrounding cement mix and buoyancy effects.

Compressive Strength

The compressive testing results strongly agree with the exponential ceramic strength model found in the literature, with a value of $q = 5.4$. This suggests that the foam models are not appropriate for high-density cement foams (foams with relative densities above 0.6) and these foams are better modeled as solid ceramics with distributed holes. This result agrees with the conclusion reached by Tonyan, where foams with high relative densities exhibited this behavior. Comparing these results to cement foams made using

the mechanical method and a protein-based foaming agent shows the similarities between the techniques. Tonyan reports a foam microstructure with pores ranging from 20 microns to 500 microns, and a q value for high-density cement foams of $q = 4.5$ (Tonyan, 1991).

Density gradients

Using the strength data obtained from the compression tests, the use of gradient structures was compared to uniform structures. In nature, structures are rarely homogeneous and instead configurations such as sandwich panels and density gradients are often seen. For example, bones are comprised of a shell of high-density cortical bone surrounding a low-density trabecular core. These structural configurations offer enhanced properties over homogenous materials and the concept can be translated to density gradients in building materials such as cement. The calculation results seen in the cylindrical beam example reveal material savings of 9%. These savings are in the material cost, the emissions produced, and the weight of the produced object. As well, the properties of cement/concrete foams can be improved by autoclave curing processes to further improve the material savings (Tonyan, 1991).

Reliably producing density gradients in cement structures poses a challenging task, though graded test samples were successfully produced with the segmented mould and gravity mould methods. The segmented mould technique offered precise control over the density and divisions between different densities, though it produces a step-wise gradient. The radial sample showed a smoother gradient, and this is likely due to the higher ratio of barrier surface area/segment volume. This ratio controls the rate of diffusion between segmented regions, which affects how smooth the gradient is between segmented pours. Using finer segmentations and having mixtures with higher water content would allow for increased diffusion to create a finer, smoother gradient.

The sample made using the gravity-dependent method showed a narrow range of porosities and the gradient was uneven at points. However, a larger range of porosities could be achieved by increasing the acceleration, for example through the use of a centrifuge. While both methods hold promise, it is noted that on-site construction techniques could not utilize these methods and they are both more suited to pre-fabricated part production. Another important note is that the concept of structural density gradients can be applied to other material systems, such as polymers or composites. Cement is not an ideal material system for structural density gradients, as the exponential strength dependence on density in ceramics results in a strong decrease in mechanical properties for foamed cement.

One important observation of the chemically foamed cement is the rise time and volume change. Like bread rising in the oven, the foamed cement samples demonstrated large volumetric expansions in a period of around five to ten minutes after the aluminum was added. During this period, the wet foam was very fragile and any disturbance popped the cell structures. This fragile expansion period is an important consideration for additive manufacturing, where layer size and strength are crucial parameters.

Conclusions of Mechanical Tests on Chemically Foamed Cement

These experiments have shown that cement foam porosity can be controlled by the ratio of aluminum powder to dry cement mix. Average pore size increases with the proportion of aluminum in the mixture, and porosity increases in the same manner until it reaches an optimum. This can be explained by surface tension in the gas bubbles during the foaming process. Surface tension prohibits gas bubbles from growing after reaching a maximum size, causing them to collapse or break due to the weight of the surrounding cement mix and buoyancy effects. The maximum porosity achieved was 40% using a weight ratio of 1.2 g/kg aluminum to dry cement mix.

The compression results strongly agree with the exponential ceramic strength model, as suggested in previous research. Thus the ceramic model should be used instead of the foam model to describe cement foams produced using aluminum powder. Finally, the implications of radial density gradients in concrete foams were explored. Through theoretical calculations of a cylinder under bending stress, a graded beam can have 9% less mass than a solid cylindrical beam of the same dimensions and support the same load. These numbers could be increased through the use of autoclave curing, which would increase the mechanical properties of the cured foam.

The qualitative observations from the production of the chemically foamed cement samples include the required rise time for foam expansion, the fragility of the wet foam, and the low viscosity of the mixture. These parameters do not bode well for direct extrusion in an additive process due to the need for low slump, layer consistency, and material robustness.

Mechanically Foamed Cement

Based on the results of the chemically foamed cement tests and analysis, the concept of radial density gradients was further investigated using mechanically foamed cement. The compression testing and stress analysis of the chemically foamed cement was promising, though the observations of low viscosity, rise time, and wet cell fragility of the cement mix did not bode well for 3D printing applications. Mechanically foamed cement, where a protein agent is foamed and mixed with cement, was investigated to determine if its properties are more suitable for additive manufacturing.

Methods

Several commercial cement foam products exist and are used for home insulation purposes. Experiments conducted in this work used a cellular concrete product made by Elastizell (Elastizell, 1998). The process to make foam cement begins by pre-foaming a

liquid protein agent using a compressed air source and foam generator system. By adjusting the ratio of concentrate protein agent to water and the pressure of the compressed air, the foam density and cell size can be manipulated. Once the foam is made, it can be mixed with cement and water to produce cement foam. The ratio of foam to cement during the mixing process determines the final density, which can be varied between 20 to 120 lbs per cubic foot (Elastizell, 1998). Sand and other aggregates can be added to the cement foam to produce concrete foams, though cement foams were studied here to reduce the number of variables.

Initial test production of mechanically foamed cement was conducted using Elastizell's JLE Concentrate diluted with water in a 1:40 ratio. This was foamed using Elastizell's smallest foam pump unit with a connected air source at 100 PSI (Figures 45 and 46). The foamed protein agent was mixed with Type 3 Portland Cement in various ratios and different water mixtures to qualitatively evaluate the pour properties like viscosity and robustness of the wet foam cells.

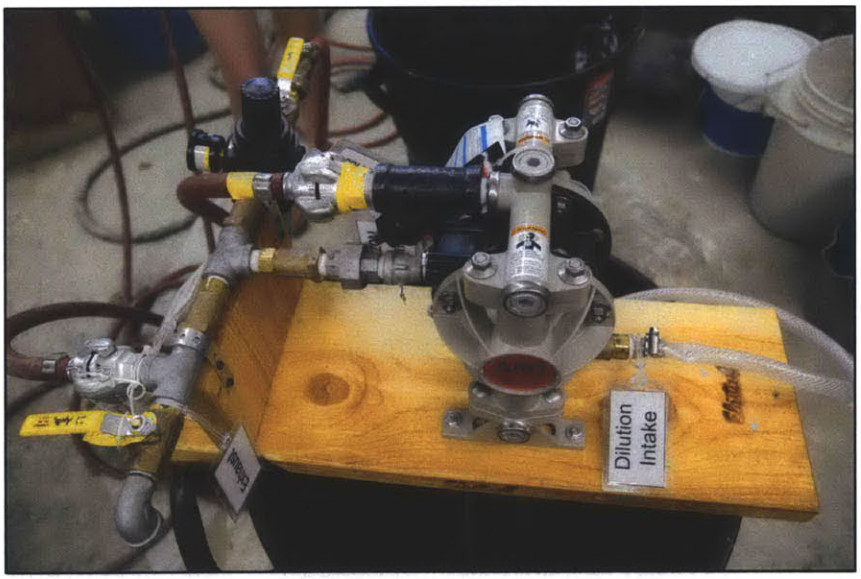

Figure 45. The foam generation unit from Elastizell used to aerate the liquid protein foaming agent.

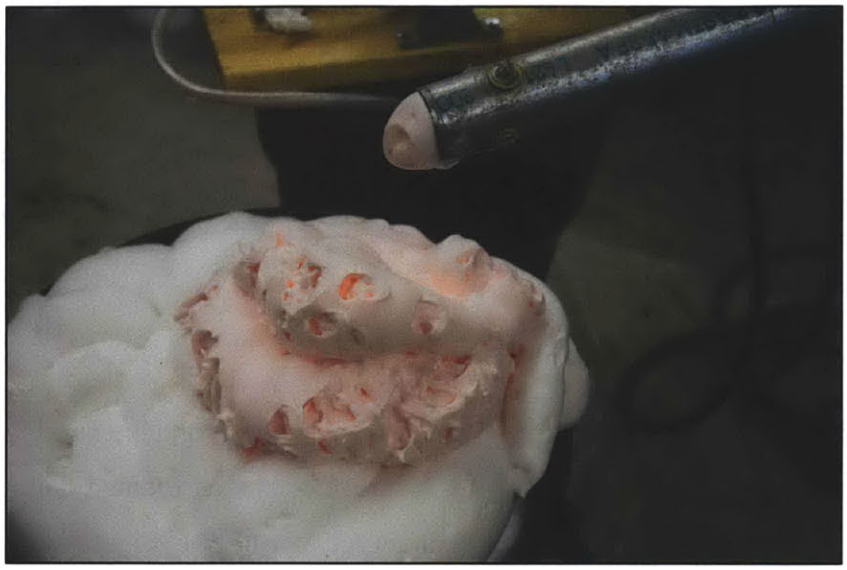

Figure 46. Foam produced by the foam generator is of a similar consistency to shaving cream. Here, the pink foam was produced by adding a food colouring dye to the liquid foaming agent to check the rate of uptake.

Results and discussion

The mechanically foamed cement samples proved much easier to work with and control than the chemically foamed cement samples. Due to the mechanical aeration of the protein foaming agent, there is no volumetric change that occurs after the cement foam is mixed, unlike the chemical foam that has a significant rise period. The foam cell structure was much more consistent and of fine structure than the chemically foamed sample and the density was easily controlled with the ratio of foam. As opposed to the chemically foamed sample, where very subtle differences of aluminum powder would drastically affect the density, the mechanically foamed cement was easier to control. Samples were produced across the spectrum of densities, with some samples even able to float on water (Figure 47).

Figure 47. The mechanically foamed cement was able to be produced at densities lower than water, allowing samples to float.

The viscosity of the mechanically foamed cement mix was still found to be very low, which indicates problems for 3D printing. To achieve higher viscosities, a plasticizer was added to reduce the water content. The effect of the plasticizer was dramatic in reducing the need for water, though the mixture still displayed very low viscosities needed to maintain the cellular structure. With the differences and properties of chemically and mechanically foamed cement in mind, a 3D printer extruder system was designed and explored.

Foam Generator

The foam generator supplied by Elastizell (seen in Figure 45) produced foam at a very high rate and was far in excess of the flow rate required for the envision 3D print system. In addition to flow rate, the generator was large, heavy, and required two people to move. To enable 3D print tests, a much small foam generator was designed and prototyped to serve the low flow rate requirement. The foam generator was built using standard brass plumbing fixtures and a foaming nozzle. The design used a high-pressure air line and a

pressurized liquid protein agent line. The liquid was pressurized using a standard painter's tank typically used for compressed air spray painting (Figure 48). The air and liquid were forced through the foaming nozzle, which consisted of a tube packed with steel wool to foam the liquid mixture (Figure 49). The design was inspired by reverse engineering the larger Elastizell foam generator and performed quite well in testing. The size was significantly reduced and the flow rate was controlled by a ball valve on the pressure line.

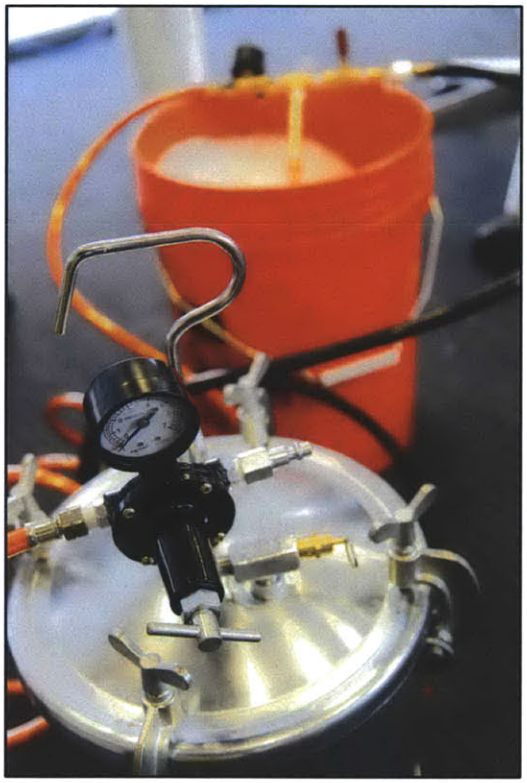

Figure 48. The smaller foam generation unit developed for 3D printing purposes is much more compact. The mixing unit is seen in the background and in the foreground a pressurized tank of liquid foaming agent is seen.

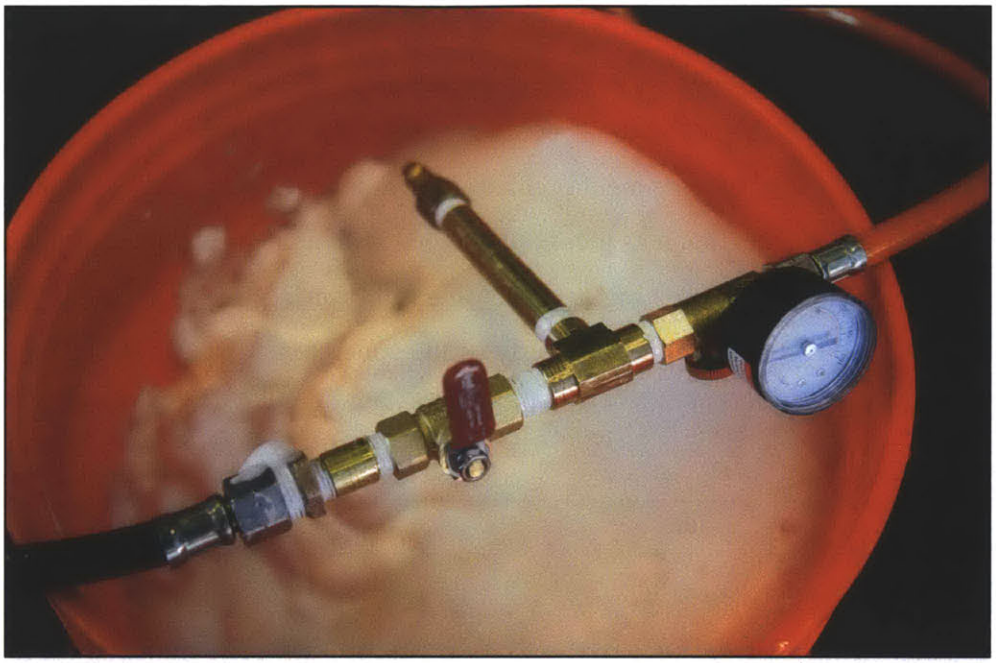

Figure 49. The smaller foam generation unit developed for 3D printing uses a nozzle filled with steel wool to act as nucleation sites for aerating the protein foaming agent.

3D Printing Functionally Graded Cement

Currently, two main groups in the literature have developed additive manufacturing techniques using concrete: Contour Crafting and Concrete Printing. They are two separate 3D printing projects that use direct extrusion of concrete to create layered objects (Khoshnevis, 2004) (Lim, Buswell, Le, Austin, Gibb, & Thorpe, 2012). These groups both use a gantry-style delivery system and direct extrusion of a special cement-based material to print large objects. These groups have pushed the boundaries of 3D printing to large-scale objects, however they are still constrained to a single material.

The concept of functionally graded 3D printing would enable a whole new realm of integrated possibilities. Looking at the concrete example, functional gradients could improve strength, reduce structural weight, and open new design possibilities. Density is the obvious property to vary, due to the ability to reduce material weight and cost as demonstrated by the theoretical analysis in earlier sections. However, many other

properties of concrete can be spatially varied in a monolithic structure. Properties like aggregate density, colour, and even aggregate type (Figure 50). By being able to control these gradients, monolithic structures could be designed specifically for a given load distribution or any other environmental constraint. This allows for local optimization of many different parameters, such as a concrete bench with a cheaper bulk aggregate and a more expensive, visually interesting aggregate near the surface for finishing. Taking the example of colour, if the colour is a property of the concrete, rather than a surface coat of paint, then the structure has an inherent colour scheme immune to weathering.

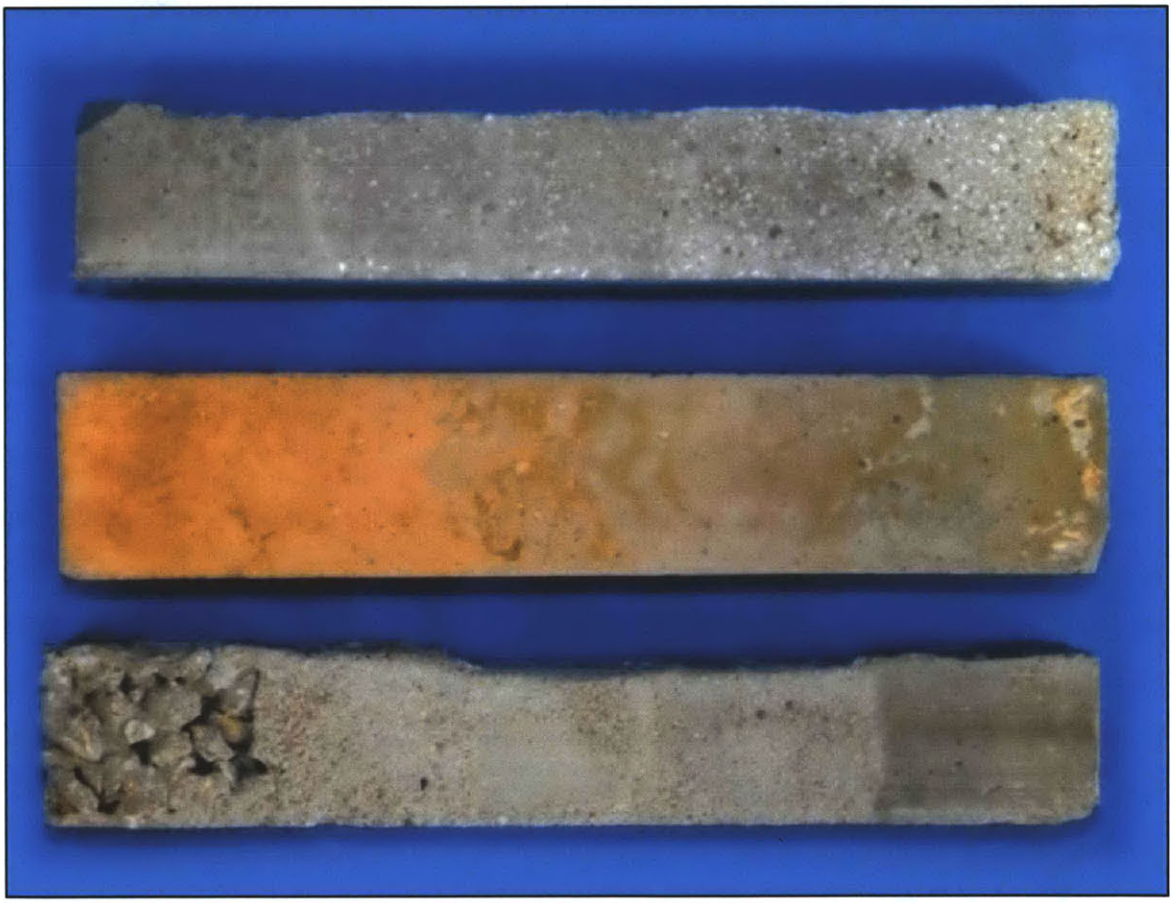

Figure 50. Many different material properties can be spatially varied in a monolithic concrete structure, such as aggregate ratio (top), colour (middle), and aggregate type (bottom).

Direct Extrusion

In order to reliably produce controlled density gradients of any shape, the design of direct extrusion 3D printer capable of extruding cement foam was investigated. To facilitate different densities of cement foam, different ratios of foam and cement can be mixed. Taking an input of pure foam and pure cement, a mixing chamber with controlled inputs could dynamically vary the inputs to control the density of the extrusion. This concept of dynamic mixing is analogous to mixing varying amounts of black and white paint to achieve different shades of gray.

With the concept of dynamic mixing in mind, a prototype extrusion system was developed. An extruder was designed around the concept of an Archimedes screw auger, due to the use of screw pumps for high viscosity applications like injection moulding and oil pumps. The action of the screw pump also functions as a mixer, able to dynamically mix components like foam and cement. By controlling the speed of the auger, the flow rate can be controlled.

After experimenting with several different auger bits, the use of a meat grinder was found to be ideal for the purpose. An STX Turboforce 3000 Watt electric meat grinder was used as the core of the extruder design and the core auger components are seen in Figure 51. The electric motor was powered through a speed controller to give fine control over the auger speed.

Figure 51. Auger components of the STX meat grinder used to serves as a material extruder for 3D printing tests with cement and concrete. Image source: STX International

The extruder was tested with different nozzles and the curvature of the nozzle was found to be very important due to the thixotropic nature of cement. When wet cement is put under mechanical pressure, the solid particles can jam and water is squeezed out, making the mixture stiffer. This is opposed to common Newtonian fluids, which yield under stress. Cement is often modeled as a Bingham plastic due to its suspended particles and thixotropic nature. As such, a 3D printed nozzle with continuous curvature was printed from ABS and sanded to produce a smooth interior finish to reduce material drag (Figure 52). Mounting the extruder along a test funnel hopper to the arm resulted in the test platform seen in Figure 53.

Figure 52. 3D printed ABS nozzle for extrusion tests with cement and concrete.

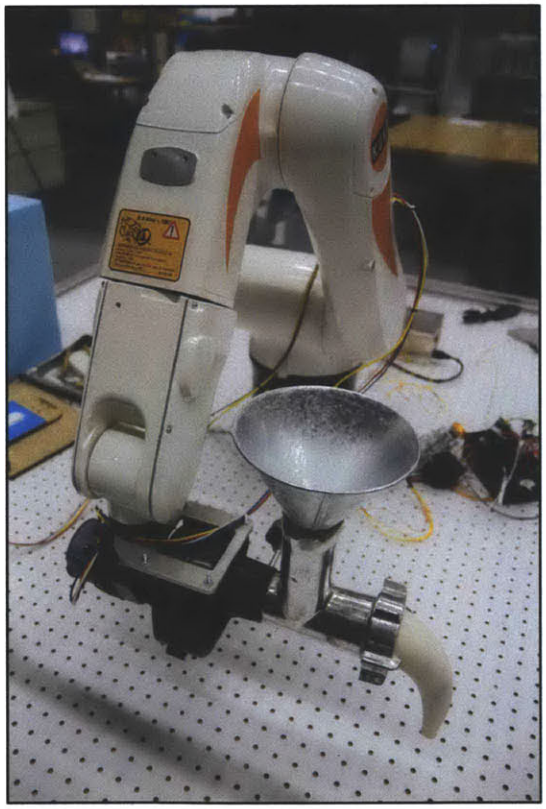

Figure 53. The material extruder attached to the robotic arm for 3D printing cement and concrete tests.

The extruder setup proved to be very robust due to the cast metal parts and heavy-duty electric motor. From cookie dough (Figure 54) to concrete (Figure 55), all types of different test mixtures were extruded to determine the extruder parameters. If the device had a problem or required cleaning, the meat grinder assembly was able to be easily detached from the electric drive and cleaned by hand.

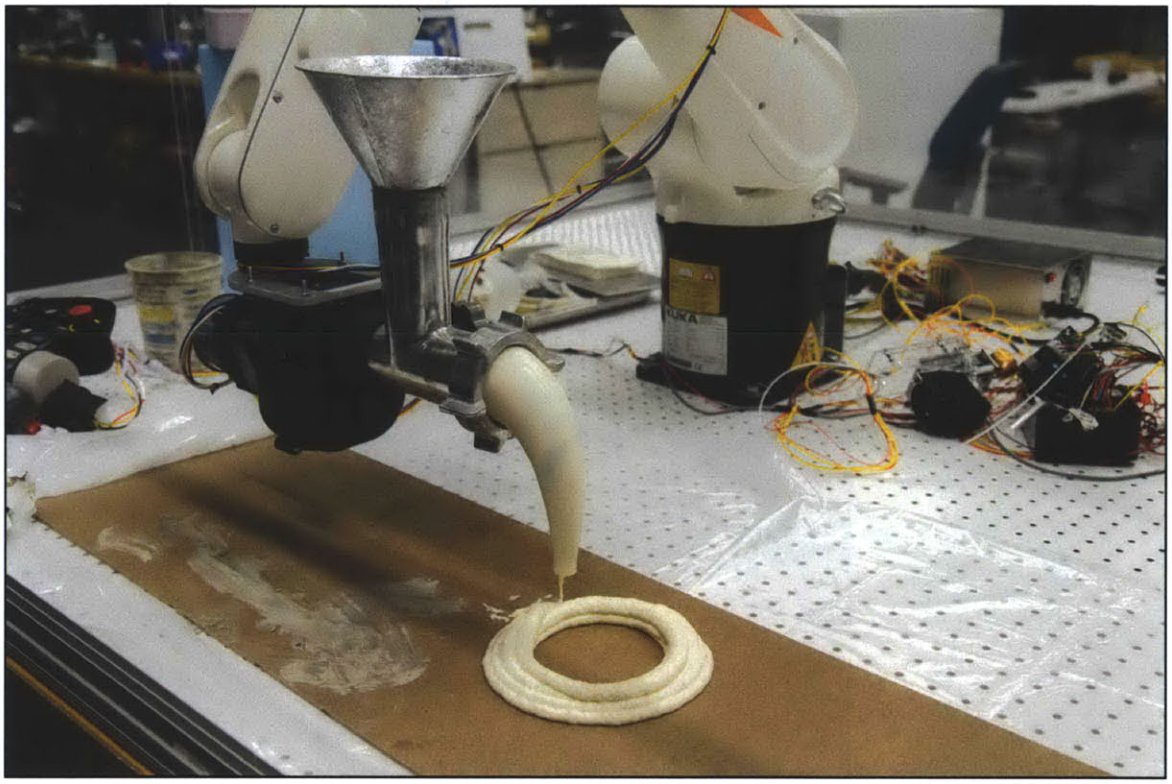

Figure 54. A material extrusion test using cookie dough to represent the texture of concrete without needing to worry about curing. The material flow rate was controllable via a speed controller attached to the motor to control the auger rotation rate.

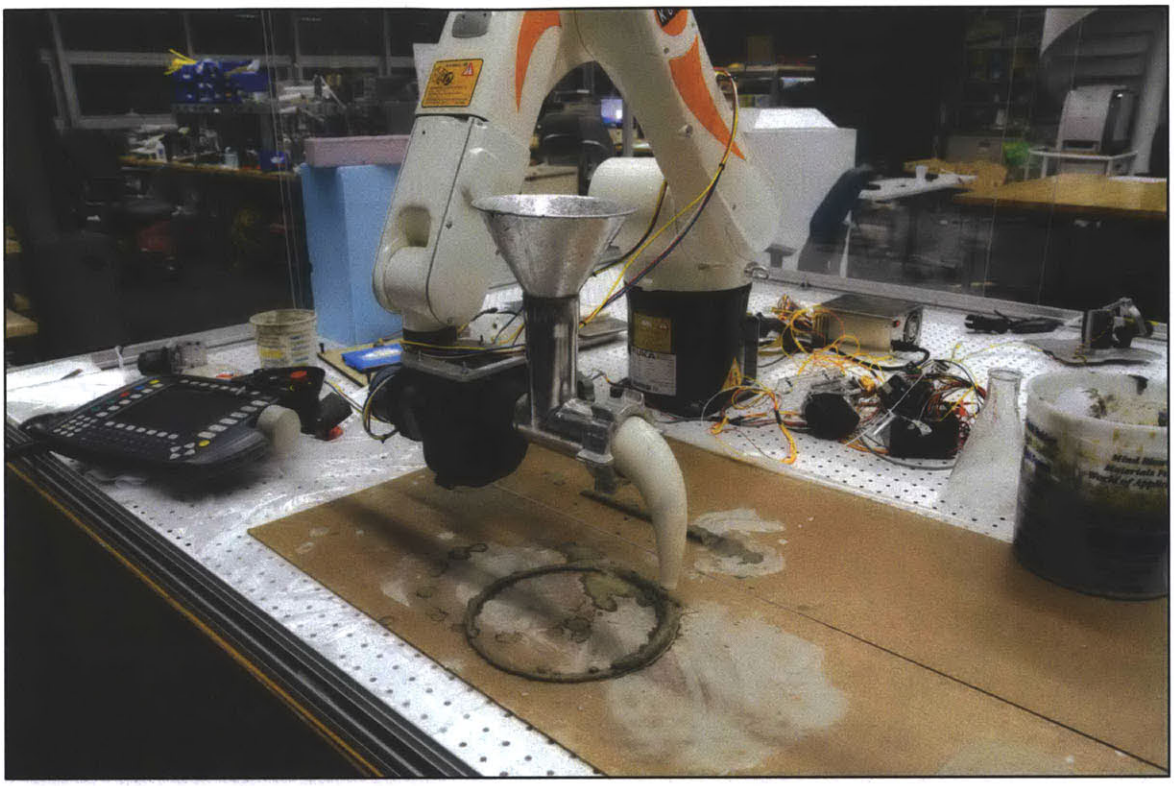

Figure 55. The material extrusion tests for cement and concrete revealed the difficult balance between viscosity, cure rate, and plug flow. As seen here, most tests started extruding for a short period of time before jamming occurred in the nozzle or auger chamber.

While the extruder was robust, able to handle a variety of material, and have a controllable flow rate, 3D printing concrete was very problematic for several reasons. All types of foam concrete were found to be too low viscosity to hold its own form once extruded. The very high slump of foam concrete is required to enable the cellular structure, but the foam concrete resulted in a liquid puddle rather than an extruded bead. This was true for both mechanical and chemically foamed cement, though mechanically foamed cement performed much better than its chemically foamed counterpart. With various fiber mixes and slump-enhancing admixes, it is conceivable that a mechanically foamed cement mixture could hold its own form during 3D printing.

However, regular cement was extruded and found to be equally problematic. Many tests were conducted and after a short while of extrusion, the nozzle or auger would jam. Upon disassembling the extruder mechanism, a solid jammed block of cement would be found

to be causing the problem (Figures 56 and 57). After experimenting with various cement mixtures, including plasticizers additives and various sand aggregates, it was determined that the system is very sensitive to the cement chemistry. Furthermore, plug flow is necessary in the system. Plug flow means that no residue is left in the system as the cement flows, as if not, over time this residue hardens and builds up. Combined with the thixotropic nature of cement, jamming and clogging occurred frequently.

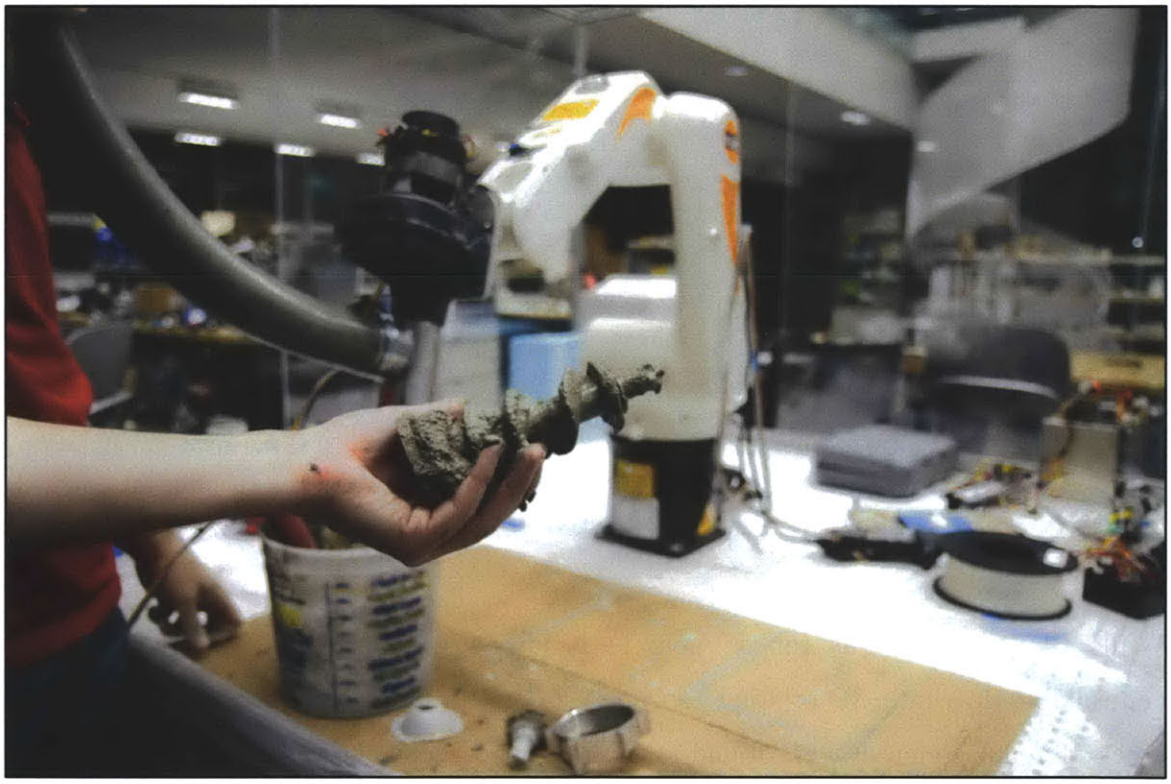

Figure 56. A jammed auger was a frequent result of extrusion tests. The thixotropic nature of cement, combined with curing properties, created jams that impeded material flow.

Figure 57. A jammed nozzle tip was a common result of the cement and concrete extrusion testing.

To determine the best cement mixture to use, Contour Crafting and Concrete Printing papers were reviewed. As both groups did not disclose their exact mixtures, the author contacted the researchers involved with the Concrete Printing project. The discussion confirmed the results and the importance of both cement chemistry and plug flow. Their Concrete Printing system took several years to refine their concrete chemistry and likewise with the Contour Crafting system. The concrete mixture used was a specialized sensitive blend with a strong balance of both being able to be pumped and extruded, and able to maintain its form upon extrusion.

From the experiments conducted and the findings of the other direct concrete printing projects, the difficulty in finding the right cement chemistry was determined to be problematic. Adding to the complexity is the notion that once the right chemistry is found, as was done in the other projects, then the properties will vary due to changing the foam ratio to control density. Changing the viscosity dynamically adds another

complicated variable to the extrusion characteristics. While potentially feasible, the practicality of such a sensitive system and the experimental time required to fine tune the chemical mixture inspired other ideas on how to achieve additive manufacturing using concrete. Instead of directly extruding concrete, several other ideas were explored including negative mould printing and print-in-place mould printing.

Dissolvable Mould Printing

Looking at other options for additive manufacturing of concrete without direct extrusion, the concept of a 3D printed mould was introduced. The tests of segmented moulds had successfully resulted in cement foam density gradients (Figure 58) from previous experiments, providing context to additively manufacture the moulds to achieve desired designs.

Figure 58. Density graded concrete samples produced using a segmented mould as described in Chapter 6.

To achieve overhang structures and complex shapes, the use of dissolvable mould printing was explored. Using a MakerBot 3D printer, polylactic acid (PLA) plastic mould structures were 3D printed. These moulds were then filled with concrete, allowed to cure,

and then immersed in hot water to dissolve away the PLA mould. This method worked quite well for small objects and the level of detail was on par with the resolution of the 3D printed mould (0.3 mm layer height). Sample produced objects made in collaboration with Sarah Han are seen in Figures 59 and 60.

The success of the prototype tests of PLA mould printing for concrete indicates that the technique could be used for an assortment of different casting materials. By printing a thin mould as a monolithic print, traditional mould problems like interior features and parting lines can be avoided. However, each printed mould can only produce a single part as the mould is dissolved away. Using a segmented printed mould and filling the different sections with different materials or blends of concrete, a graded structure could be produced. Still, the dissolvable PLA moulds are limited in scale by the size of the 3D mould printer. In terms of architectural concrete structures, dissolvable mould printing is impractical using PLA and the setup explored here due to the slow speed, material cost, and scaling problems. For larger structures, a different mould printing technique was developed, termed *Print-in-Place* construction.

Figure 59. A concrete object produced using a dissolvable PLA mould which was 3D printed. The resolution is similar to the resolution of the 3D printed mould, which was printed with a layer height of 0.3 mm.

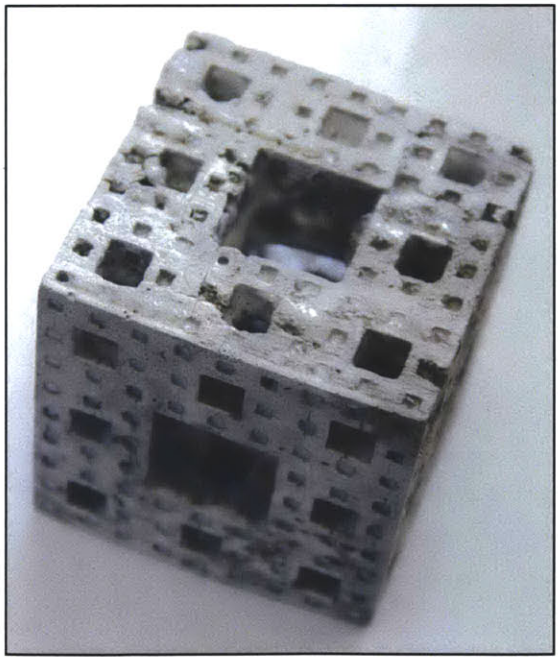

Figure 60. A concrete model of a Mernger-Sierpinski cube produced using a dissolvable PLA 3D printed mould. For scale, the cube is approximately 3 inches tall.

Print-in-Place Mould Printing

To achieve the enormous scale required for architectural additive manufacturing, a mould printing system was developed where the mould is left in place after casting. Termed *Print-in-Place* construction, the idea involves 3D printing foam moulds for concrete walls where the foam moulds are left in place to serve as thermal insulation. This concept is similar to using insulated concrete forms, which is a widely used construction method, but the forms are printed in place as opposed to manually assembled. The concept eliminates many of the problems encountered with direct concrete extrusion, such as jamming concerns, cure time, layer adhesion, material flow, weight, and robustness. By 3D printing a mould, the concrete can be cast as a monolithic structure and elements can be placed inside the mould to enable integrated functionality. The resolution of the process can also be easily fine tuned, as the foam can be finished using subtractive processes like milling to perfect the mould before casting. Finally, the process is mould-based, meaning it is not inherently linked to a single type of building material. Any castable structural material, ranging from plastic wood composites to biological-based growth media, could be used inside the mould.

This concept was born out of the original concrete 3D printing work and was pursued as a separate project due to its success and promise. The Chapter 7 details the Print-in-Place construction-scale additive manufacturing work.

Conclusions

Using a robotic arm platform, a functionally graded cement 3D printer system was investigated. The potential structural benefits of weight reduction and improved material efficiency using radial density gradients in cement column structures was shown through analysis using experimental test data. Segmented moulds were used to produce cement foam samples with radial density gradients. As well, gravity can be used to produce reliable density gradients as well.

Both chemically foamed cement and mechanically foamed cement was tested for applicability in 3D printing and found to have insufficient viscosity for use in direct extrusion. A 3D printing test platform was prototyped using the robotic arm system and samples of cement and other materials were tested using direct extrusion. Difficulties with jammed nozzles and with plug flow resulted in new directions for additive cement and concrete manufacturing other than direct extrusion.

Dissolvable moulds and print-in-place moulds were two developed methods that produced strong results for the creation of 3D printed cement structures. The interior features and resolution of the dissolvable mould make it a good candidate for producing complex, small objects out of ceramic materials. The print-in-place method holds promise for additively manufacturing architectural scale structures like buildings and will be further discussed in the next chapter.

Chapter 7: Construction-Scale Digital Fabrication

"The time will most certainly come when whole houses will be turned out in one piece."

— Biography of Thomas Edison

Introduction

3D printing has grown significantly in the last decade and the number of applications for it are ever widening. However, 3D printing has so far been limited to a small printing space, with the typical 3D printer only able to produce objects smaller than a few square feet. This size limitation is primarily due to the difficulty of making a large machine (to print a building, a printer larger than a building is required), printing time (small objects often take up to a day to print), and material limitations (cure mechanisms and stability). Robotic arms are well suited to large-scale printing due to the significant reach, small physical footprint, and the range of motion required for multi-axis printing and pick-and-place operations.

Work discussed in the previous chapter examined concrete printing, which is inherently suited for large-scale manufacturing such as walls and buildings. However, efforts to directly print concrete resulted in difficulties due to the material properties of concrete. In this chapter, a new technique was created to avoid direct extrusion of concrete but still produce additively constructed large structures.

As oppose to directly extruding concrete, a mould can be printed in which concrete (or any other structural material) can be cast. The method, termed Print-in-Place Construction, uses quick-curing materials that serve a dual purpose: as a mould for cast structural materials and as thermal insulation. In this sense, the construction system is similar to insulated concrete forms (ICFs), which are assembled moulds that are left in place as insulation.

To construct a building, the CAD design of the structure is programmed into the mould extrusion machine. This machine (which could take several forms, such as a robotic arm, a gantry system, or mobile robotic agents) then prints mould structures for all of the wall components of the building. The printed material is a lightweight, strong, and fast-curing material, which enables rapid construction at great heights. Expanded polyurethane foam was utilized for this experimental proof-of-concept. Once the wall moulds are printed in a successive layered fashion, a structure filler material (such as concrete) is poured into the wall moulds and allowed to set. The printed moulds then act as an insulative layer for the wall, eliminating the need for additional insulation. With the structure complete, a weatherproofing coating can be applied to the external surface of the building and the interior can be fitted with drywall to create a finished building. More complex operations can also be automated in this process, such as addition of embedded objects (rebar, electrical wiring, plumbing, etc.) to the printed moulds before the filler material is added.

This novel method provides a means of rapid construction of custom structures (the estimated construction time for a house structure is well under a day). The cost of construction is radically reduced in comparison to traditional construction methods due to the efficiency of application, the lack of waste materials, and the reduction in labour. The cost of construction is minimized to the raw material stock and the machine's operational cost (electricity and maintenance).

History of Construction Automation

Ever since Henry Ford's automobile assembly line, inventors and thinkers have proposed different ways to automate large-scale construction techniques. Residential construction is a difficult task to automate, due to the scale, one-off designs, and varying environmental conditions and requirements. The first significant attempt occurred in 1917 with Thomas Edison's patent on single-pour concrete housing (Edison, 1917; American Heritage, 1980). Edison proposed a novel system where a large single reusable

metal mould could be used to cast concrete houses, including furniture, indoor accessories, and even pianos all made with concrete! His motivation was to provide extremely low cost housing through applying mass manufacturing to residential housing. Several houses were poured as seen in Figure 61 and are still standing today. However, the prototype moulds proved to be far too complex with expensive moulds consisting of over 2,300 pieces and the project became a well-documented failure.

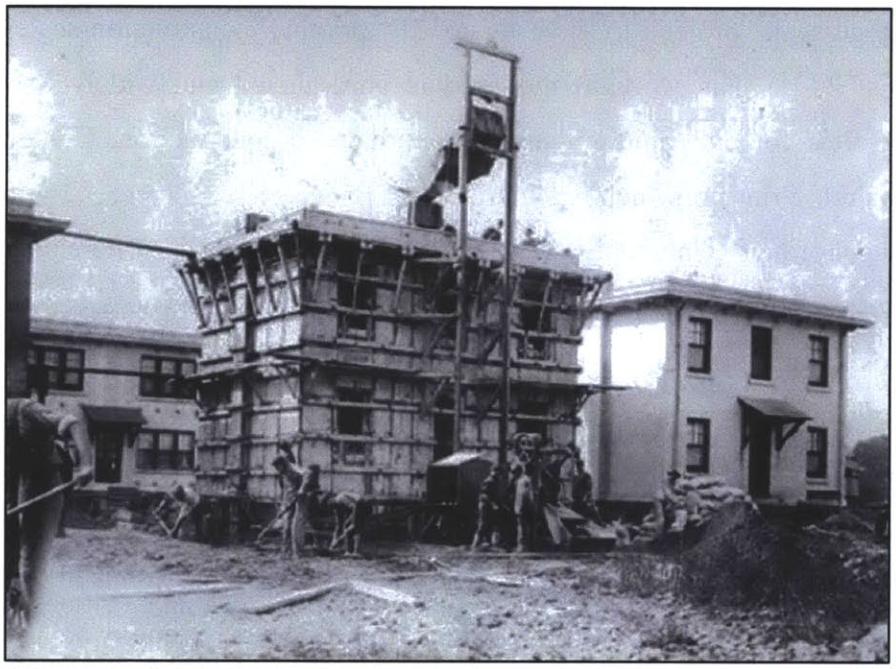

Figure 61. Edison's single-pour housing construction used a reusable metal mould. Image source: Wikimedia Commons

In the 1980's, Japanese companies developed large-scale construction automation systems to reduce the amount of human labour required. These systems included hundreds of tele-operated robotic devices ranging from excavators to assemblers to floor trowelling machines (Taylor, Wamuziri, & Smith, 2003). The development of these automated systems was a technical success, though the cost and the difficulties of an unconstrained environment reduced their impact (Bechthold, The Return of the Future: A Second Go at Robotic Construction, 2010).

Current research efforts into large-scale 3D printing have resulted in several projects such as Contour Crafting, 3D Concrete Printing, and D.Shape (Khoshnevis, 2004; Lim, Buswell, Le, Austin, Gibb, & Thorpe, 2012; Dini, 2009). While these projects have successfully printed large objects, transitioning to full building-scale structures has yet to be proven and several inherent challenges exist in their methodologies.

Contour Crafting, a process developed by Bohrokh Khoshnevis in the early 2000's, was the first large-scale project to investigate 3D printing construction-scale structures (Khoshnevis, 2004). His work in the field is unparalleled and widely known in the architecture field for his paradigm-shifting approach to construction. Contour Crafting and 3D Concrete Printing, which is a more recent project into concrete 3D printing based out of Loughborough University, both use a similar approach whereby concrete is extruded from a moving nozzle to generate layered structures. The nozzle is moved using a gantry positioning system in the XYZ space. Both projects have produced wall-like elements several feet long (Figures 62 and 63). The main concern for the scalability of these projects is related to the direct printing of concrete. The extruded concrete must be a very precisely controlled chemical mixture to obtained the required slump and cure time. As concrete is thixotropic and cures with time, precise extrusion is difficult and any pause of the machine would requires nozzle cleaning. The cure time is another problem, as the concrete needs to cure quickly, but not too quickly, in order to prevent it from hardening inside the print hopper before extrusion. The result is that each printed layer requires significant time to cure before printing the successive layer. Finally, direct printing of concrete is difficult due to the weight of concrete. The print head must be rigid enough to support the weight of the extruded concrete, which is becoming challenging with large scales and spans.

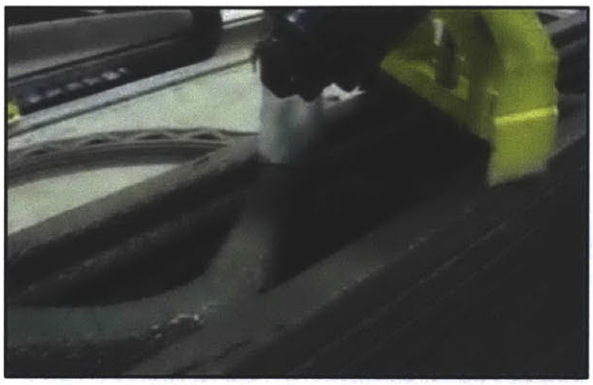

Figure 62. The Contour Crafting project uses a direct extrusion process combined with a trowelling process to additively create large concrete structures, like the wall seen here. Image source: Contour Crafting, University of Southern California

Figure 63. The 3D Concrete Printing project uses a direct extrusion process similar to Contour Crafting, but with a finer resolution. Image source: Freeform Construction, Loughborough University

D.Shape takes a different approach, where a powdered stone material is spread over a volume and small amounts of liquid binder are selectively deposited from an array of nozzles. After each binder deposition, a new layer of powdered material is spread over the surface and the process is repeated (Figure 64). To remove the structure, the excess powder must be removed. This approach allows for true 3D structures, unlike the 2.5D geometry of Contour Crafting and Concrete Printing, due to the unused powder acting as support material. This process also has the highest resolution of the three methods and has produced large-scale, complex structures (Figure 65). However, D.Shape is significant limited by the large volumes of material required as the process scales up.

Printing a building with this method would require a building full of powder that would subsequently demand enormous support systems and removal processes.

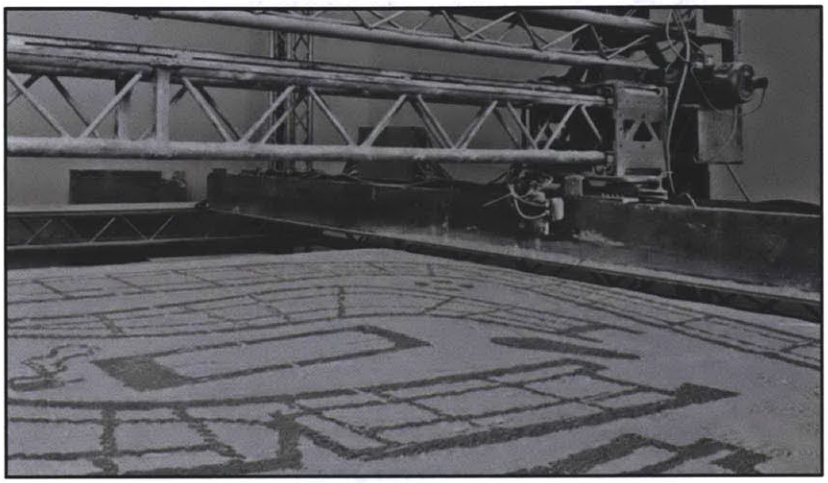

Figure 64. The D.Shape process deposits a liquid binder on successive layers of a powdered stone material to create large structures, similar to the printing technique used by Z Corporation powder printers. Image source: D.Shape

Figure 65. One of the large 3D printed structures produced using the D.Shape process. Image source: D.Shape

Finally, all of the described systems utilize a gantry setup, where the printed objects must be smaller than the mechanical gantry system in order to move the nozzle(s) to the

required edges of the structure. At small scales, this requirement is simple. However, moving to construction-scale is problematic due to the increased moment arms, the physical setup, and the portability of the system for on-site fabrication.

Print-in-Place Construction

Developed Method

Looking at these problems associated with direct concrete extrusion and gantry systems, a different approach to construction-scale fabrication was developed. Rather than directly extrude concrete as the printed material, a rapidly cured mould is printed and the moulds is used to cast concrete (Figure 66). The process is termed Print-in-Place Construction, as the mould is printed directly on the final building location. Print-in-Place Construction allows the sidestepping of the complexities associated with direct concrete extrusion, for instance cure time, slump issues, and weight of the hopper material. In addition, mould printing allows for a stronger product as the concrete is cast at once instead of successively layered.

Figure 66. The developed Print-in-Place process is based around 3D printing an insulative foam mould (left) and then filling the mould with a structural material like concrete (right). The insulative mould can be left in place for thermal insulation purposes or removed if designs are milled into the printed foam.

Another interesting benefit is the dual purpose that the mould fulfills. After serving the purpose of a mould for the concrete interior structure, the mould is left in place and serves as a thermal insulative layer. After printing and pouring, the result is a fully insulated building. This is accomplished by using a mould material with insulative properties, which was polyurethane spray foam for all of the experiments conducted.

The polyurethane spray foam utilized in the prototype system (Dow Chemical FROTH-PAK foam) is a two component chemical foam which has cure time of 30 seconds. It is an expanding foam that is strong, lightweight, and designed for a high insulative value. The rapid cure time allows for a large structure to be printed very quickly, for example the curved twelve foot long wall structure shown in Figure 67 was printed in approximately five minutes using a robotic arm to control the nozzle position. It is estimated that an entire house structure could be printed in under a day.

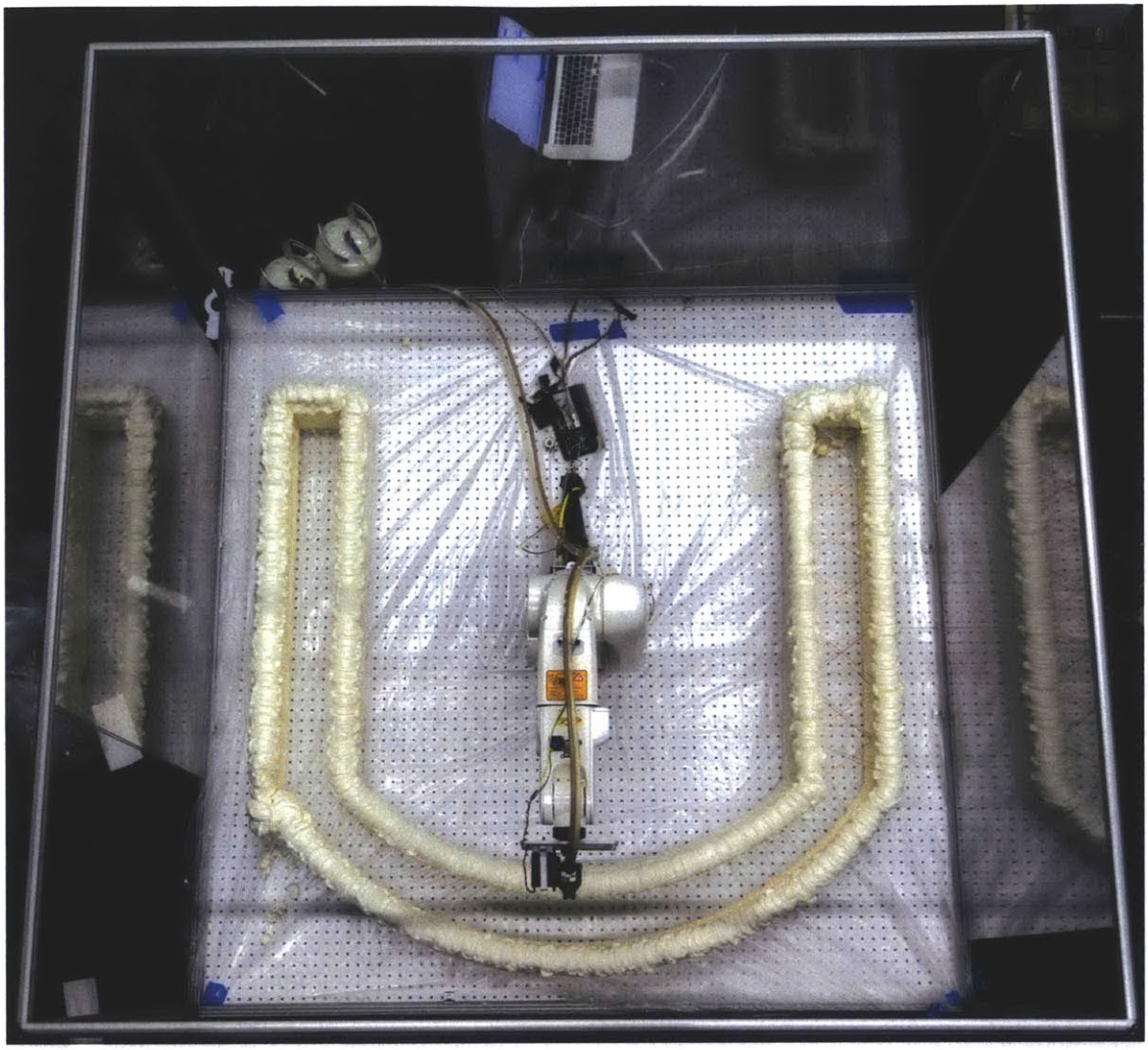

Figure 67. A curved wall mould is printed using the robotic arm platform (top view). The resulting polyurethane mould structure can be filled with a castable structural material and finished with traditional methods.

Separating the mould printing from the concrete pour also simplifies the process. A building's mould can be printed and then a concrete truck can do a single pour at another convenient time. As well, the hollow mould can be adjusted for the inclusion of embedded objects (like plumbing, rebar, or electrical wiring) before the concrete is poured (Figure 68).

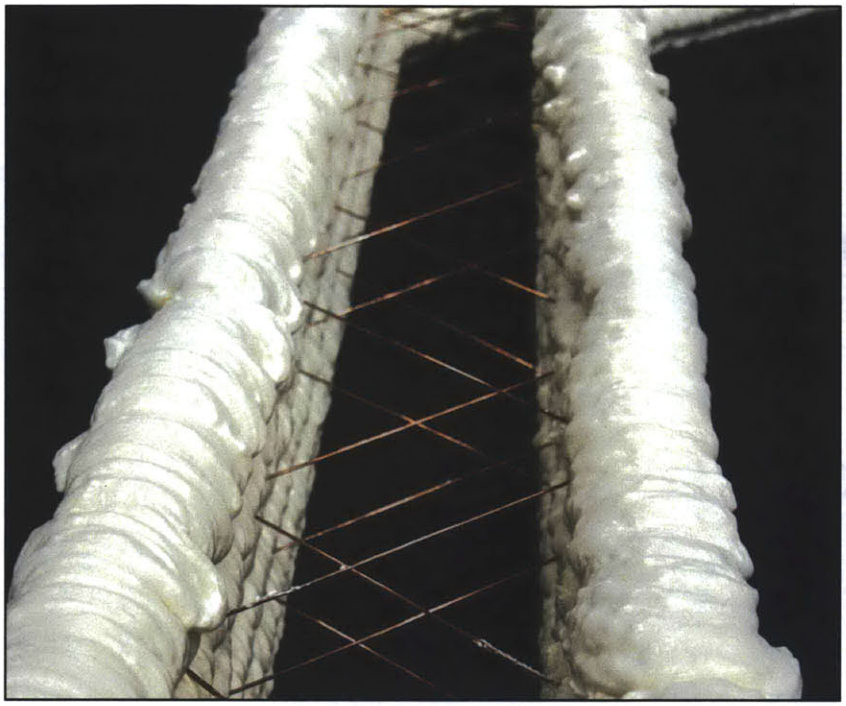

Figure 68. Different structures and integrated features can be incorporated into the 3D printing process, such as these metal reinforcement rods.

A proposed full-scale implementation would function like this: a large boom lift drives up to a construction site which contains all of the needed printing mechanisms and material to fully print the entire foam mould for a house. The crane is equipped with a small, precise robot arm on the end with a nozzle that will first 3D print the outline of the house, layer by layer (Figure 69). Then, a milling bit attached to the robot arm performs detailed work to mill out the edges of the framework and any custom reliefs or designs into the structure. Voids are marked off by foam cross sections that will be cut out to insert doors, windows, plumbing, electrical, and other utilities. Rebar is then mechanically placed between layers for reinforcement, and once the mould is printed, fiber-reinforced concrete is poured into the mould using a three-part nozzle to achieve a concrete wall with a density gradient. This gradient functions as a sandwich panel to provide additional thermal insulation and increase material efficiency.

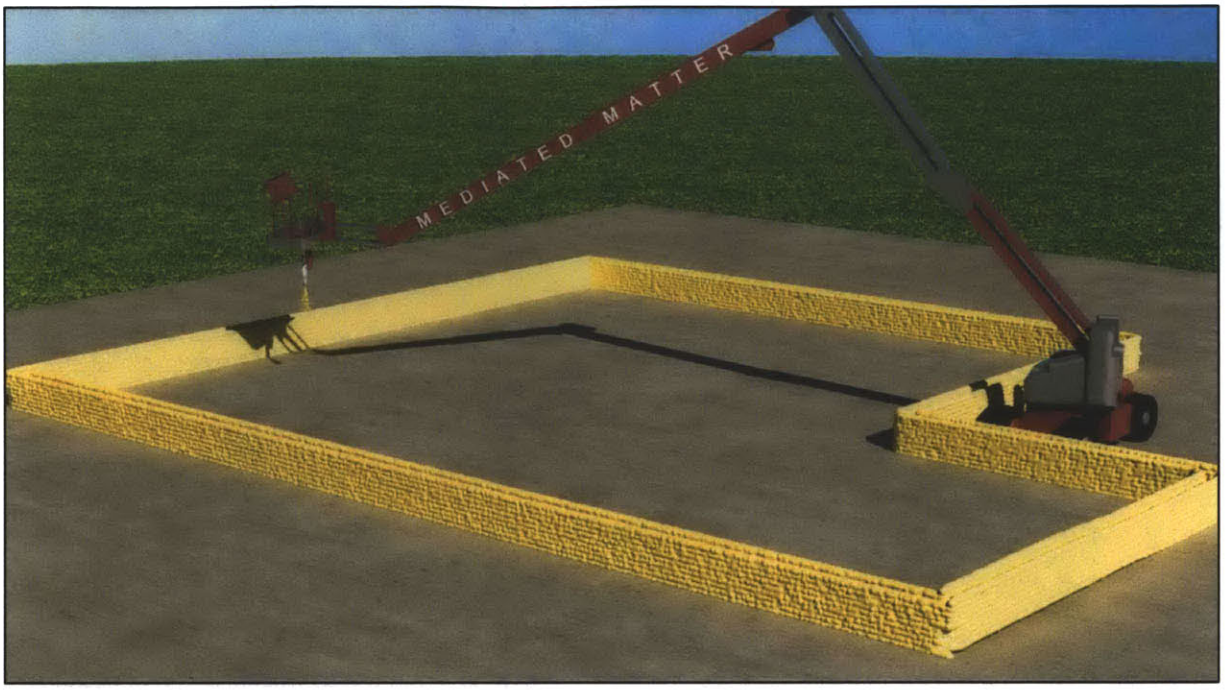

Figure 69. A computer rendering details a mould for a residential building being 3D printed using the Print-in-Place method. Layers of foam are successively printed according to a CAD design to create an insulative mould for concrete and other castable structural materials.

In order to create this density gradient and sandwich panel, three nozzles distribute concrete of varying density and the resulting mixture forms a diffusion gradient (Figure 70). Concrete foam, made using mechanical agitation of a protein foaming agent, is used to control the density of the mix. The outermost two nozzles extrude higher density concrete, as the skin bears most of the structural load, while the middle nozzle extrudes low density concrete that supports the shear loads. The foam is then waterproofed, covered in drywall, finished, and painted.

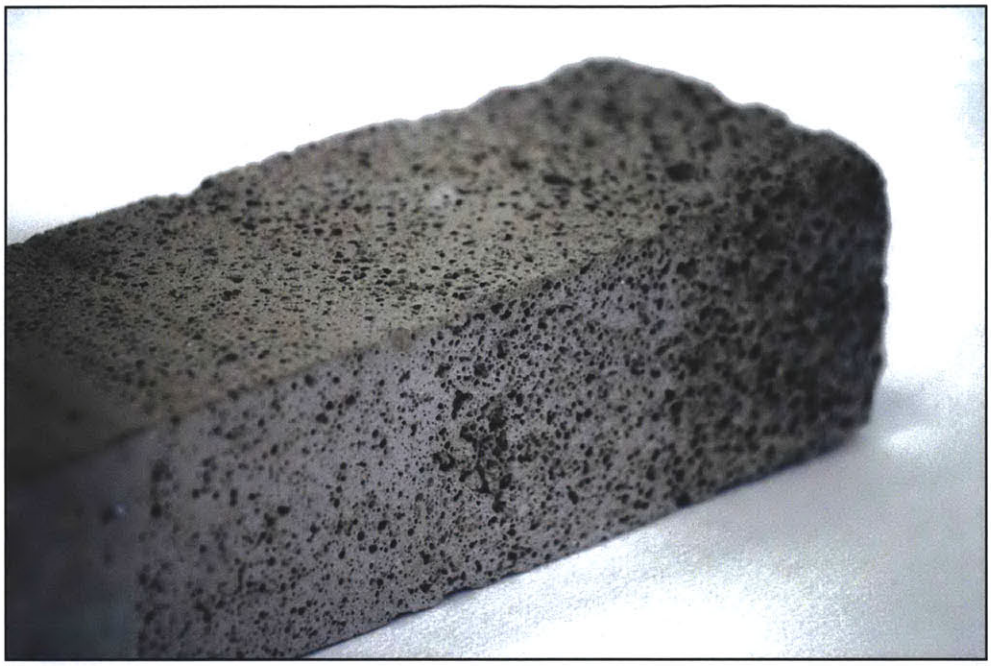

Figure 70. Using a multi-nozzle extruder, density gradients in concrete walls could be achieved using the Print-in-Place process. This would result in gradients similar to the structures seen in this sample, which was produced using a segmented mould as detailed in Chapter 6.

One of the advantages of the spray foam is that the curing process is initiated through chemical mixing. This allows for precise control of the extrusion process, including pausing it by closing the chemical valves. Extra material not used in one printing project could be saved for the next structure to be printed.

3D curvature can be generated through offsetting successive printed layers laterally, as seen in Figure 71. The excellent adhesive properties of the spray foam allow for significant overhangs to be generated without support material. This enables the option of a dome construction for a roof. Multi-floor structures could be constructed in a similar way, though to achieve flat floors on multi-floor buildings would require the addition of lateral supports.

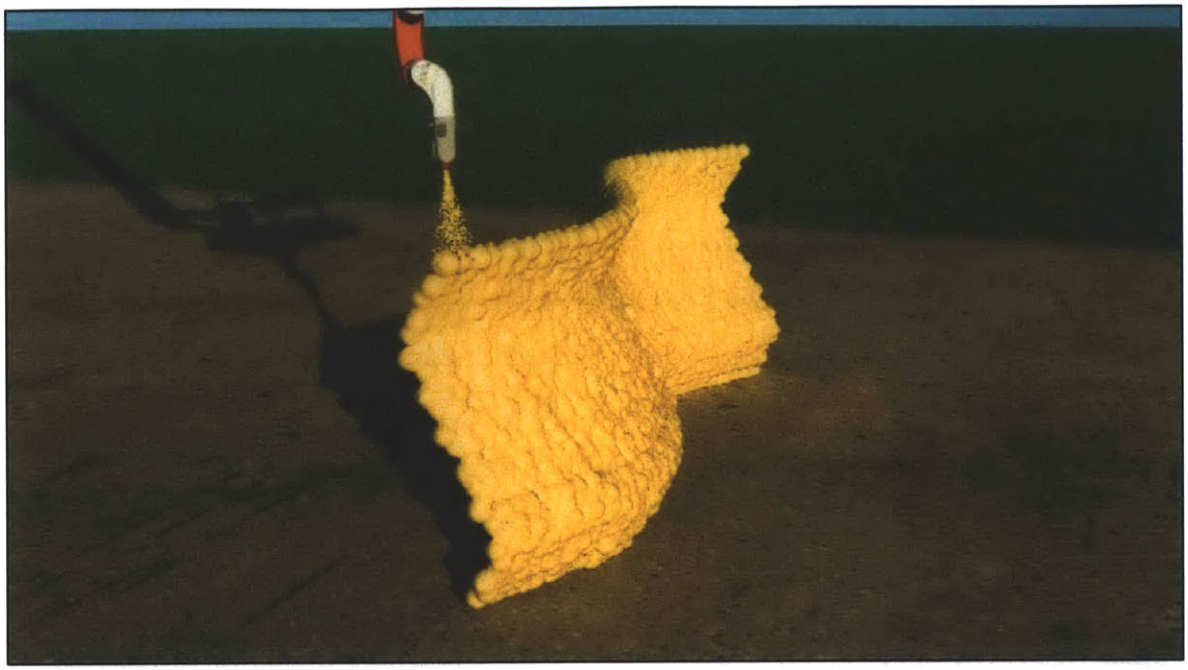

Figure 71. Doubly curved structures, such as the rendering above, can be produced using the Print-in-Place process due to the low-density and adhesive properties of the spray polyurethane.

When compared to traditional construction practices, the benefits of the designed system are substantial. Whereas the former method requires human labour and large construction machines, the latter allows for buildings to be printed with cost-effective mobile printing units. From a material standpoint, this system wastes no resources and uses only the exact amount of bulk material needed for construction. This reduces the price of construction down to the bare minimum based on the price of the bulk material components (insulating foam and concrete). From a speed standpoint, reducing the construction site time by orders of magnitude offers enormous savings. Finally, custom aesthetics are easily achieved, as the geometry is not constrained by rectilinear paths. With no more effort than inputting a design into a printer, every building can be unique.

Overall, printing the mould is an effective method that offers benefits over the difficulties involved in printing concrete directly or using a powder/binder process. In concrete extrusion, the slump and consistency of the concrete are critical to the success of the print. By printing dual-purpose foam that acts as a mould for the concrete and insulation

for the building, Print-in-Place Construction is significantly more versatile and can incorporate different materials or variations of concrete. The process can also be rapidly integrated into current building strategies and regulations as the Print-in-Place Construction method aligns directly with traditional insulated concrete form (ICF) technology. Once the mould is printed, conventional methods and regulations that apply to ICF construction are applicable to the Print-in-Place process.

Technical Analysis

Materials Characterization

The Print-in-Place process is based around printing the mould for a large structure. The main material used in the printing process, two-component spray polyurethane, has properties well suited for 3D printing. First, the cure time is very quick (under 30 seconds) which allows for layers to be built up rapidly. Secondly, the material is lightweight with a density around 1.75 lb/ft^3 and it expands to around 40 times its original volume upon mixing (Dow Chemical Company, 2012). These characteristics allow for ease of shipping and reduce the weight carried by the printer. The material strength of the cured foam is 21 PSI in compression and 27 PSI in tension, which creates a strong mould structure. The strength of the foam also determines the proper concrete lift size to pour at once and will be experimentally tested in future work. Finally, the sprayed foam is incredibly sticky, allowing for very strong layer adhesion and the ability to print overhang structures.

Five different commercial spray urethane foam products were qualitatively evaluated through spray tests to determine the optimum material. Based on the desired properties of fast cure time, high strength, and low density, the Dow Chemical FROTH-PAK Insulative Foam product proved best.

System Integration

Another important consideration is how other components of the building (such as the foundation, wiring, plumbing, floors, and ceilings) will come together. To begin, the printing process needs a rigid surface to work on. Typical excavation and foundation building techniques could be used to create a level concrete slab to print on. The techniques for incorporating other building components into the walls are similar to those adopted by ICF construction. By cutting voids in the foam outline after it is printed, electrical components and other utilities could to be placed using the robotic effector or by hand. Components like pipes and wiring conduits could also be placed inside the foam mould and embedded in the concrete walls.

The mould printing process could be capable of printing roofs and floors with the addition of simple support material. Another option is to pre-cast these structures and lift them into place with a crane. Also, a traditional wood-framed floor for additional stories and a wood-framed roof could be installed as is commonly done in ICF construction.

For reinforcing the concrete walls, a rebar system was developed to allow for flexible and full 3D structures. As detailed below, it consists of a cross beam with two side components that stick in parallel to the foam, acting as ties to hold the foam mould together during the concrete pour (Figure 72). Traditional rebar or steel fiber additive also could be used for reinforcement.

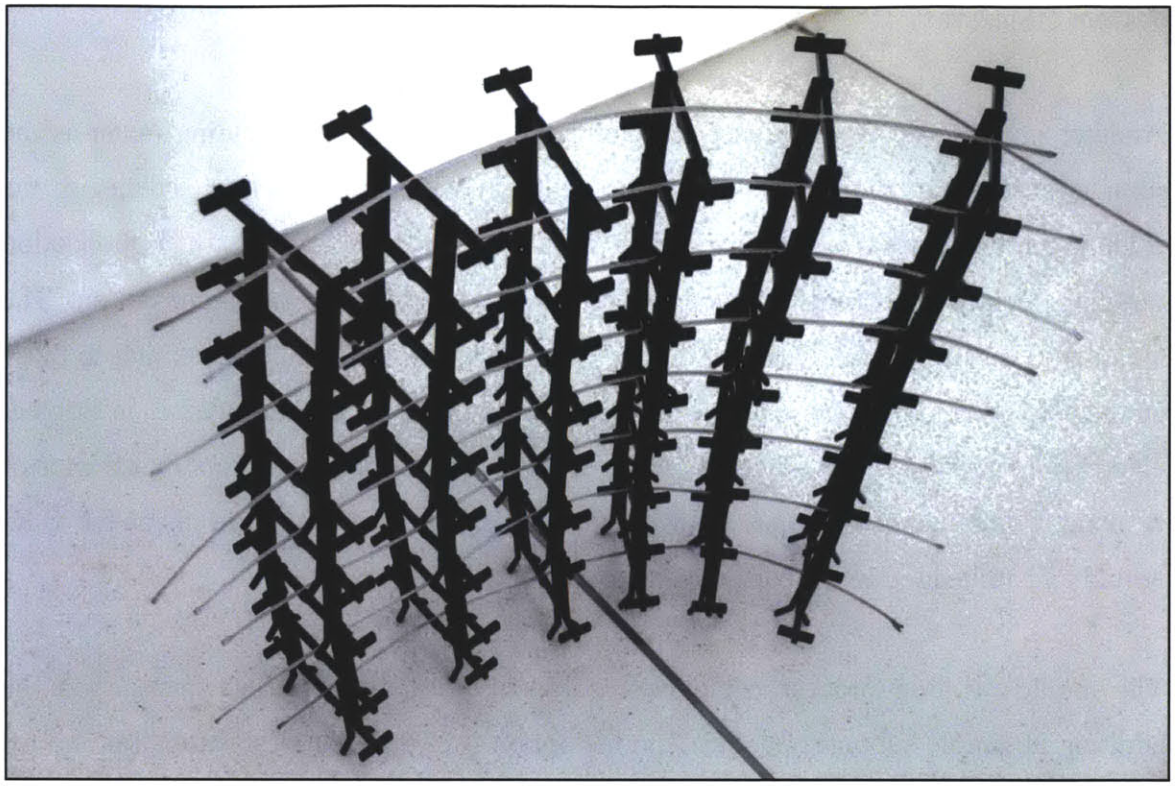

Figure 72. An example reinforcement system that could be integrated into the printed mould structure to serve as rebar for concrete, ties for attaching screws to the wall, and to improve structural strength of the mould.

Delivery Systems

Several delivery mechanisms are possible for implementing building-scale 3D printing. The simplest is for a crane or boom to have a robot arm attachment at the end for precision (Figure 73). This robot arm would move around the building and print the mould. It would also hold the liquid foam supply on board and have different effectors for inserting rebar and milling, making it an all-in-one construction device. This boom platform would be an easy extension of current construction machine technology.

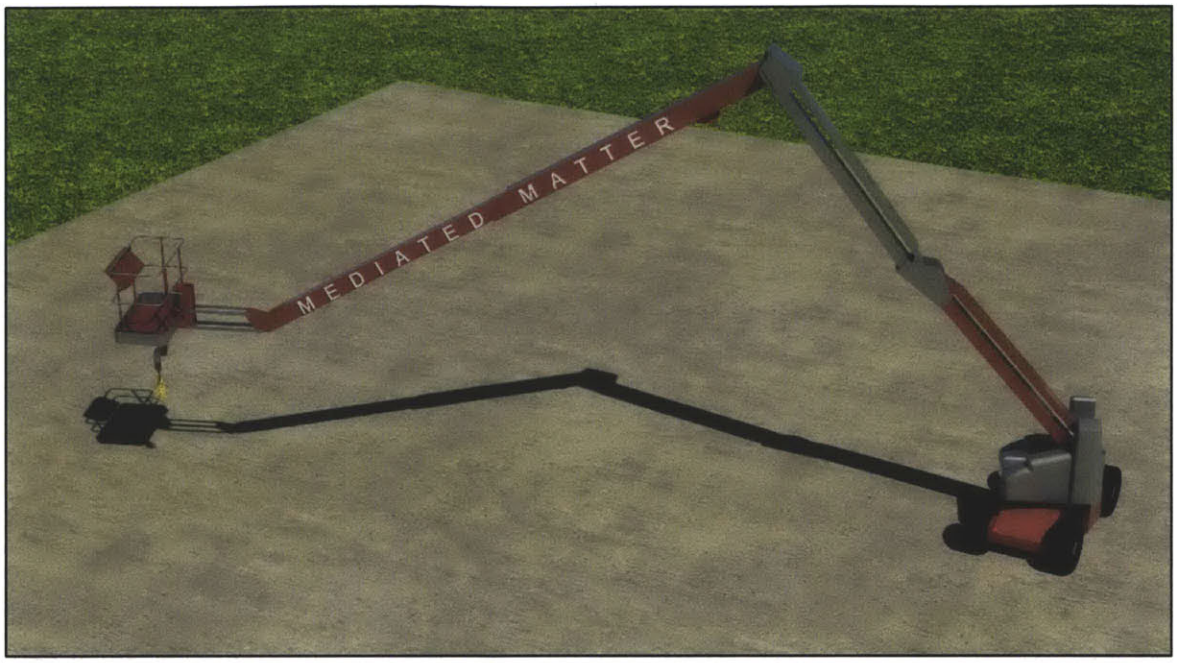

Figure 73. A boom lift system could be used as a delivery mechanism, as seen in the rendering above. Using a smaller robotic arm at the end of the boom could be used to compensate for vibrations and improve the coarse resolution of the boom lift.

While this method can be employed using any nozzle positioning system, such as a gantry system or robotic arm, another interesting option is available due to the low density of the mould material. The chemicals significantly expand during curing to offer only a small volume of material needed for initial transport. This characteristic enables the concept of mobile printing; where robotic agents print structures much larger than themselves. Using the foam printing method, mobile robots could extrude the mould material while it travels, leaving a trail of printed foam. As the foam cures quickly and support significant load, these robotic systems can travel up previous printed layers to enable large structures to be printed. The mobile printers carry the chemical mixture onboard or have flexible tubes connected to a main chemical tank. In the prototype concept, the mobile robot has two extrusion nozzles that are aligned with the wheel distance. This allows for the robot to drive up the previously printed structure using the foam mould as tracks for its wheel-base (Figure 74). In this setup, the mobile printer would follow the perimeter of the desired building and spiral upwards on its previously printed tracks. Different mobile robotic forms could also be used, from ground-based

system (wheels, tracks, legs, etc.) to air-based systems (helicopters, quadcopters, etc.). Precise positioning tracking can be accomplished through a number of systems ranging from GPS, to wheel encoders, to optical tracking from a stationary position. Multiple mobile printers could also be used to expedite the printing process or serve different roles (Figure 75). For instance, some of the units could do the foam printing, while others provide supplementary roles such as rebar insertion, pluming configuration, or wall painting.

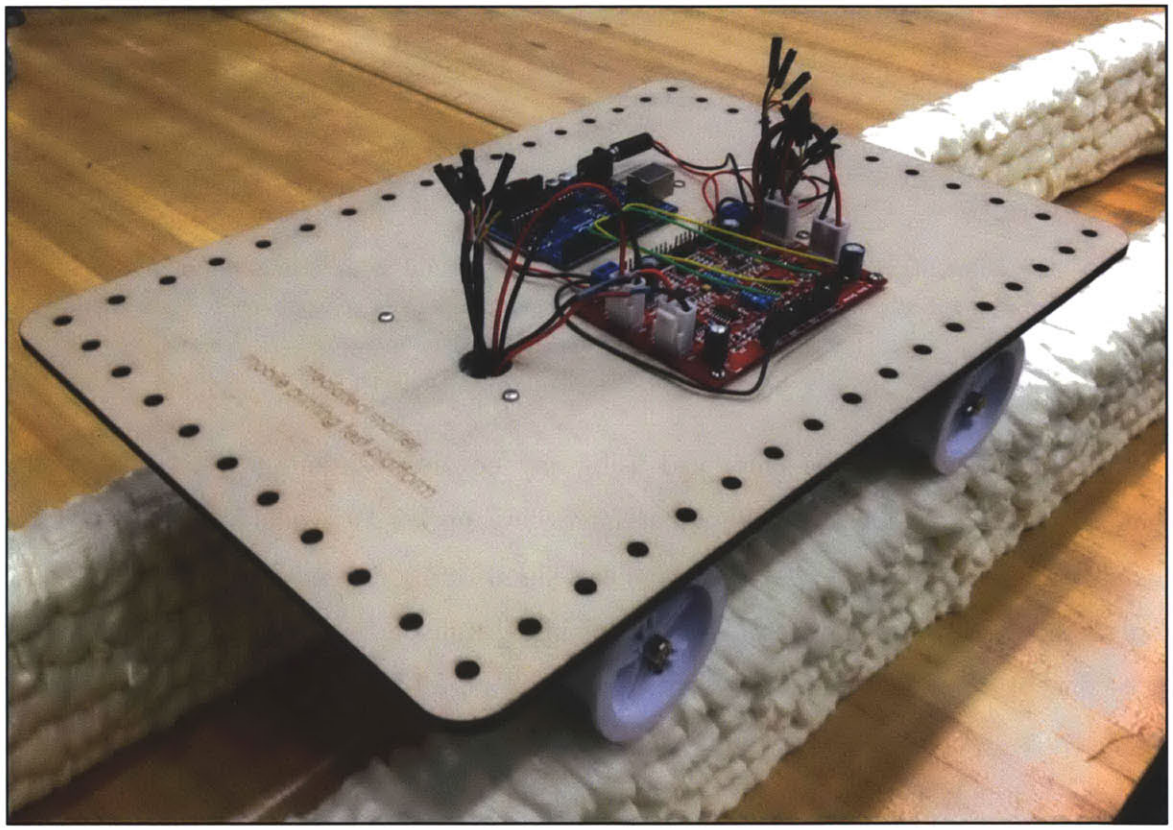

Figure 74. An early mock-up prototype of a mobile printer that can drive on top of the foam moulds to print structures larger than itself.

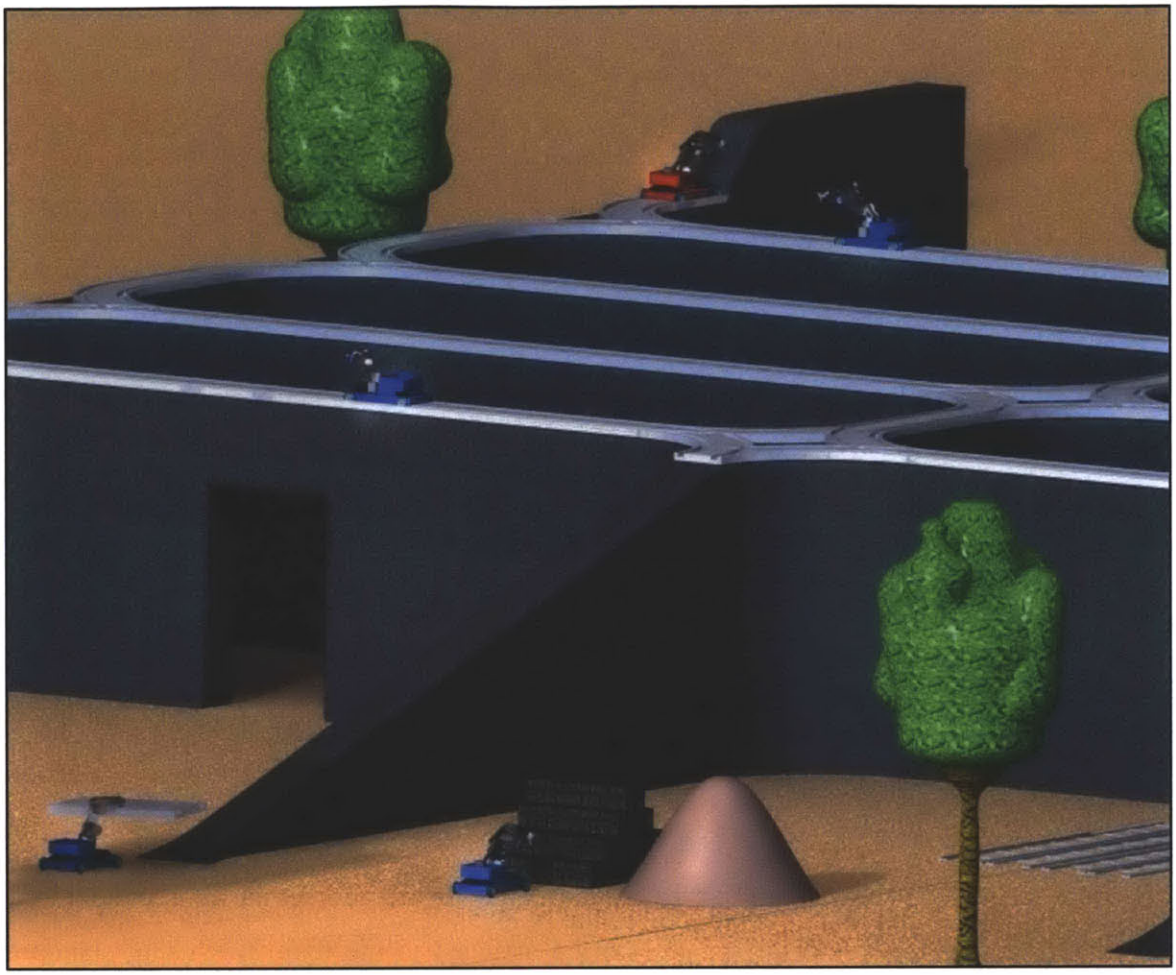

Figure 75. A rendering detailing how a group of mobile robots could work together to construct larger structures using swarm printing techniques.

A final possibility is a cable-driven printing platform inspired by spiders and the camera-positioning platform *SkyCam* (SkyCam, 2012). This platform could be used for extremely large structures or for printing neighborhoods with a single setup. Using supporting cables mounted to static connection points above the printing area, the cable-driven platform allows for a massive print volume (Figure 76). This could be set up in a large area by attaching each of the cables to static points in a city or large cranes. This concept and an early stage prototype was introduced and developed by Benjamin Peters, a graduate student in the Mediated Matter group.

Figure 76. The SkyCam technology uses a cable-gantry system to move a camera around a stadium for videoing sporting events. A similar cable-gantry could be used as a delivery mechanism for large-scale 3D printing.

Finishing

There are several available options for finishing the surface of the printed building. For detailed design work, the foam can be milled to give exact surface designs or textures. Drywall or other interior wall finishes can be attached to the foam ties using standard techniques. On the exterior, a number of options exist including siding and spray able finishing products. Also, for pre-cast structures such as panels, slabs, benches, sculptures, and other artwork, one can simply pressure-wash the foam off after the concrete cures.

Print tests

A number of printing tests and prototype walls were constructed using the robotic arm to experiment with different materials and techniques. These tests were helpful in proving the concept, determining proper parameters, and evaluating the large-scale feasibility. An end effector for spraying the foam and milling the foam was constructed (Figure 77). The end effector uses an interchangeable mixing nozzle produced by Dow Chemical to allow for easy replacement (Figure 78). A servo connected to a valve controlling the chemical

flow allows for the spray flow rate to be manipulated. A small controller was constructed to operate and change the flow rate (Figure 79). For milling, a Porter-Cable handheld router was mounted to the effector. A number of sample printed structures are seen in Figure 80.

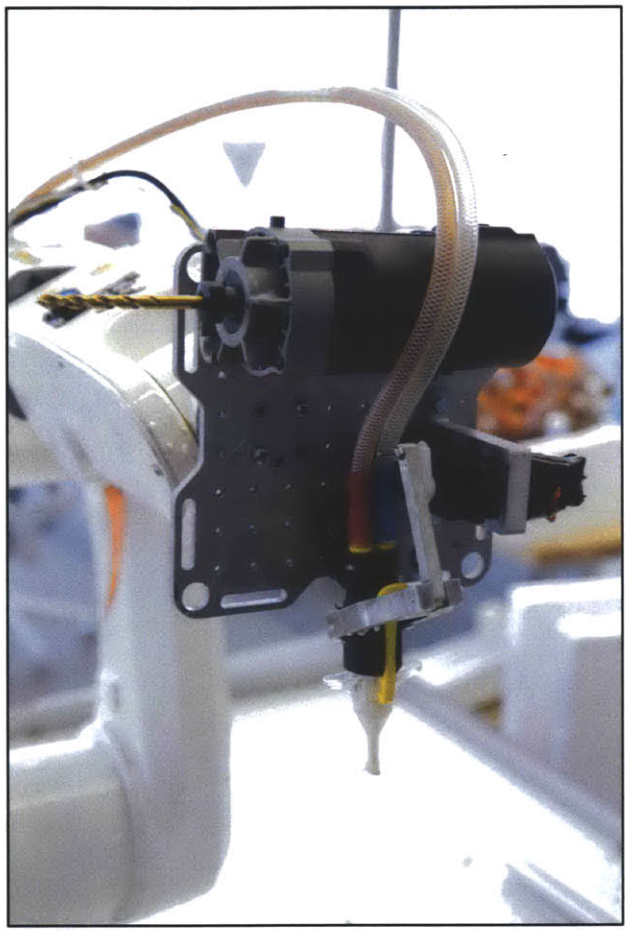

Figure 77. The foam printing and milling end effector used for all Print-in-Place testing. The chemical lines connected to the nozzle are connected to pressurized tanks located behind the robotic arm.

Figure 78. Replaceable mixing nozzles for the spray urethane foam made by Dow Chemical. Different spray widths and nozzle shapes can be used for various layer widths.

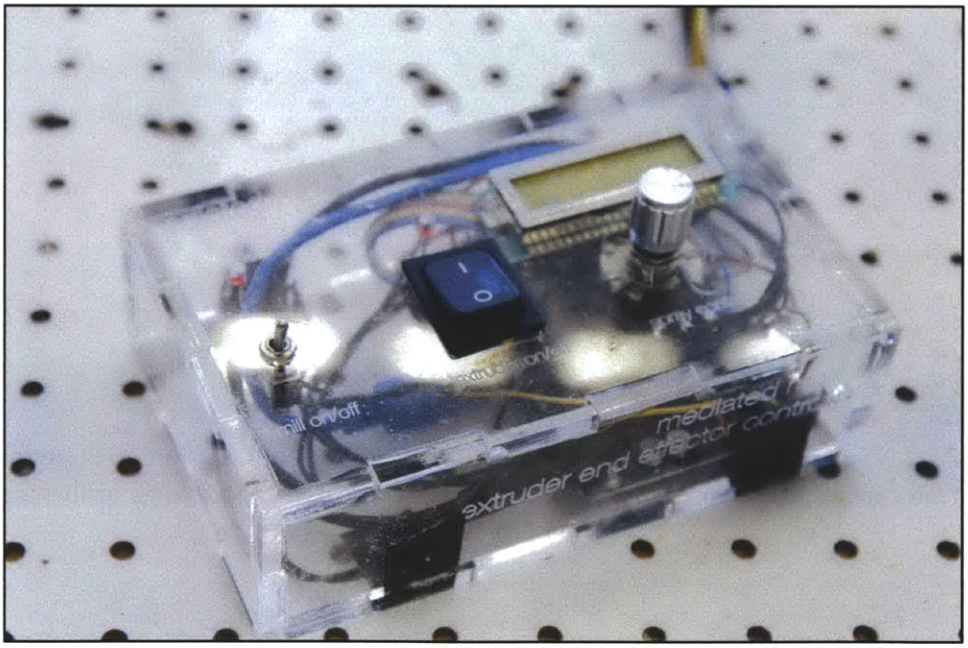

Figure 79. The foam extruder controller box was built to driver the servo controlling the foam flow rate.

Preliminary overhang foam tests confirmed that walls with overhangs can be printed, which would allow Print-in-Place Construction to print very complex structures. To

achieve overhangs and sloped structures, both horizontal offsets (Figure 81) and angular extrusion (Figure 82) can be used. In fact, the spray foam is adhesive enough to facilitate printing at angles larger than 90° in respect to the previously printed layer. The foam can even be printed upside down to spray on surfaces above the nozzle. As opposed to the 2.5D structures that Contour Crafting and Concrete Printing are limited to, the Print-in-Place method allows for full 3D geometries with interior voids. These tests confirmed that the foam printing process is capable of creating even more radical structures than other large-scale 3D printing methods to date.

Figure 80. A few of the printed test sections are seen in this photograph.

Figure 81. A print test of a cone where the layers were printed with horizontal offsets to achieve the slope of the cone. The nozzle was kept perpendicular to the build platform the entire time.

Figure 82. Angular print tests were done by spraying the foam at different angles. All angles produced satisfactory layer adhesion due to the low density of the foam and its adhesive properties.

Milling tests also successfully tested the combination of foam printing and milling to obtain smooth finishes and high-resolution moulds (Figure 83). This technique would not only allow drywall and other finishes to be easily applied to the foam insulation, but it would also allow an architect to add artistic etches to a building.

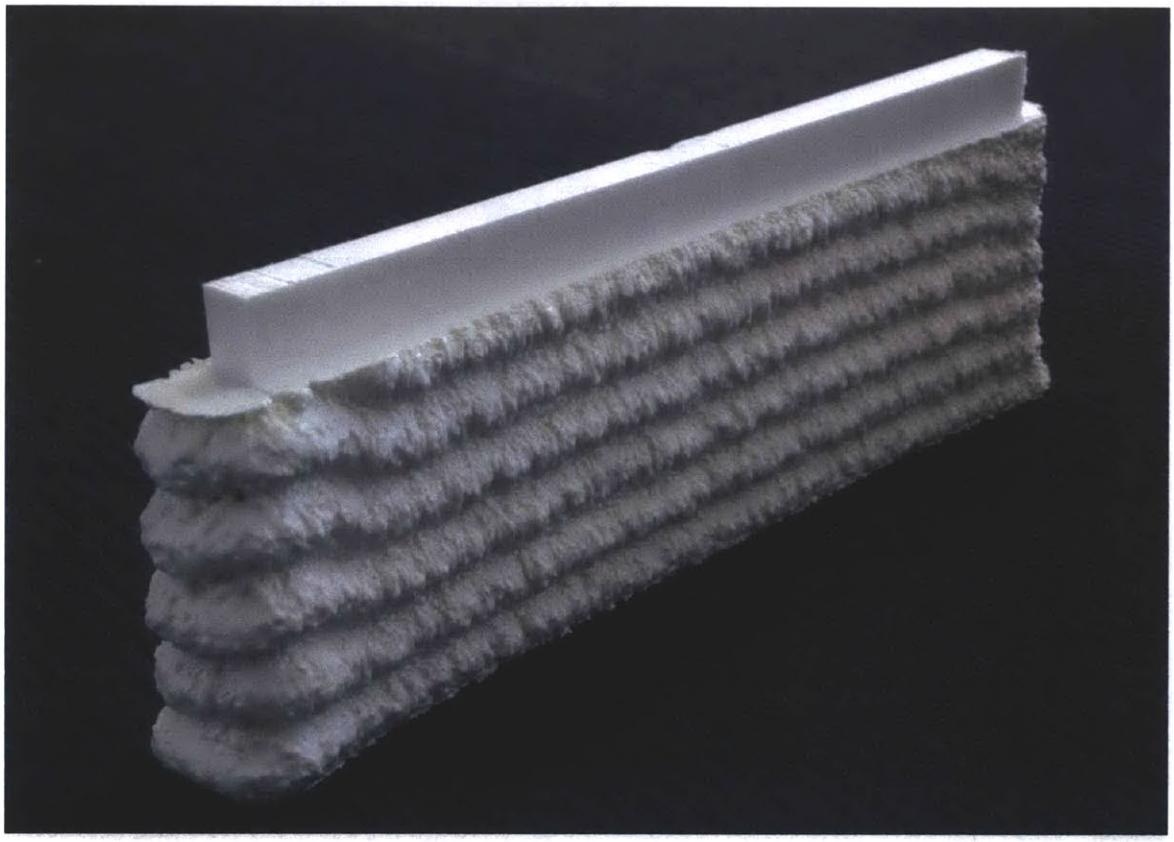

Figure 83. A foam printed wall that was robotically milled on the top layer. Milling can be done to achieve a more consistent surface finish, to add details and designs to a cast structure, or to carve out features for functionality such as electrical routing.

Detailed 3D features milled into the insulation foam could translate into decorative or functional surfaces if the foam was then pressure-washed off. Using this technique, artistic surfaces, signs, and more can be created that are completely custom without the need for a repetitive pattern as is traditional used in creating cast reliefs (Figure 84).

Figure 84. A printed foam panel was robotically milled to create a designed mould that was filled with concrete. After removing the foam mould, the cast concrete sign was produced. Features like this could be milled into the sides of wall moulds to produce very elaborate and precise architectural scale buildings and sculptures.

Comparison to traditional construction methods

The primary methods of modern construction—wood and steel framing, brick laying, and traditional concrete formwork—have not fundamentally changed in centuries. While other industries have seen revolutions in technology, materials, and automation, construction remains an industry constrained to traditional techniques and regional knowledge. The Print-in-Place process has the potential to revolutionize the construction industry by using automated techniques that offer benefits over traditional methods. To understand how Print-in-Place Construction compares to industry standards, an overview of the current primary methods of building construction is warranted.

Wood

Wood is used in modern construction primarily to frame houses (Figure 85), in fact, 85% of all houses in the US and Canada are built with a wood frame. Metal frames are also used and it is the preferred material for framing commercial buildings due to their strength compared to wooden frames (VanderWerf, The Concrete House: Building Solid, Safe and Efficient with Insulating Concrete Forms, 2007). Wood framing is the most common method of construction for residential buildings despite the fact that wooden homes are vulnerable to water, fire, insect, and storm damage. In fact, the main benefit of wood are its low costs. As such, the only countries where wood is used more commonly than metal are the US, Canada, Scandinavia, Siberia, and other locations where lumber is particularly cheap (VanderWerf, The Concrete House: Building Solid, Safe and Efficient with Insulating Concrete Forms, 2007).

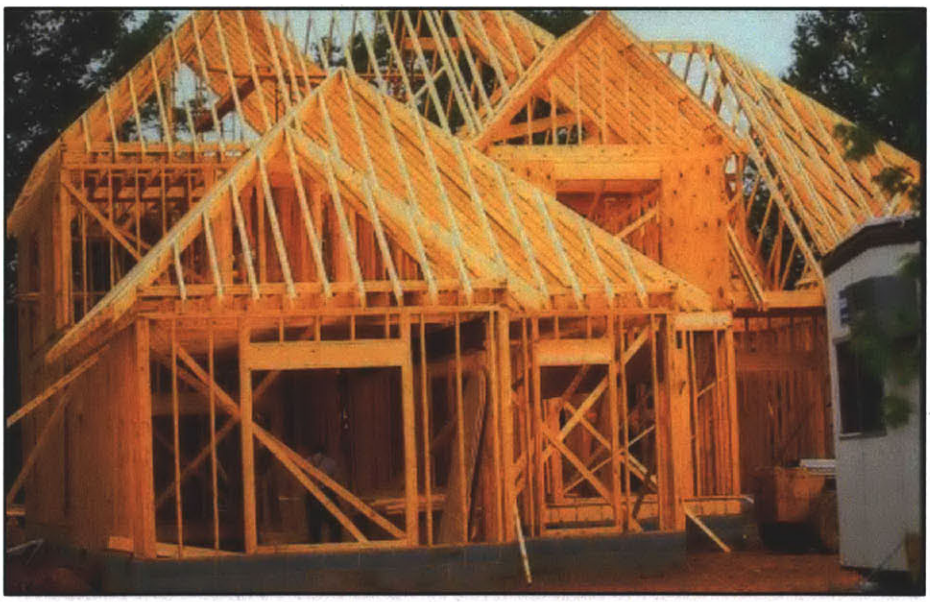

Figure 85. A typical wood frame construction of a residential building. Image source: New Home Construction

Concrete Blocks

Concrete blocks are reinforced with rebar and used in conjunction with concrete columns and tie beams. Concrete Block Structure, or CBS, construction is commonly used for the load-bearing walls of buildings. In suburban houses especially, concrete blocks are used for perimeter walls, with a concrete slab and foundation below (Figure 86). Larger structures, however, tend to use steel instead (National Concrete Masonry Association, 2012).

Figure 86. Concrete blocks are often used for perimeter walls in construction, as seen here. Image source: Home Designs and Furniture Gallery

Steel

Steel is used as an external surface covering or as structural framework for large buildings, especially high rises (Figure 87). The main benefits of steel include strength and flexibility, while corrosion is one long-term disadvantage. For use in construction,

steel requires a significant amount of labour. In terms of Print-in-Place concrete buildings, it would be difficult to replicate the strength and structure of a steel high rise.

Figure 87. Large skyscrapers are constructed using a backbone of steel. Image source: Denver Infill Blog

Insulated Concrete Forms

Insulating Concrete Forms are a relatively new technology that has numerous energy and strength benefits. ICFs are type of concrete formwork that stays in place as permanent building insulation after concrete is poured: an energy-efficient method of creating reinforced cast-in-place walls, floors, and roofs (Figure 88). In current construction, the forms are interlocking units that are poured in four-foot lifts. The modular units are typically 10x16x48 inches and are dry-stacked to assemble the building (VanderWerf,

The Concrete House: Building Solid, Safe and Efficient with Insulating Concrete Forms, 2007).

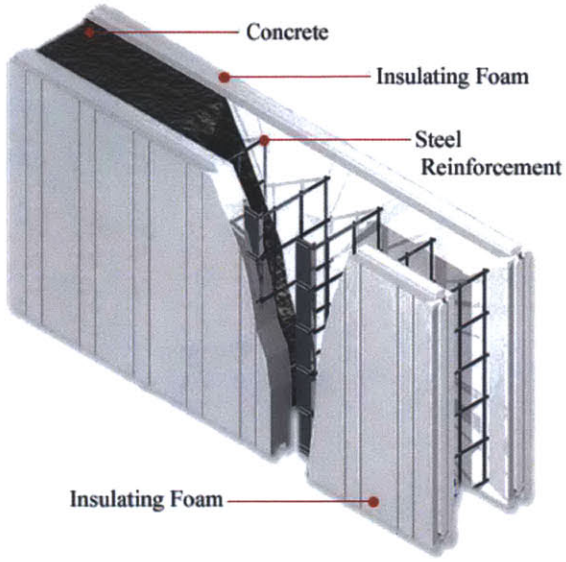

Figure 88. A schematic of a typical ICF block shows the foam walls, steel ties, and cast concrete. Image source: Concrete Works

Recently, ICFs have become an increasingly common technology for building homes and low-rise commercial buildings. In 2006, over 90,000 houses were built at least partially with ICFs in US and Canada, a figure that has shown 20% growth annually (VanderWerf, The Concrete House: Building Solid, Safe and Efficient with Insulating Concrete Forms, 2007).

The combination of expanded polystyrene insulation foam and concrete as building materials provide strong benefits. The concrete has a large thermal mass, and the foam has a large unit thermal resistance, or R-value, of 16 to 23, making ICFs much more insulative than typical fiberglass insulation, which produces walls of an R-value between 8 and 12 (Panushey & VanderWerf, 2004). The foam and concrete also results in an excellent fire rating of two to four hours, as compared to normal wood-framed walls' rating of half an hour to an hour. ICF houses can resist very high temperatures for a much

longer time than traditional houses (VanderWerf, The Concrete House: Building Solid, Safe and Efficient with Insulating Concrete Forms, 2007).

Once completed, ICF houses are nearly identical in appearance to traditional houses, the only difference being that ICF houses have thicker walls. However, ICFs are much more energy efficient, stronger, and more resistant to natural disasters (such as fires, tornadoes and hurricanes) than traditional wood-frame houses. Concrete is far less likely to burn than wood, and though the foam exterior will melt when exposed to fire, it cannot hold a flame to feed a fire. Provided that the rebar is adequate for local seismic conditions and building codes, ICF houses see no significant damage in earthquakes either. ICFs are also incredibly sound resistant: less than one-third as much sound can pass through an ICF wall as a traditional wall (Panushey & VanderWerf, 2004).

Unlike other construction methods, no additional structural support is needed when using ICFs other than temporary scaffolding for openings. As compared to wood frame construction, using ICFs can sometimes increase construction costs by 3-5% (NAHB Research Center, 2001). However, ICF houses use an estimate of 44% less energy to heat and 32% less energy to cool than traditional wood-frame houses (VanderWerf, Energy Comparisons of Concrete Homes Versus Wood Frame Homes, 2001). This can save upwards of a thousand dollars on heating and cooling costs annually, which makes ICF construction an excellent long-term investment.

The concept of Insulating Concrete Forms is very similar to what to printing foam moulds for building-scale 3D printing. However, instead of placing the insulation, robotic devices 3D print the mould, creating Print-in-Place Construction.

Benefits

The building-scale printing work is motivated by the problems currently plaguing the residential construction industry. The proposed method aims to have comparable energy,

strength, and durability benefits as ICF construction, but with additional safety, design, speed, environmental, energy, and financial benefits.

Traditional construction methods are unsafe, slow, labour intensive, costly, and hard on the environment. The significant decrease in building time and labour proposed here through the use of automated methods will greatly reduce costs and improve safety in an inefficient and dangerous industry. According to the United States Bureau of Labor Statistics, in 2010 4 out of 100 full-time workers were injured or contracted a work-related illness. According to the U.S. Bureau of Labor Statistics, in all, 802 fatalities were reported in 2010, the largest number of deaths in any sector, making construction arguably one of the most dangerous professions in the country. A powerful benefit of this process is its potential to significantly decrease the number of injuries and deaths in construction industry by eliminating many of the dangerous and labourious tasks of constructing a building.

Print-in-Place buildings also have structural benefits and can be built more easily than traditional buildings. Although ubiquitous due to their simplicity and low cost, rectilinear buildings are actually weaker and more dangerous due to stress concentrations. Curvature improves structural integrity, but curved shapes are extremely challenging to form using traditional methods. With the Print-in-Place method, creating curved structures is as simple as designing them on a computer, which allows architects to create more stable, unique, and versatile structures (Figure 89). By encouraging creativity and increasing the possibility for unique and doubly curved structures, Print-in-Place Construction could facilitate complex architectural expressions for the same cost as a rectangular building. Imagine what buildings would look like in the future if the total cost were completely independent of the shape and merely tied to the cost of raw materials!

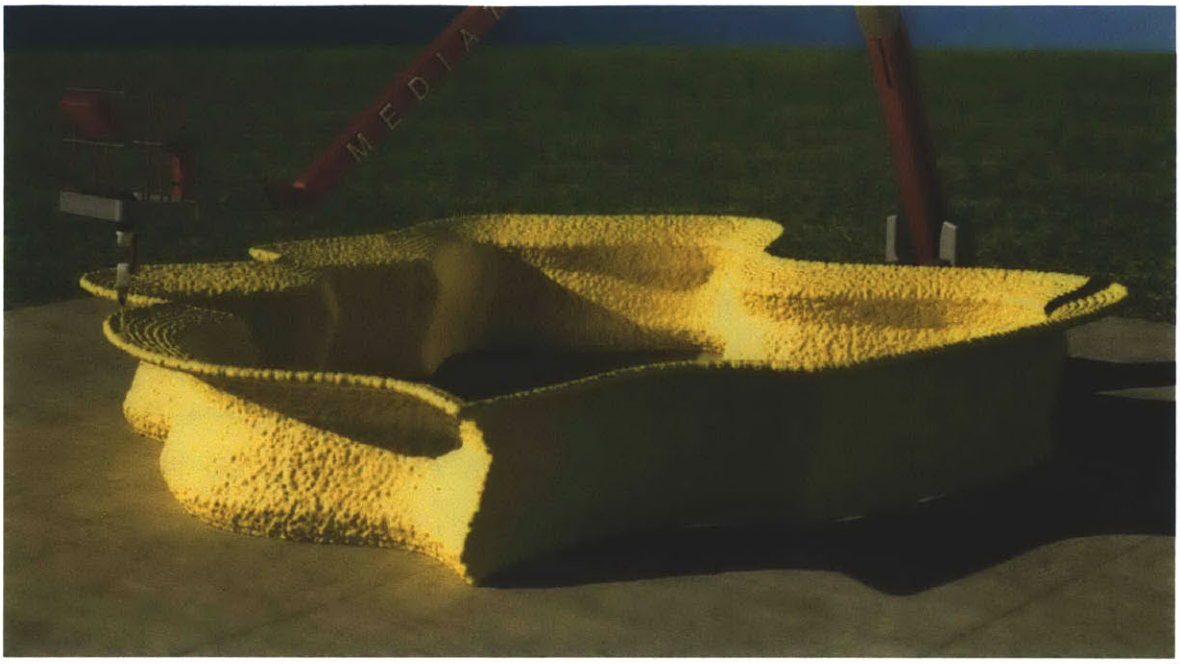

Figure 89. A rendering of a complex structure being printed using the Print-in-Place method. Doubly curved structures, like this one, would cost the same as rectilinear forms of the same mass.

Additionally, automation enables highly detailed process control – parameters such as wall properties and construction time can be controlled and precisely predicted. By removing human error and variation, civil engineering calculations can be much more accurate, allowing for a house to be built to exact structural and thermal specifications. Having a correct time prediction is also very useful for planning purposes and ensuring a project finishes on time. Time calculations, based on prototype test conditions in lab, estimate that the mould for a typical one-story house with 10-foot walls and a perimeter of 170 feet could be printed in 8 hours and 35 minutes[1]. Automation of the building process also eliminates the scheduling difficulties of having multiple contractors on a jobsite at the same time and saves construction time and, consequently, labour costs.

---

[1] Calculations based on parameters used in lab prototypes where various wall sections have been successfully printed. This time estimation is based on a robotic arm moving at a speed of 0.2 m/s, one-inch layers, using a dual nozzle foam extruder end effector.

Not only would the Print-in-Place method reduce waste, but it would also save money on energy bills. While traditional construction methods have walls with a thermal insulation R-value from 8 to 12 and ICFs have an R-value from 16 to 23, the standard thickness polyurethane foam and concrete combination would provide a highly insulating R-value of approximately 36, significantly greater than that of both traditional and ICF walls. This value is a conservative estimate that only includes the R-value of the foam and not the cast concrete. As well, the R-value of the printed walls can easily be adjusted by telling the robotic system to print thicker or thinner foam insulation sections. By offering complete control over a building's parameters from a keyboard, the Print-in-Place process allows buildings to be customized and adjusted for any environment or culture.

According to a life cycle analysis study conducted by the Concrete Sustainability Hub at MIT that analyzed residential concrete buildings and traditional wood frame homes, there are many benefits inherent to ICF construction due to the higher R-value and lower thermal bridging (Ochsendorf, 2010). Researchers reported operational energy savings of more than 20% compared to traditional buildings in cold climates. These energy benefits would be greater for Print-in-Place walls due to the larger R-value and offer significant financial savings for homeowners.

The outlined 3D printing method has numerous versatile applications, the most practical and effective of which is residential construction. However, other potential extensions include low-rise commercial buildings, emergency or impoverished housing, civil infrastructure, pre-cast panels or slabs, benches and other small concrete structures, sculpture, and art. This method could also potentially be used in highly constrained environments such as disaster zones, military bases, and even outer space.

Future Plans

To continue this project, a scaled up test to build a full-scale building as a proof of concept is planned. This test building would help discover any issues not seen at the smaller scale prototypes.

An investigation of the different delivery mechanisms—robot arm, mobile robots, and cable-driven gantry—is required to determine which is most appropriate to be scaled for building-scale 3D printing. Since the mould is being printed rather than the concrete, the building material can be varied, which makes the method quite versatile and open to new possibilities, such as recycled plastic wood alternatives and novel composites. Testing these alternative materials in place of concrete could result in novel building structures.

Conclusions

Overall, the goal of the Print-in-Place Construction method is to improve upon the limitations of modern construction methods. Through using a robotic arm as a flexible extruder system for spray polyurethane foam, the developed process additively produces insulative forms for building-scale components like walls. The developed Print-in-Place process uses mobile industrial robotic arms in a new environment: the outside world. By mounting a robotic arm on a mobile delivery system, such as a boom lift, the speed and precision of the arm can be used to compensate for inaccuracies and vibrations of the larger delivery system. This facilitates a fast and flexible construction-scale digital manipulator. While a number of challenges exist to facilitate outdoor robotic positioning, the possibilities of large-scale industrial robotic arms operating in the external environment are novel and exciting for many applications, such as construction.

The Print-in-Place construction process holds potential to save material, energy cost, time, money and labour while increasing safety and architectural possibilities. By putting the power of design and construction directly into an end users control, allowing imagined structures to be constructed at the touch of a button. Buildings of any shape could be created in hours, not weeks, using a machine process that is quantifiable, accurate, and customizable.

Chapter 8: Direct Recycling

"Plastic should be a high value material... [It] should be in products that last a long time, and at the end of the life, you recycle it. To take oil or natural gas that took millions of years to produce and then to make a disposable product that last minutes or seconds, and then to just discard it — I think that's not a good way of using this resource."

—Susan Freinkel

Introduction

Recycling is typically thought as an off-site process requiring large machines and a complex retrieval and distribution center. Most cities have a few central recycling centers that are feed by a network of recycling trucks and depots. This chapter explores the idea of distributed recycling using a robotic arm 3D printer, where individuals can recycle their disposables into new products for themselves through additive manufacturing.

The ubiquity of disposable thermoplastic containers in today's society offers an interesting opportunity when combined with additive manufacturing. Most low cost 3D printers function using a thermoplastic feedstock that is melted inside an extrusion print head. If the thermoplastic waste could be converted into a feedstock for a 3D printer, then an object could be directly recycled into a new product. In this sense, direct recycling is a type of formative fabrication process, akin to forming. The input material is re-shaped into a new form through the addition of heat and mechanical forces.

In this chapter, the concept was explored through the rough prototyping of a direct recycling machine using the robotic arm platform. The goal was to allow a user to have the experience of converting their trash into a designed product of their choice, all in a single machine operation. The motivation behind this project was to look at alternatives to centralized recycling and manufacturing. Instead of collecting and sending out

recycling to a central facility and then having another centralized manufacturing factory send out their products to a store, the concept of direct recycling allows both of these processes to happen at distributed locations. This would save an enormous amount of embodied energy due to the reduction of transit and labour. In addition, the machine encourages recycling through a tangible reward and enables distributed manufacturing.

Direct Recycling Prototype Machine

A prototype 3D printer that uses recycled materials as feedstock was designed around the common thermoplastic high-density polyethylene (HDPE). HDPE was selected as it is commonly found in beverage container products and it has a low melting point. Used milk containers were standardized as the source material to reduce material variability. The direct recycling system is built around three components: a shredder to reduce scrap HDPE into a uniform shard size, an extruder to melt and extrude the HDPE, and a delivery system to move the extruder around programmed tool paths to print the desired object.

Feedstock shredder

In order to use scrap plastic as a printing medium, the input material has to be reduced to a small size to be able fit inside the melting chamber and extruder. A shredding mechanism from a standard diamond cross cut paper shredder was used for this purpose (Figure 90). HDPE milk containers were flattened and run through the shredding mechanism to produce plastic shards sized around 5-10 mm. Paper from the milk label was left in the mixture but could be removed through a blowing or washing operation if desired.

Figure 90. A piece of an HDPE milk jug is inserted into the shredding component of the direct recycling process to facilitate a uniform recycled feedstock for 3D printing.

Extruder

A plastic print head was constructed to melt down the shredded plastic and extrude a bead of molten HDPE. The extruder uses an auger to feed the shredded HPDE particles from a funnel hopper into a heated melt chamber. A 12V motor with attached gearbox and a speed controller drove the auger bit. The assembly is seen in Figure 91. Similarly to the ABS print head described in Chapter 4, a Nichrome heating element is used with a thermocouple to maintain a desired melt temperature. The temperature is regulated through a solid-state relay and an Arduino microcontroller. For the HDPE plastic, a temperature of 150 °C was experimentally found to produce the best results. The print head could be used for other thermoplastics by altering this set temperature. An aluminum turned nozzle controls the bead width of the molten plastic being extruded. The bead width, along with the layer height, controls the resolution of the printed objects. For this experiment, a nozzle width of 5 mm was used, though smaller nozzles could be used for better resolution.

Figure 91. The extruder system for the direct recycling prototype uses an auger bit to force the material from the hopper into the melting chamber and nozzle.

Delivery System

The KUKA robotic arm was used as the delivery system for the extruder, which was mounted to the wrist faceplate as an end effector (Figure 92). The programming of the arm uses the same code workflow as for the ABS 3D printer described in Chapter 4.

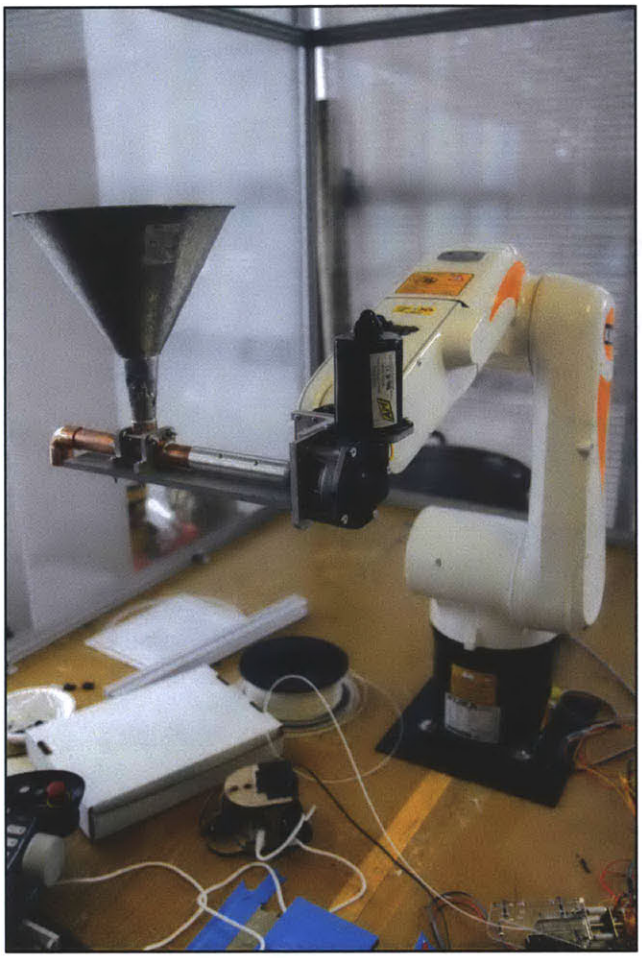

Figure 92. The robotic arm and extruder system for the direct recycling prototype.

Results

The HDPE print head successfully printed parts using ground milk containers as a feedstock. Facilitating direct recycling, a user can grind a milk container using a standard paper shredder and place the shredded particles into the hopper of the extruder head (Figures 93). Due to the large nozzle size (5 mm), one of the main issues was thermal stresses and cooling rates. Warping of the initial printed layers was noticed in early iterations and was improved through the use of a heated print platform. Another issue noted was the extra vibrations incurred when the rotating auger sheared plastic grounds.

This offset the extruder head slightly and reduced the accuracy of the printed parts. A sample print test is seen in Figure 94.

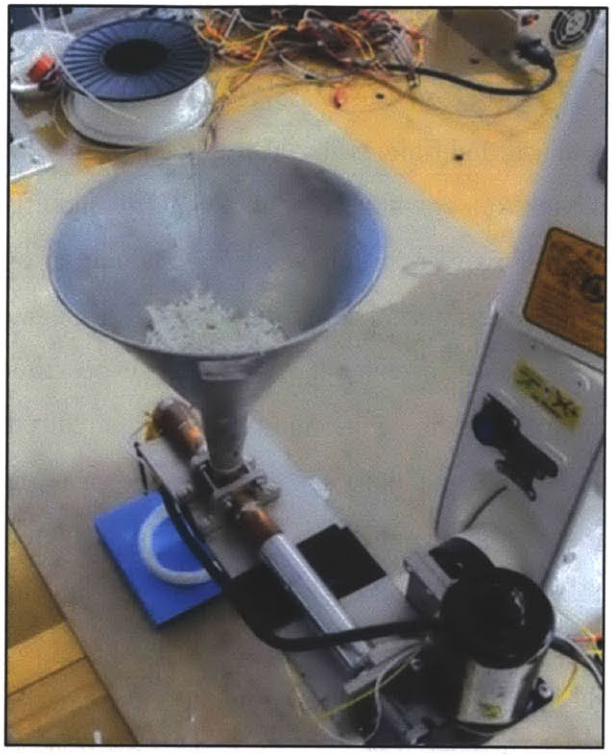

Figure 93. Shredded HPDE particles from used milk jugs are held in the hopper and extruded to print new objects.

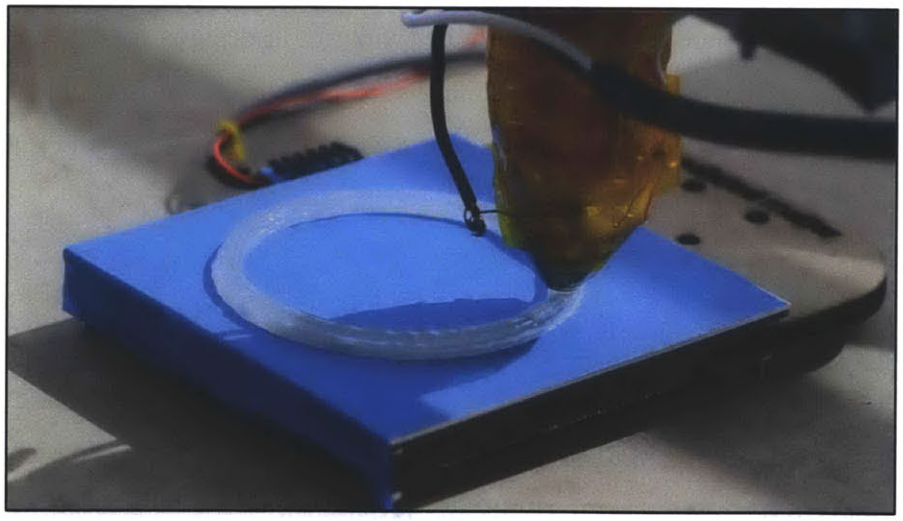

Figure 94. A print test shows the molten HPDE being extruded onto the heated build platform. The layer consistence was affected by the vibration of the auger bit and small pieces of label paper from the milk jugs.

Discussion

The direct recycling printing experiment is a strong visual demonstration that emphasizes the ability and strength of recycling. A discarded object can literally be transformed into any arbitrary shape or design before a user's eyes. The concept of direct recycling saves the step of transporting discarded objects to a centralized facility and the transport of the finished recycled good back to a consumer. From an energy and efficiency viewpoint, the concept is very attractive. However, the present implementation of direct recycling as a single step process incurs several challenges that currently relegate the piece to a more artistic and representative proof-of-concept. As there are no filtering mechanisms, the printed material is an amalgamation of the input-recycling stream that yields inferior and inconsistent properties. In fact, the output parts from the printing tests contain bits of paper that can jam the nozzle and interfere with layer consistency. This filtering issue would also be useful to sort HDPE materials from other recyclable materials that cannot be directly printed. Another issue noticed was the extrusion rate was difficult to control due to different sizes of shredded input material passing through the auger feed at various rates. Both issues point to the idea of converting the recycled material into a filtered, uniform feedstock as an initial step before input into a 3D printer. This notion of a two-step method offers more process control and could be implemented in future iterations of the design. Currently, there are several groups working on designs for converting waste thermoplastic shreds into a uniform feedstock, such as Recyclebot (Baechler & Pearce, 2011). If successful, these machines will allow for a more uniform feedstock that can be used in a variety of 3D printers.

Conclusion

In summary, the direct recycling machine provides a unique example of how distributed recycling could work in the future. While the prototyped machine was fairly simplistic and only capable of a single thermoplastic type (HDPE), the machine made the recycling process clear, apparent, and understandable to users. The robotic arm platform as a direct

recycling system functioned properly and objects were printed from recycled plastic. While a gantry-system could be used for this purpose, the robotic arm system allowed a large print volume and an unimpeded view for users. For the first time, people could take their waste containers and direct recycle it into a new digitally designed form in front of their eyes. The implications for direct recycling in the future are significant, especially as energy and material costs continue to increase. Imagining a world where products can be printed and recycled into new products directly at distributed locations offers many benefits over the current centralized model. In order to make that reality a possibility, vast improvements in 3D printers, software, user interface and materials need to occur, but the field is rapidly advancing.

Chapter 9: Jammable System Design and Fabrication

"I hope you're jammin', too."

— Bob Marley

Introduction

Manufactured parts are typically made from a single homogenous material with properties that do not change over time. In analyzing the differences between man-made materials and natural materials, these two characteristics – gradient structures and time-varying properties – stand out. Taking a look at natural materials, such as bone or muscle, these characteristics are very apparent and functional. For instance bone, with its radial density gradient, creates a stiff and strong structure without the added weight of a fully dense structure. In addition, bone has time-varying properties such as the ability to heal cracks and redistribute material and structure according to loading. Chapter 6 investigated functionally graded materials that utilized gradients of material properties spatially distributed in a part to enhance functionality. This chapter investigates a time-variant material system where stiffness and strength can be dynamically controlled using the mechanism of granular jamming. This effect is used in various design and fabrication prototypes and can be used alongside a robotic arm to facilitate digital casting or used within robotic arms as a structural and control mechanism.

When granular media is put under external pressure, the particles are compressed together and the system as a whole becomes jammed, as the particles are unable to freely slide past one another. This natural phenomenon is referred to as granular jamming and occurs in many natural systems (Liu & Nagel, 1998). In this chapter, the term 'jamming' or 'jammable system' will refer to this granular media transition between a liquid-like state and a solid-like state, with the controlling factor being the amount of external pressure applied to the granular system. Most people are familiar with jammed granular systems, even if they are not familiar with the term or inner workings. As a person walks

on a sandy beach, the free-flowing sand becomes jammed underneath the foot of the person and the jammed sand supports the person's weight. Another common example is vacuum-packed coffee bags. One a vacuum-packed bag of coffee is opened; the bag becomes much less stiff as the jamming pressure from the vacuum is removed once the seal is broken. Jamming occurs on many scales in nature, such as the microscopic jamming of molecules to form an amorphous glass instead of a crystalline structure and the macroscopic jamming of cars during a traffic jam (Liu & Nagel, 1998).

The increase in system stiffness under jamming pressure is due to the friction and Van der Waals forces increasing between particles when the system is compressed. As well, the physical shapes of the grains play an important role due to physical locking of particles against one another. In the beach sand example above, there would be a large difference in the jamming characteristics between a fine sand beach and a larger pebble beach. Likewise, if the sand beach were made of perfect spherical grains of sand, the jamming characteristics would be significant different as the spheres would be able to slide past one another with less force. In jammed granular structures, the grain shape, size, material, and external jamming pressure all influence the structural characteristics of the resulting system. The specific mechanisms and physics of jammed granular systems are under significant research in the current literature (Lu, Brodsky, & Kavehpour, 2008; Ludewig, Vandewalle, & Dorbolo, 2006; Corwin, Jaeger, & Nagel, 2005).

For this work, jamming is looked at from a design and fabrication perspective. As the jammable system is a closed system (with the exclusion of air), the changeable geometry falls into the formative fabrication category. Jamming is a unique type of formative process, as the material can be easily reset and reformed into a new structure by controlling the jamming pressure. In this sense, jammed granular systems can be compared to tunable clay that responds to external pressure through system rigidity.

Jamming has been studied as a component of soil mechanics in civil engineering for many years, but only recently has jamming become an area for design. In 2010, a jammable robotic gripper was introduced by a team from University of Chicago, Cornell

University, and iRobot (Brown, et al., 2010). The developed gripper allowed complex gripping control of complex foreign objects through a single, simple, and low-cost device. Following the introduction of the gripper, significant interest around jammable systems in design has emerged and applications in architecture, medicine, and robotics have been investigated (Huijben & Herwijnen, 2007; Loeve, Ven, Vogel, Breedveld, & Dankelman, 2010; Steltz, Mozeika, Rembisz, Corson, & Jaeger, 2010). However, the design field around jamming is still very experimental and lacking in design guidelines and scope.

In this chapter, mechanically jammed system characteristics are analyzed to determine suitable design parameters for engineering applications and a number of potential product fields are investigated with novel prototypes. The applications and developed prototypes include structural uses, fabrication uses, and artistic/aesthetic/toy uses for jammable material. More specifically, the structural inventions developed consist of jammable furniture, mechanical joints, conformable vices, and floors with controllable stiffness. The fabrication techniques outlined focus on a mould-making technique for casting objects and use of jammable materials for producing robotic arms. Finally, the artistic/aesthetic/toy applications focus on a reconfigurable sculpting technique and an optical effect where the granular media is transparent and a light source is present.

System Architecture

Granular media (for example, sand), will readily display macro-scale properties of a liquid, such as the ability to flow when agitated and assume the geometry of a container holding the media. However, when an outside jamming pressure is applied to the granular media, the interparticle forces (mainly friction and Van der Waals) increase and the granular system displays solid-like properties such as rigidity and a defined shape. This results from the formation of force networks throughout the jammed media that can support external loads as seen in Figure 95 (Tang & Behringer, 2011).

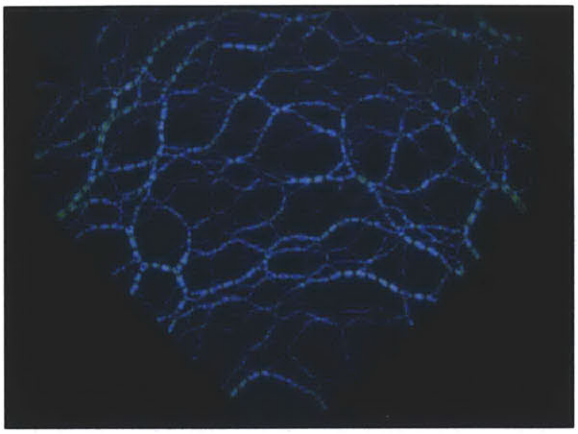

Figure 95. Jammed granular force networks are imaged using photoelastic disks to show which particles are load-bearing. Image source: Tang & Behringer, 2011

There are several ways of generating a jamming pressure, such as mechanical pressure, gravity (as seen in the hopper example), air pressure, or other fluid pressures. The systems described in this chapter primarily use air pressure to create a jammed granular system, though other pressure-generating methods could be used. The basic jammable system is shown in Figure 96 and uses a vacuum pump to create a pressure difference to establish the jamming force.

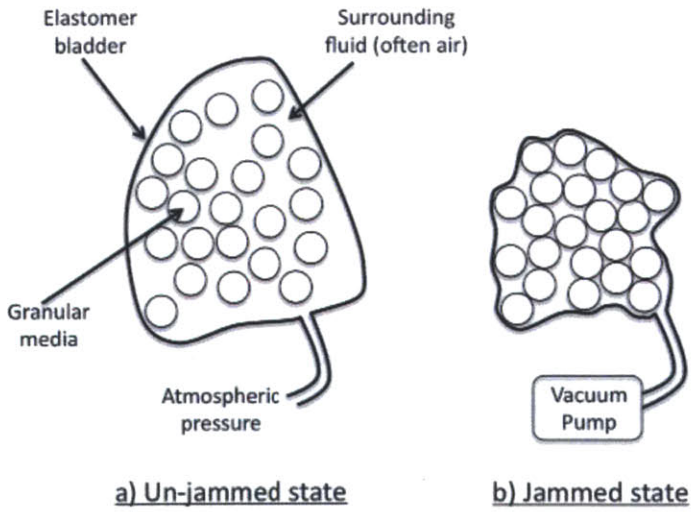

Figure 96. A diagram illustrating the basic concept behind using granular jamming for designed systems. An elastomeric bladder containing particles (a) can be jammed by applying vacuum pressure (b) to pack the particles together and increase frictional forces.

An elastomeric bladder contains the granular media and allows for a vacuum to be established, as air does not readily penetrate through the bladder. In the unjammed state (a), the granular media is not under a net pressure difference and the grains can readily slide past one another, creating an easily deformable shape. Upon the application of vacuum pressure applied to the bladder, the grains are packed tightly together due to the weight of the atmosphere and the increased forces between grains create a rigid system where it is difficult to have grains sliding past one another. This densely packed state with an applied pressure is referred to as the jammed state (b). The mechanical properties of the jammed system (i.e. strength, stiffness) depend on the pressure applied, as well as on the particle geometry, material, and surface friction. Particles with irregular surfaces and high surface friction will result in a jammed system with higher rigidity. The use of smoother particles will have a lower jammed strength, but will also flow easier when in the unjammed state. A variety of granular media, such as sand, beads, or other small particles can be utilized in a jammable system. As well, other fluids instead of air can be used both inside the elastomeric bladder and the outside the elastomeric bladder to achieve different properties. For example, water could be used to achieve higher external jamming pressures; this would result in increased system rigidity.

A block diagram of a jammable system is shown in Figure 97. Adding a control loop to the basic elastomeric bladder and enclosed granular media allows for automated control of the jamming state. A pressure sensor inside the bladder can provide data to a microcontroller to allow for a vacuum pump to reduce the internal pressure to a certain level and create a jammed state when desired. A vacuum reservoir is an evacuated tank that acts as a buffer in order to reduce the time that the vacuum pump has to operate. Control valves regulate the pressure inside the jammed system, which controls the rigidity of the system.

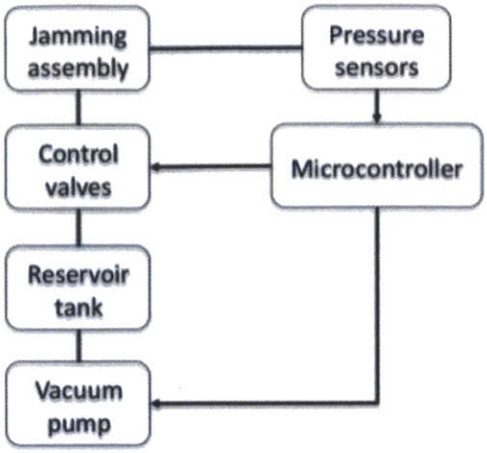

Figure 97. A block diagram showing the basic system architecture of a controllable granular jammed system.

The design factors of jammed material systems are investigated below to provide insight into the overall system properties and dependence on pressure and material type.

Material System Characteristics

To understand the material properties of jammed system for use in design, a number of experiments were conducted to characterize a number of common granular materials and the effects of grain size and applied jamming pressure.

Methods

To understand the qualitative properties of the jamming effect and get a sense for the basic construction techniques, several jammable cylinders were fabricated with different elastomers and granular media (Figure 98). These cylinders were cast from two-part silicones (Smooth-On EcoFlex and Vac Bag Silicone) using cylindrical moulds. Sand, glass beads, and metal jacks were used to fill the cylinders and air tubes were added before sealing the cylinders with silicone caulking. A small fabric filter on the end of the

air tubes was applied to prevent the granular media from being sucked up into the tube. One of the cylinders was fabricated with a removable metal cap to allow different granular media to be tested.

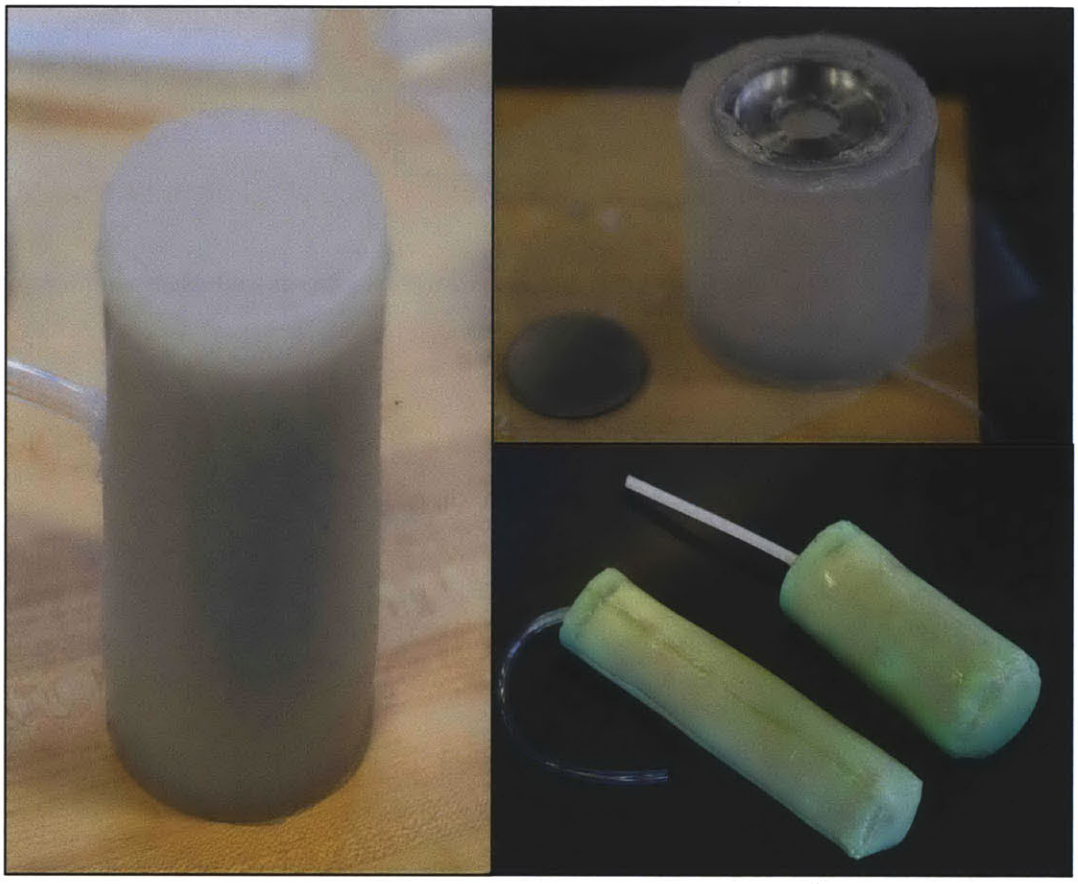

Figure 98. Different test cylinders were fabricated using various silicones to determine the qualitative properties and construction techniques of jammable devices. The top right cylinder has a removable metal cap for experimenting with different granular media.

The constructed elastomeric cylinders were attached to an electric vacuum pump and different levels of vacuum were pulled to investigate the effects of jamming in the cylinders. An Instron testing machine was utilized to quantitatively measure the material system characteristics at different vacuum pressures.

To reduce the effects of the elastomeric bladder on the measured properties and standardized the testing, an experimental setup based on ASTM D2850, the unconsolidated triaxial compression test, was developed. Instead of the thicker silicone, an extremely thin membrane was desired to reduce the effects of the elastomeric skin on the measurements of the granular jamming properties. Prophylactic latex condoms served this purpose well. Ends caps were machined from aluminum and a support stand to ensure uniform size and filling was printed on an Objet 3D printer (Figures 99 and 100). The size and shape of the support stand created the shape of the jammed cylinder, which was 4 inches tall with a diameter of 2 inches to provide the correct 2:1 height to diameter ratio.

Figure 99. Aluminum end caps were fabricated for compression testing granular samples. The bottom cap has an air line to apply vacuum jamming pressure and a canvas filter to prevent grains from entering the air line.

Figure 100. A support stand was 3D printed to give the granular samples a standardized shape and volume for compression testing. Vacuum lines were used to ensure the latex bladder was pulled to the shape of the support stand.

The sample preparation procedure began by assembling the support stand and stretching a prophylactic condom (with the top cut off to create a latex tube) inside the support stand to create a tube. The bottom aluminum end cap was then placed on the end of the assembly, to create a container to pour the granular material inside. A vacuum was pulled between the support stand and the latex to ensure the latex took the exact form of the support stand. The granular material was then poured inside and loosely packed by tapping on the side of the assembly. The top end cap was then attached and the ends of the latex tube were unrolled onto the support stands and rubber bands secured the latex to the ends of the aluminum caps (Figure 101a). A vacuum was then pulled inside the latex tube via a air line running through the bottom aluminum end cap and filtered with a piece of canvas cloth. The support stand was then removed, leaving a cylinder of jammed media encased in thin latex ready for mechanical testing (Figure 101b).

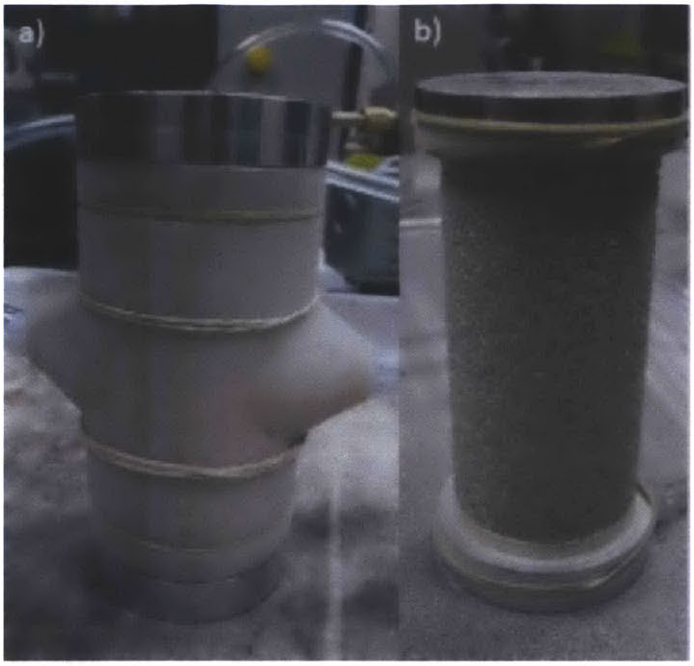

Figure 101. The support stand was used to give the sample a standardized shape (a), which was maintained by vacuum pressure after the support stand was removed (b). The sample seen in (b) consists of glass spheres.

During testing, a FJC vacuum pump with a brass ball valve and vacuum gauge were used to control the jamming pressure. Compression tests occurred at a strain rate of 2 mm/min and continued for a displacement of 15 mm or until the force-displacement curve flattened. Samples were jammed using differential vacuum pressures of 25, 50, 75, and 100 kPa. The compression test setup in seen below in Figure 102.

Figure 102. A compression test of jammed coffee using the test setup for granular jamming characterization.

Materials that were tested included coarsely ground coffee, finely ground coffee, sawdust, glass spheres, hollow glass spheres and diatomaceous earth. To investigate the effects of grain size, different sized glass spheres were tested. The diameters tested were 300-425 um, 800-1200 um, 1500-2000 um, and 2000-2500 um. The different materials were imaged using an optical microscope to view the grain size and shape (Figures 103 and 104). The measured sizes of the glass beads are listed in Table 3.

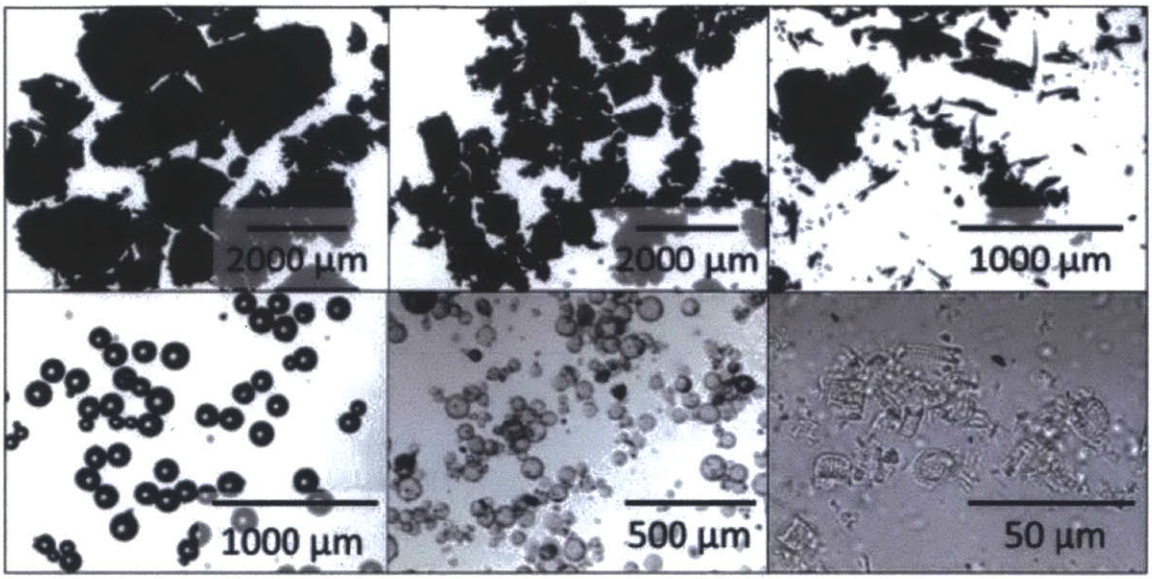

Figure 103. The different granular materials were microscopically imaged. Top row, left to right: coarsely ground coffee, finely ground coffee, sawdust; bottom row, left to right: solid glass spheres, hollow glass spheres, and diatomaceous earth.

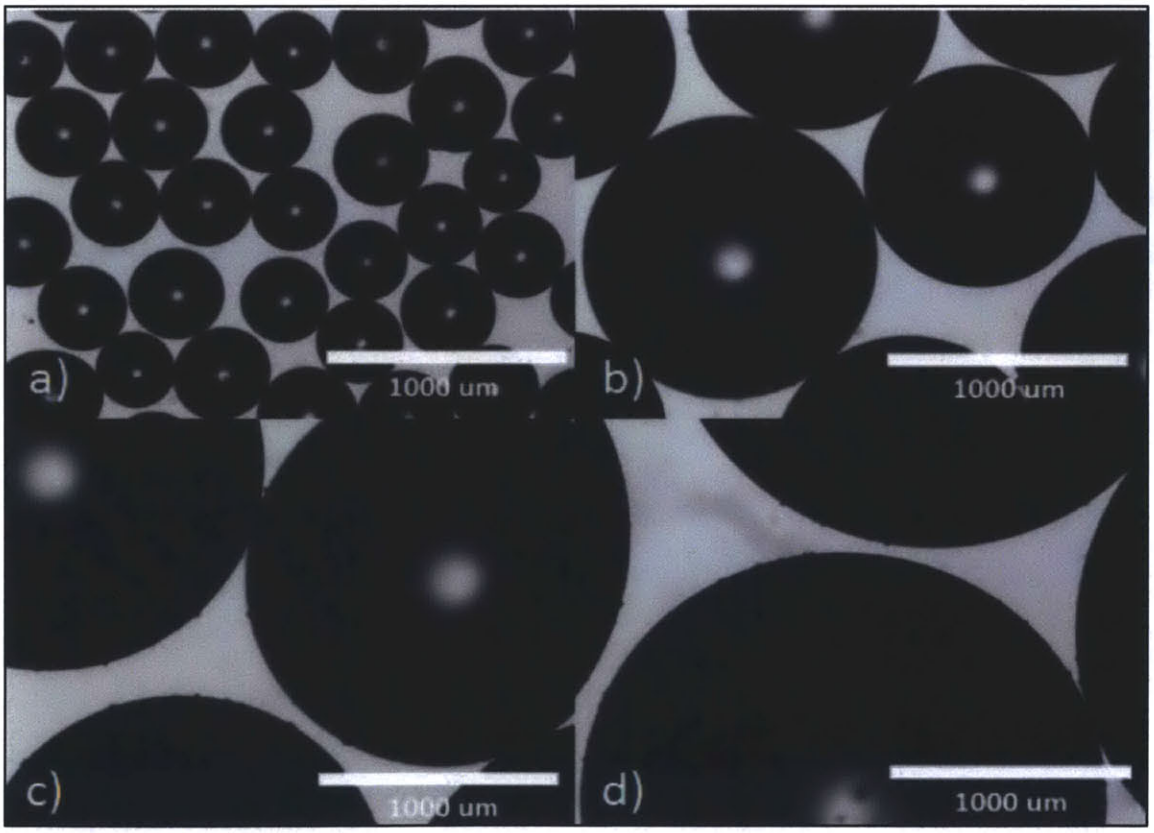

Figure 104. The different sizes of glass spheres were imaged to determine exact size and distribution.

Table 3. The nominal size of the glass spheres as provided by the manufacturer and the measured size from microscopy.

Nominal Size (um)	Measured Size (um)
300-425	349 ± 22
800-1200	1071 ± 112
1500-2000	1775 ± 201
2000-2500	2239 ± 149

The mechanical testing of the jammed granular materials was completed in collaboration with Nadia Cheng, a fellow mechanical engineering graduate student, and Shaymus Hudson, an undergraduate research assistant in the Mediated Matter group. Shaymus' thesis on mechanical testing of granular materials contains further details on the conducted compression tests (Hudson, 2012).

Results

The compression test results on the varying sizes of glass beads are shown below in Figures 105 and 106. Both yield stress and Young's Modulus are well represented by a linear dependence on applied jamming pressure.

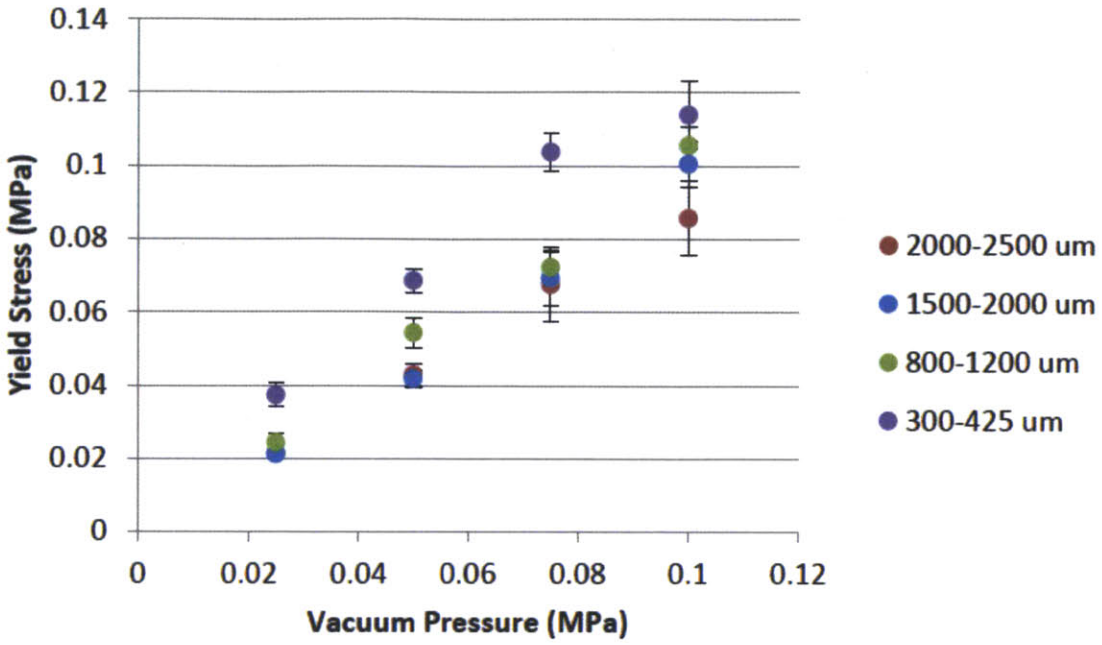

Figure 105. Plot of yield stress vs vacuum pressure for the different sizes of glass spheres.

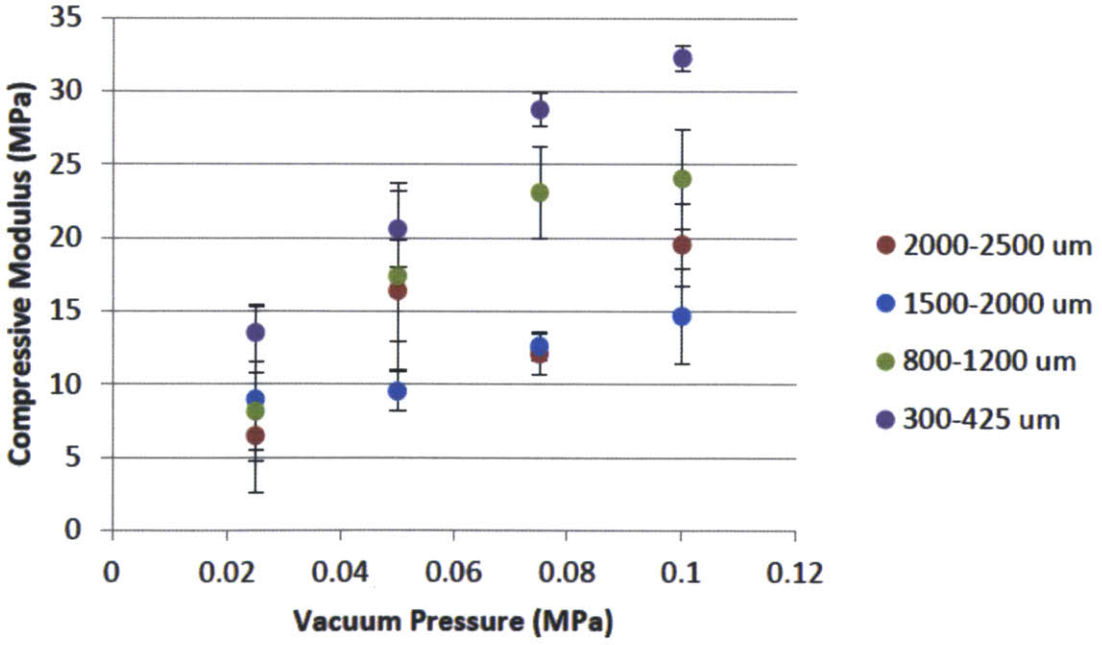

Figure 106. Plot of Young's modulus vs vacuum pressure for the different sizes of glass beads.

Yield stress was also influenced by the size of the spheres and showed a linear dependence (Figure 107). Compressive modulus also varies with size, but a clear linear dependence was not observed (Figure 108).

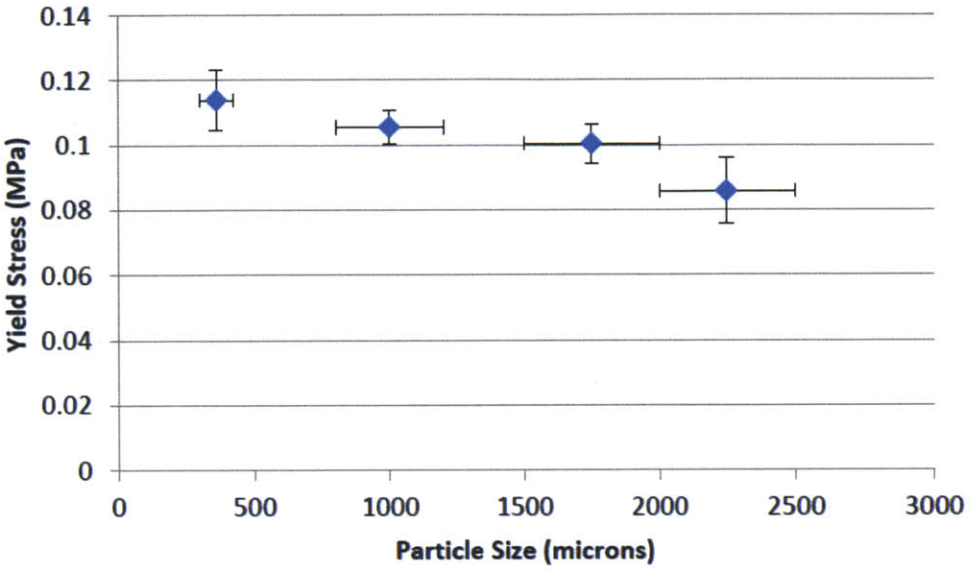

Figure 107. Plot of yield stress vs particle size for the glass spheres tested in compression.

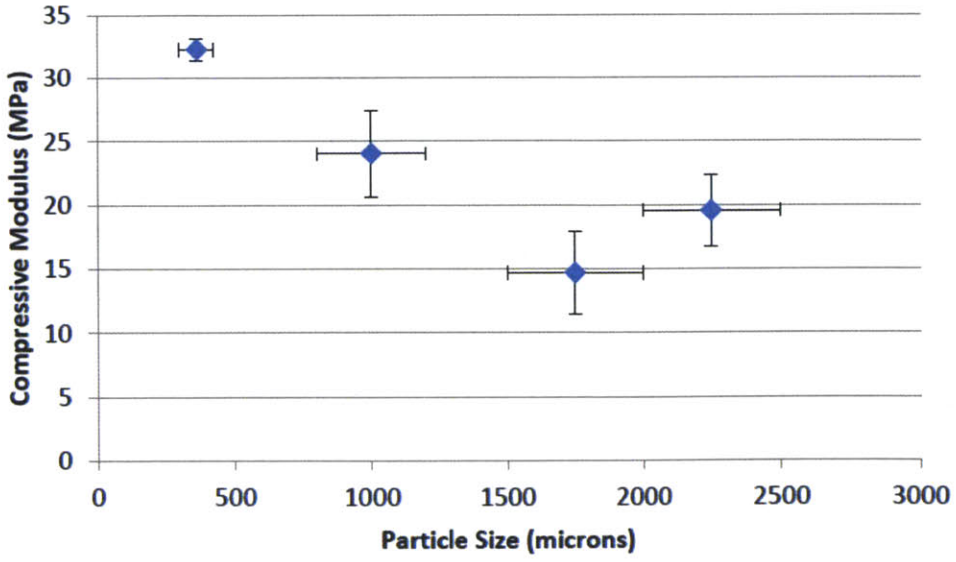

Figure 108. Plot of Young's modulus vs particle size for the glass spheres tested in compression.

Comparing different granular media resulted in the results shown below in Figure 109. For design purposes, often the important properties are effective modulus and also the effective modulus per unit mass, both of which are calculated in Table 4.

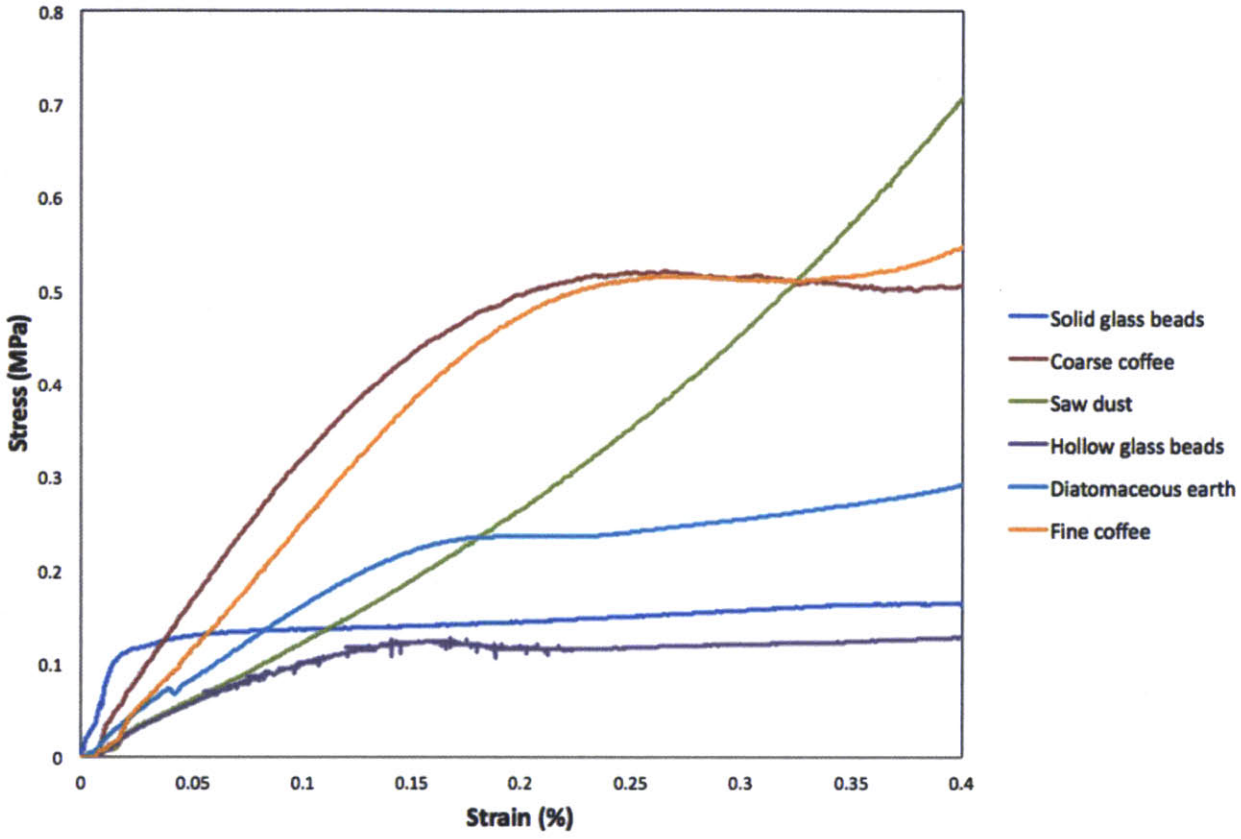

Figure 109. Plot of stress vs strain for different granular materials tested in compression at a differential vacuum pressure of 75 kPa.

Table 4. Density and modulus values found for different jammed granular materials at 75 kPa differential pressure.

Granular Media	Density (kg/m^3)	Modulus (MPa)	Modulus/Density (kN*m/kg)
Hollow glass beads	83.0	1.1	12.8
Coffee (coarse)	445.5	3.0	6.8
Solid glass beads (100 micron)	1443.5	8.5	5.9
Coffee (fine)	505.5	2.7	5.4
Saw dust	397.5	1.7	4.2
Diatomaceous earth	484.1	1.5	3.1

Discussion

The results of the materials testing on the glass beads showed a linear trend between jamming pressure and yield strength. As well, a linear trend between jamming pressure and compressive modulus was observed. This agrees with the qualitatively observations and theoretical simulations (Somfai, Hecke, Ellenbroek, Shundyak, & Saarloos, 2007). The dependence of modulus and yield strength on jamming pressure is a result of the increased frictional forces, which is a product of the normal force and the coefficient of friction. This relationship allows granular systems to have a controllable stiffness, directly related to the applied jamming pressure.

The negative relationship observed between the particle size and yield strength is potentially a result of a few different interactions. First, the glass spheres are a distribution of sizes, not strictly a single size. This distribution in sizes means that the smaller spheres will have a higher packing fraction and coordination number. This suggests that the higher yield strength is due to higher frictional forces between particles due to more contact area from the increased coordination number for the smaller sizes spheres. The impact of coordination number and packing fraction has been shown in the literature to have a positive relationship on strength and modulus (Somfai, Hecke, Ellenbroek, Shundyak, & Saarloos, 2007; Durian, 1995). The observations on compressive modulus can also be explained with the increased coordination number and higher packing fraction, however other effects may also be involved and explain the discrepant data point for the 1775 um spheres. More tests and data are needed to investigate the effects of grain size.

For design purposes, it is important to determine which type of granular material to use for different applications. The results from the materials testing showed the variability in compressive modulus and yield strength between different media. Often for design applications, the important properties are effective modulus and also the effective modulus per unit mass. Hollow glass beads were found to display the highest modulus per unit mass, however if weight is not critical, coffee is also a very good candidate for

jamming applications with a higher overall modulus than the hollow glass beads. Saw dust displayed a convex curve, indicative of a material that is collapsing and densifying, like a soft foam. This behavior indicates the sawdust is very porous and will undergo a large volumetric change before jamming, in contrast to the other materials. This characteristic makes sawdust a poor candidate for jammable designs, as the compressibility does not give a fast jamming response and the compressed sawdust is difficult to return to a flowable state after the jamming pressure is removed. Sawdust made from a harder wood or larger grain sizes of sawdust would likely perform better.

The ability to reversibly transition between jammed and unjammed states was shown in this testing. The effect allows for a system's rigidity and geometry to be controllable, which is implemented in several applications as discussed below.

Design Experiments Using Jammable Systems

With the system characteristics and properties in mind, a number of design applications were explored for jammable materials. These investigations and early prototypes demonstrate a wide range of areas for jamming applications, indicating the potential for tunable stiffness systems.

Structural Applications

Granular materials can be jammed into a solid-like state that can support both dynamic and static structural loads. In addition, the granular system can be tuned by controlling the jamming pressure to attain a desired rigidity or a specific shape. This concept is investigated for structural purposes through the creation of several prototype applications: a tunable joint, a robot arm, soft jaw vice grips, and a morphable chair.

Tunable Joint

The first structural utilization investigated was a joint where the number of joint arms and the degrees of freedom are unconstrained until a jamming pressure is applied. This joint was made using joint arms that have one end inside of a bladder containing a granular media (Figure 110). Upon the application of a jamming pressure (via an air tube), the joint become rigid and all degrees of freedom are constrained. In addition, the joint has tunable stiffness (as the stiffness varies with pressure), and can be used for active dampening applications as well. The joint can have any number of arms that can fit within the bladder. The ends of the joint inside the bladder can have a rough shape in order to increase friction and the strength of the joint. As well, the arms can be loosely interlocked (like a hook and ring interlock) in order to prevent an arm from being torn out and to improve strength. The prototyped joint proved very strong and could be rapidly switched between being jammed and unjammed. This style of joint can transmit all types of mechanical movement (rotational, translational) about all axes. The working prototype was constructed using common silica sand as the granular media, a silicone bladder, three brass joint arms, and a tube with a sand filter (Figure 111). This low cost joint could be useful in a variety of applications from robotics to earthquake dampening in buildings.

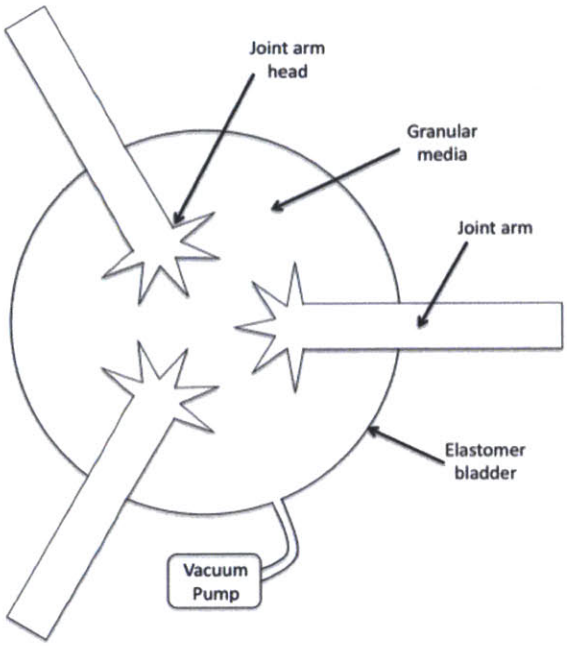

Figure 110. Diagram detailing a jammable joint which allows degrees of freedom for the joint arms to be constrained with controllable pressures.

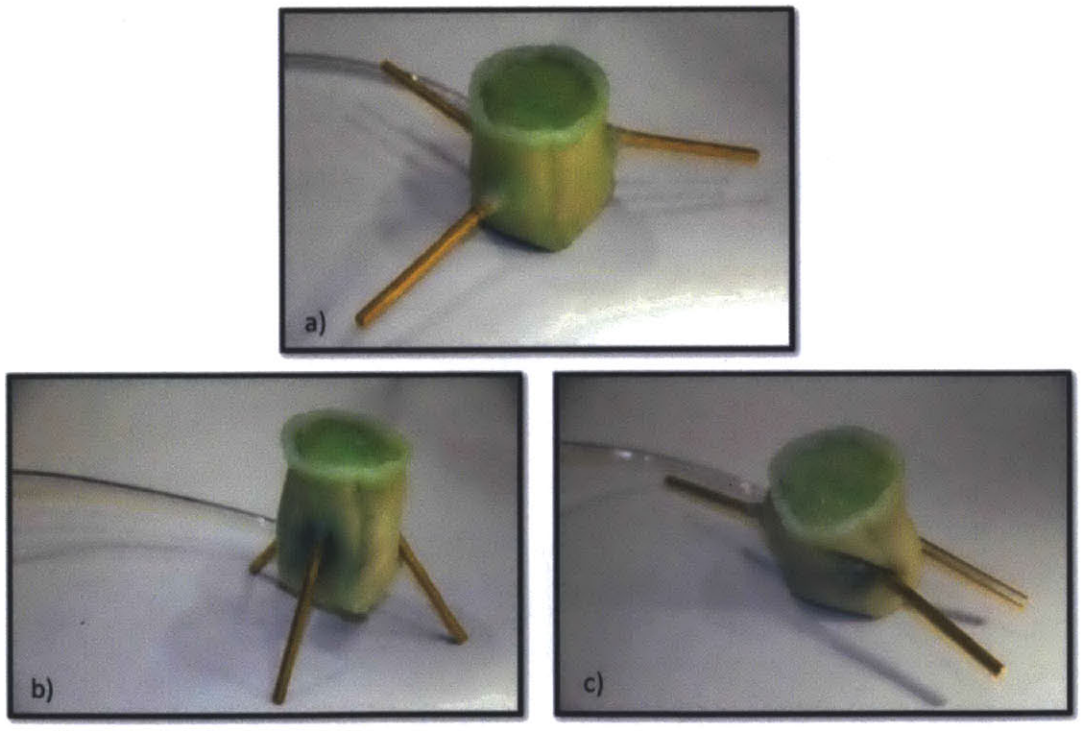

Figure 111. A prototype jammable joint that can be in a relaxed, flexible state (a) or jammed in different configurations (b and c).

Morphable Soft Jaws for a Vice

Jammable systems allow for custom shapes to be easily formed and held with impressive strength. This combination is well suited for devices that hold irregularly shaped objects. One practical implementation explored was a pair of soft jaws which attach to a regular vice in order to hold objects securely and prevent indentation damage from the typical gripping teeth. These soft jaws can be very useful in machining, where the traditional method of holding oddly shaped parts is to mill out aluminum blanks in order to hold the part properly. The jammable soft jaws can be jammed using vacuum pressure and then further mechanical pressure from the vice results in an even higher jammed strength. A working prototype was constructed using a fabric-impregnated silicone bladder (the tough fabric improves puncture-resistance), common silica sand as the granular media, and a tube with a sand filter (Figure 112). The soft jaws were used in various qualitative holding tests including milling aluminum as seen in Figure 113. The jaws performed well and a smooth cut was obtained. A workshop is ideal for a jammable system since an air supply can provide an easy access point to vacuum pressure through an inexpensive Venturi nozzle.

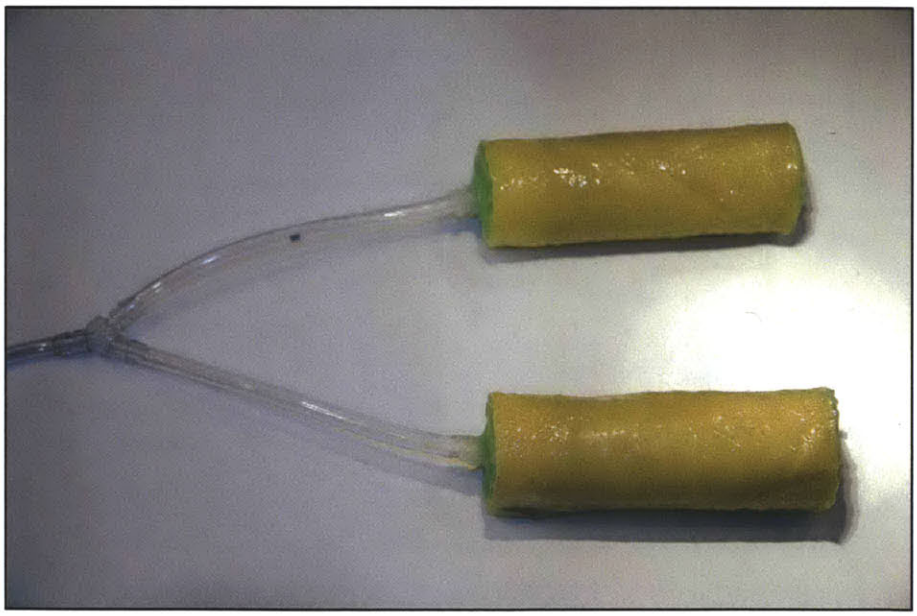

Figure 112. Prototype jammable soft jaws used to hold odd shaped parts securely in a vice.

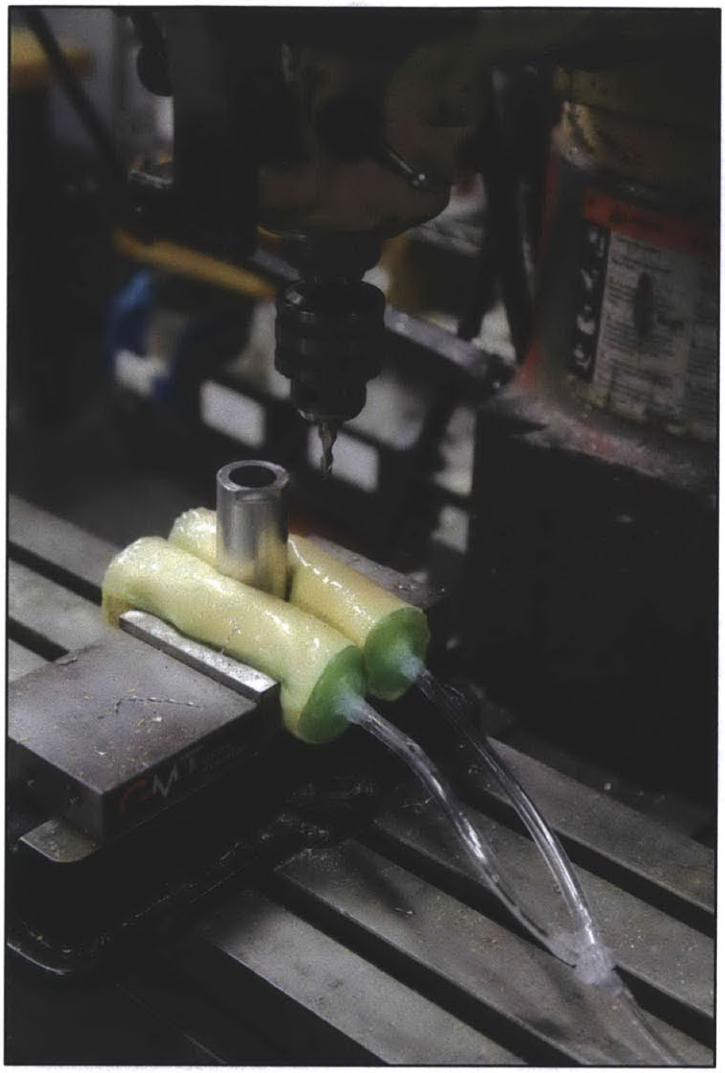

Figure 113. The jammable soft jaws being used to secure an aluminum tube for machining.

Morphable Furniture

A chair was produced which, when unjammed, is completely flexible and can be arranged into any custom configuration of shapes and angles, and then through the use of jamming pressure, the chair can be 'frozen' in any particular configuration and can support a person's weight (Figures 114).

Figure 114. Jammable chair that is flexible when not jammed (left) and rigid when a vacuum pressure is applied (right).

Once jammed, the system does not require further energy input, except to periodically maintain the vacuum pressure as some air does slowly diffuse through the elastomeric bladder. This allows for pieces of furniture to be arranged in any position imaginable and then jammed and locked into place (Figure 114). The chair was created using common silica sand as the granular media and a high strength silicone elastomer as the bladder. Figure 115 shows the mould used to create the elastomeric bladder for the chair. Sand was used as the granular media due to its low cost, high friction, and irregularly shaped particles, which result in a high-strength jammed system. Other granular media, such as coffee or ceramic hollow microspheres, could be used to make the chair lighter and maintain similar strengths. The chair's silicone bladder was cast and the sand was added

before sealing the sand inside and attaching a tube to allow for vacuum pressure to jam the system. The tube provides a pathway for the air to be removed from inside the chair, creating the pressure difference that jams the system. In order to prevent sand from entering the tube, a small cloth filter is used to allow air to pass through while holding the sand back. An interesting feature of jammable structures like the chair is its ability to remove dents. If an object strikes the jammed chair, the impact energy is absorbed by the structure through the formation of a dent. To remove the dent, positive pressure can be applied to the chair (essentially blowing the chair up) and then a vacuum can be reapplied to re-jam the system. The dent is quickly removed as the granular media flows back into the region of impact when positive pressure is applied. This combination of infinite geometric configurability and dent-removal makes the range of structural applications quite vast.

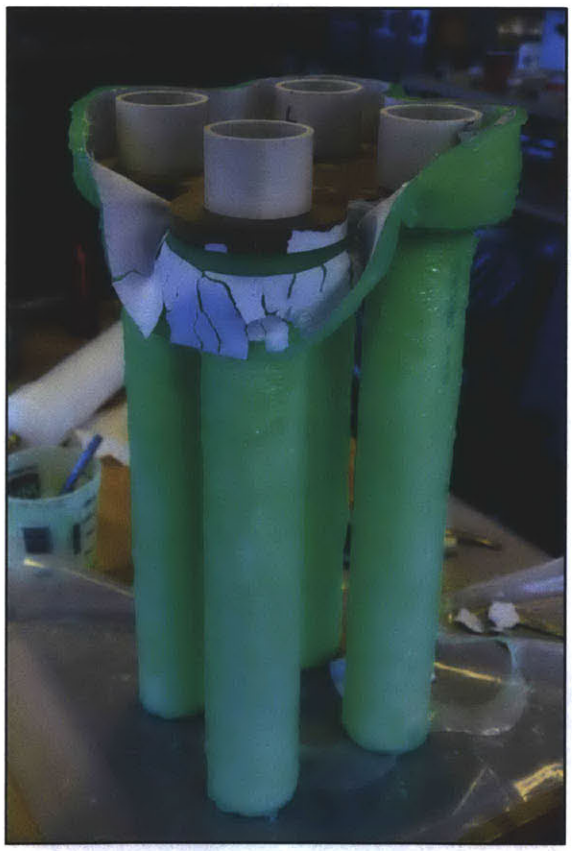

Figure 115. The jammable chair was fabricated by painting a two-part silicone onto a form. Once cured, the chair was filled with sand and sealed with an air line and filter to allow jamming pressure to be applied.

Morphable Foam Floor

Most of the jamming systems described thus far utilize granular media within the elastomeric bladder. An interesting extension of the structural jamming concept is to use an open cell foam (such as a soft urethane foam) encased in an elastomeric bladder instead of a granular media. Upon the application of vacuum pressure to the inside of the bladder, the foam system decreases in volume until the foam pressure matches the external atmospheric pressure. This collapsed foam structure is much stiffer and provides a framework for floors that can vary in stiffness, either locally or globally. The air pressure into the foam floor tile dictates the stiffness of the floor. This could be useful for environments like a gym, where traditionally mats are needed to cushion a hard floor for various sports. Having an automated system would allow for fine-tuning of the stiffness of the floor. In addition, individual floor tiles can be separately controlled using a network of pneumatic valves, allowing for a type of large 3D display where each tile acts as a pixel. This controllable floor could also act to decrease injury by rapidly turning soft if a controller determines that a person is falling down. A working prototype foam floor tile is shown in Figure 116, in various states of compression due to vacuum pressure. In the unjammed state, the tile is very soft, while in the compressed state, the tile is significantly stiffer.

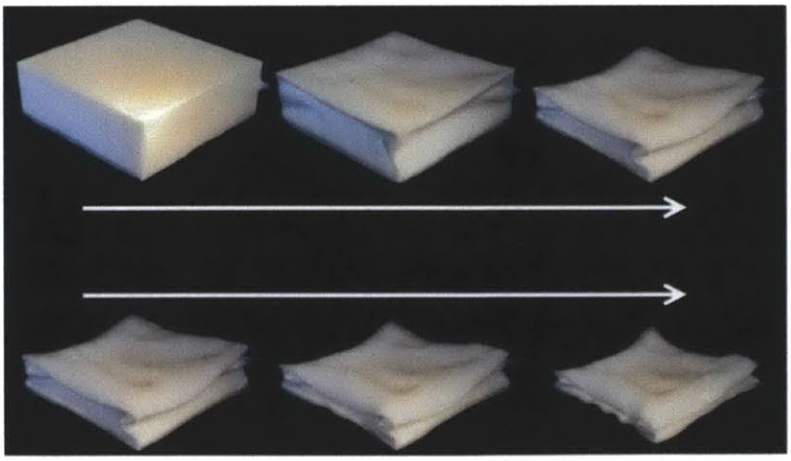

Figure 116. An open cell foam can be jammed by applying vacuum pressure and densifying the cellular structure. Here a polyurethane soft foam is encased in a silicone bladder and jammed.

Composite Jammable Media

Structural jammable systems typically need high strengths, which require granular media with high friction coefficients and irregular shapes. Experiments using composite granular media, meaning a mixture of different grain types, resulted in significantly different properties that could improve strength. To achieve a higher strength, small interlocking particles were mixed with sand (Figure 117). These interlocking particles (for example, metal jacks) formed lattice networks when jammed, which improved both the compressive and tensile strength immensely. Other interlocking shapes could be used for specific mechanical property improvements. X-ray tomography tests were conducted with a sand and metal jacks composite jammed system to view the volume fraction and interconnectivity (Figure 118). These early tests suggest that a rich field of granular composites, akin to fiber and particle composites in material science, could significant improve properties of jammed systems for specific applications. Further investigation and testing is needed to expand on this concept in the future.

Figure 117. Composite granular jamming, such as this combination of metal jacks and sand, could allow designers to create custom mixtures to achieve specific stress vs strain curves and other material properties. Sand and jacks were found to create a very strong jammed material due to the jacks interlocking.

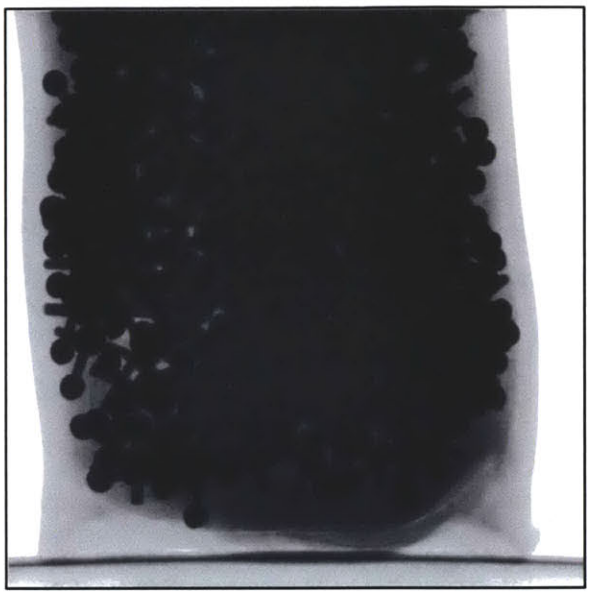

Figure 118. An x-ray image of a jammed mixture of sand and metal jacks shows the jacks interlocking with one another.

Fabrication Applications

Jammable Mould-Making

Another design avenue is fabrication. As jammable materials can maintain a shape very easily, the use of jammable materials for fabrication was explored through the creation of a rapid moulding/casting solution. Sand casting has been around for centuries, but the process is slow and messy. Using jammable materials and a flexible elastomer, an object can be pressed into the media and then once the system is jammed, the shape is retained and casting can be completed immediately. The use of an elastomeric bladder allows for quick casting of plastics and even low temperature metals, and de-moulding is simplified by applying positive pressure to pop the cast object out. This casting solution achieves similar resolution to a thermoformed mould, but requires no heat source, wastes no material, and is a faster technique. As well, the cost of a jammable casting system is a fraction of the cost of a traditional thermoforming system.

A working prototype system was developed and is shown in Figure 119. The system is comprised of a glass microsphere granular media, a thin soft elastomer (silicone in this particular prototype), a tube with a cloth filter to apply the vacuum pressure, and a vacuum pump.

Figure 119. A jammable device consisting of a silicone elastomeric bladder, glass media, and a small electric vacuum pump.

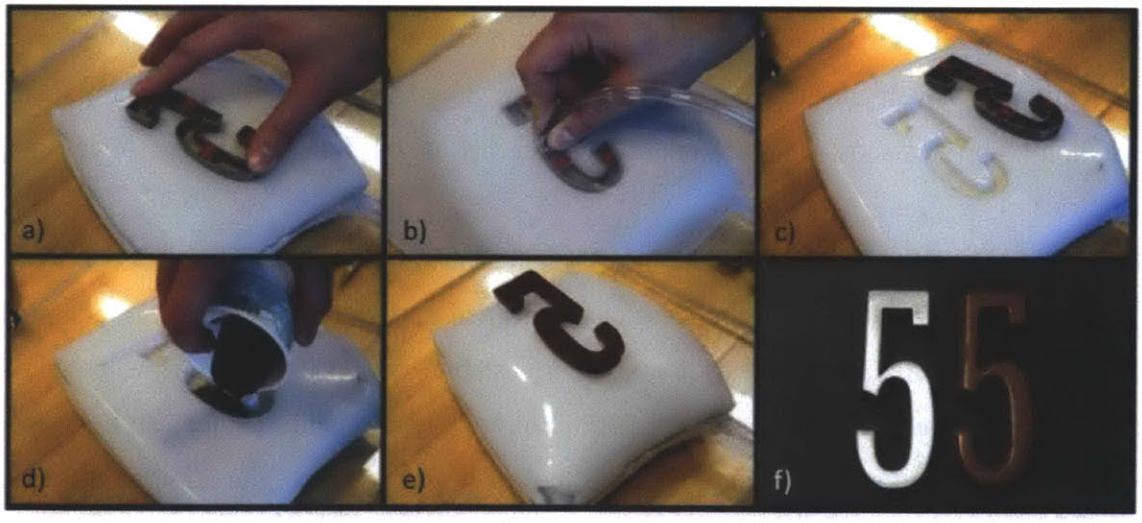

Figure 120. Casting using jammable materials involves depressing an object into the bladder (a), pulling a vacuum between the object and elastomeric bladder (b), pulling a vacuum inside the bladder to jam the granular media and make the mould (c), pouring a castable material into the mould, chocolate in this example (d), and using positive pressure to eject the casting (e). The final cast object is seen beside the original (f).

Figure 120 shows the entire process of replicating an object using this technique. First, the object is pressed into the unjammed elastomeric bladder that is filled with the fine glass microsphere media (a). A vacuum is then drawn between the elastomer and the part to be replicated, using a plastic sheet to create a seal (b). This plate could be substituted for another elastomeric bladder if a two-part mould were to be made. With a vacuum formed between the elastomeric bladder and the object, a second vacuum is drawn inside of the elastomeric bladder, jamming the granular media and creating a rigid mould. At this point, the plastic plate and the original object can be removed and the jammable media holds the shape of the object (c). Any type of casting material can then be poured into the resulting mould (d). In this figure, chocolate has been melted down and is being used as a casting material. Once the casting material has hardened, the cast object is easily de-moulded by applying positive pressure into the elastomeric bladder, which pops the cast object out of the mould (e). The final product, alongside the original part, is shown in (f). This method proved to be very rapid, inexpensive, and easy to complete. The resolution of this casting method depends on the size of the granular media (the finer the particle size, the higher the resolution), and the thickness of the elastomer (the thinner the elastomeric bladder, the higher the resolution). Fairly good resolution (comparable to thermoforming) has been achieved with this prototype, as detailed by sample cast objects in Figure 121. This replication method holds promise for many uses, from prosthetics fabrication to novelty ice cube/chocolate moulds, to hobby castings. In particular, the simplicity and low-cost of this method could be useful for projects in developing countries.

In addition to hand-casting, the process can be turned into a digital fabrication technique through the use of a robotic arm to impart a castable form. Using the same technique developed in Chapter 4 of a depressible sculpting tool, a jammable surface can be shaped into a form dictated by a compute designed tool path. In this sense, the jammable system can be viewed as a digital clay, able to be moulded and reset using air pressure.

Figure 121. Various castings produced with jammable moulds are seen. In the top, the left object is the original, the middle is a cast urethane copy, and the right shows a cast pewter copy. The bottom right key was cast in white urethane from the original key, seen on the left.

Jammable Robotic Arm

The concept of jammable joints was taken a further step by investigating an entire manipulator fabrication from jammed joint sections. A robotic arm consisting of segmented jammable sections were designed and actuated using tension cables (Figure 122). By controlling the stiffness of each segmented section using vacuum pressure and applying controllable tension in the cables, the robotic arm is capable of a trunk-like motility (Figure 123). The prototyped robotic arm has the benefits of cost, simplicity, and robustness compared to traditionally actuated manipulators. In addition, the jammable

materials provides compliance for human interaction, a unique conformable geometry, and impact-resistance due to the lack of solid parts. This jammable manipulator project was led by Nadia Cheng, a mechanical engineering graduate student, and more details on the design, construction, and testing can be found in a recent joint paper (Cheng, et al., 2012).

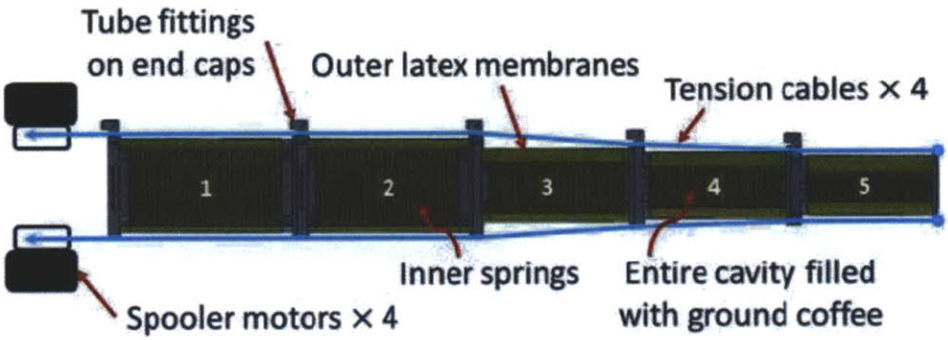

Figure 122. Diagram detailing the design of the jammable manipulator. Image source: Nadia Cheng

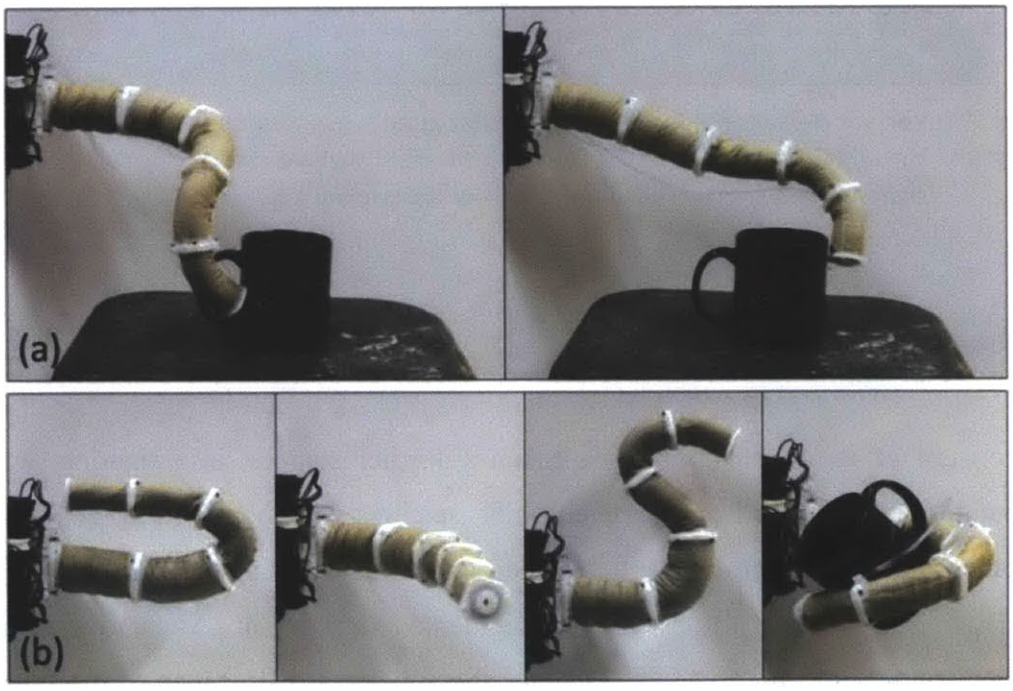

Figure 123. The prototype jamming manipulator can reach targets in a variety of paths (a) and maintain various rigid shapes. Image source: Nadia Cheng

Artistic, aesthetic, and toy innovations:

Artistic and aesthetic uses for jammable innovations exist due to the ability to have a structure with a reconfigurable geometry. A working desktop toy with the ability to have a jammable structure was constructed. The toy consists of small glass beads as the granular media, a soft silicone as the elastomeric bladder, an aluminum frame, an internal light source, and a compact electric vacuum pump (Figure 124). In its unjammed state, the toy is soft to the touch and a variety of odd shapes can be made by moulding the elastomeric bladder by hand (Figure 125a). The user can then press a button and the jammable material (elastomer and glass beads) become rigid and maintains the current shape (Figure 125b). This shape can remain as long as the vacuum pressure is adequate to maintain the jamming effect. If the vacuum pressure is released, the shape morphs back down into the unjammed state. This toy allows for a custom sculpture to be made over and over again is very inexpensive and makes for an interesting desk piece.

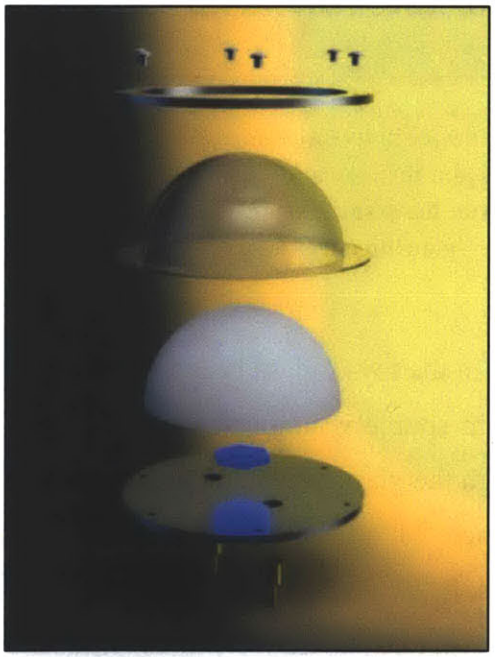

Figure 124. An exploded view of the prototype desktop toy shows the silicone bladder, glass media, light source, air valve, and fill port.

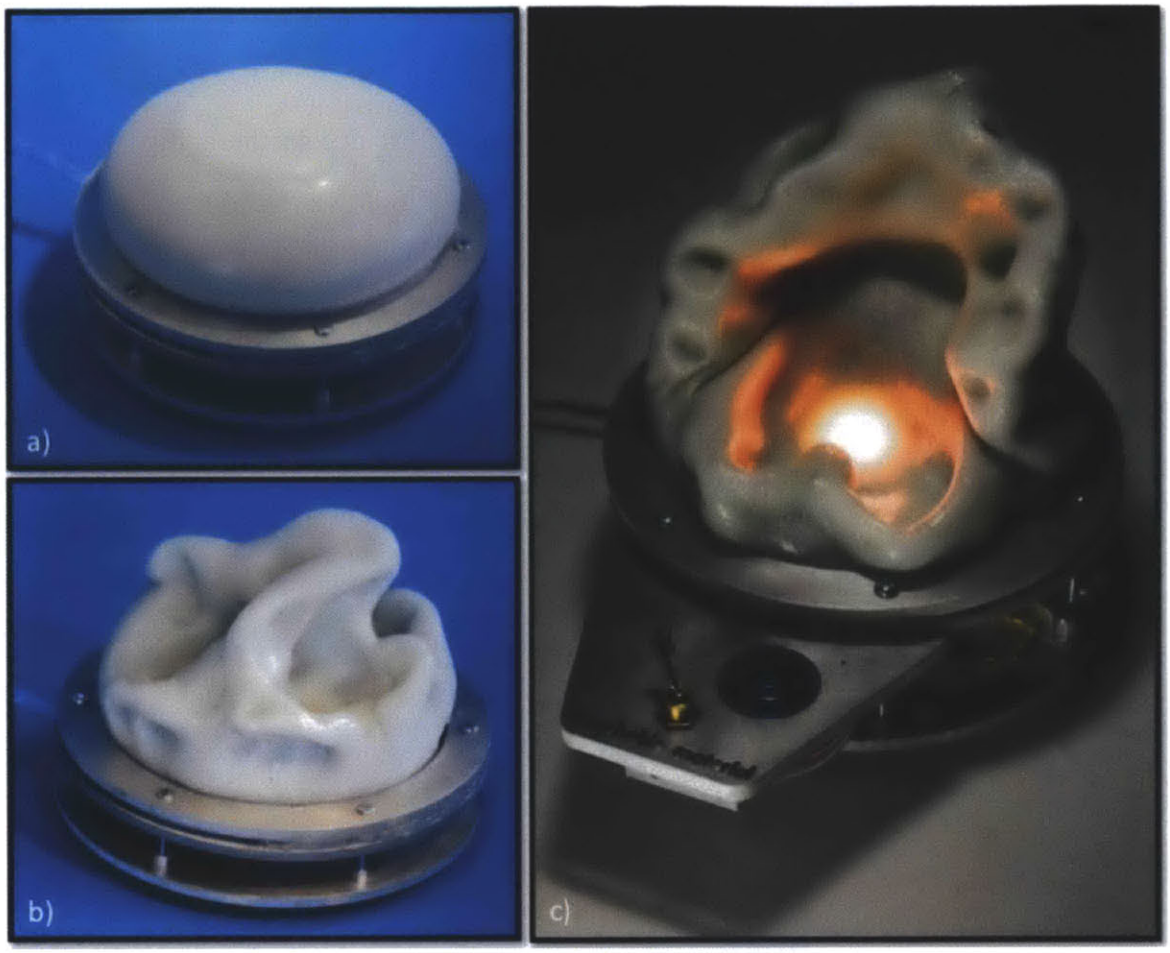

Figure 125. The jammable device in its unjammed state (a) is flexible and can be shaped by hand. When a vacuum is pulled to jam the media (b), the rigidity of the media increases and maintains its last configuration. The device has a small electric vacuum pump and an internal LED to create a glowing effect through the glass media.

The granular media used in the toy is glass beads, which are transparent. This leads to an optical effect when a light source is immersed in or is behind the granular media. The light is transmitted through the glass beads, but the internal reflection creates a very steep cutoff rate for transmittance, which depends on the thickness of the layer of glass beads. When combined with a soft, clear elastomer (such as the silicone used in the toy), this optical effect allows for regions to glow with a brightness that is dependent on the thickness (Figure 125c). This is clearly seen in Figure 126, where a user can touch the jammable media and the impressions glow. If the system is jammed, the shape is maintained and 3D glowing structures can be rapidly generated, such as the hand print

seen in (Figure 126c). The glowing impression can easily be erased by releasing the vacuum pressure and unjamming the system. The entire toy unit is seen in Figure 126d and the optical effect is apparent. A reconfigurable light made of jammable materials offers a unique method of creating custom glowing structures. This effect can be utilized in artistic pieces, toys, or lighting applications.

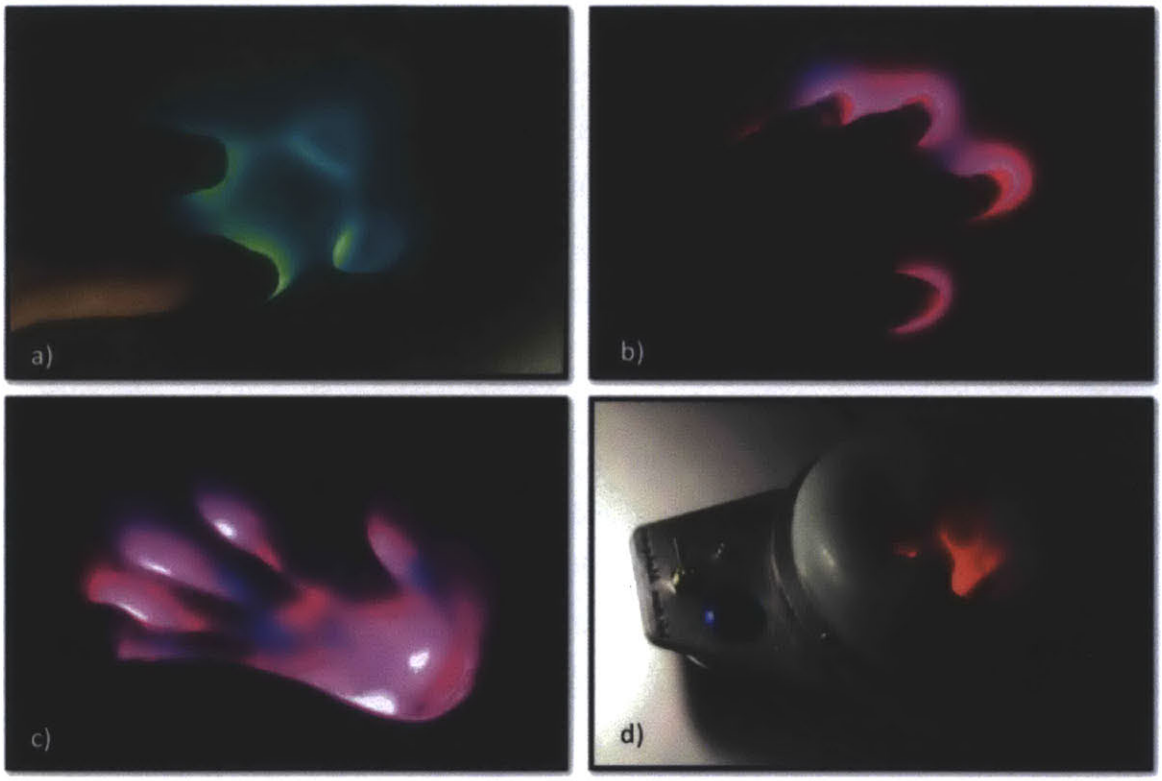

Figure 126. The optical effects of internal reflection in granular media is seen by mounting an internal tri-colour LED underneath a layer of glass beads in an elastomeric bladder. The brightness of the light corresponds to the depth of the depression in the jammed media, allowing for interesting light sculptures to be made by hand.

Discussion

The range of applications explored in this chapter demonstrates the vast possibilities that exist in design for jammable materials. While only skimming the surface of potential applications, the work demonstrated the feasibility of structural uses, fabrication

possibilities, and interactive devices. One of the most interesting observations from the work was the response of colleagues and the general public to the constructed prototypes. People loved how such a simple concept could be applied to different uses. Almost without fail, every person who saw the work would propose new applications and possibilities for jammable systems. From dental moulds to car seats, hundreds of ideas were proposed by people excited and enthused about jamming.

Looking at the broader scope and appeal of jamming, the concept can be categorized as a material system with time-dependent properties. Specifically for jamming, the material properties that change are stiffness and strength (system volume changes a small amount as well). This ability to change material properties in a fast, repeatable, inexpensive, and controlled manner is what makes jammed granular systems so appealing to designers. An interesting parallel to the spatially graded material properties discussed in Chapter 6 is the time-graded properties seen in jammable systems. Functional spatial gradients allow different areas of a monolithic structure to be designed for specific functionality; with jammable designs, different properties and functionalities are time-resolved through external control. Both types of systems allow new functionalities over conventional, homogenous material structures. In the future, if material systems with both spatial and time gradients can be designed, the possibilities and opportunities for design will be immense.

Moving forward, more work into the physics and material characterization are needed to better understand jamming and optimize the system properties. By changing the particle size, material, and shape, it is feasible that a material system can be specifically developed to have a desired mechanical response when jammed. 3D printers could be used to create precise shapes of granular particles to achieve desired characteristics. As well, the jamming pressure could evolve into more complex mechanisms than air pressure. Any type of force that compresses the particles together can facilitate jamming. For example, the use of magnetic fields could be used to manipulate granular structures and enable jamming without an external elastomeric bladder. Conversely, if the particles themselves increase in size, a jamming pressure will be developed if the particles are

constrained by an external bladder or container. Interesting jamming possibilities exists where water absorption or thermal expansion of particles would result in a granular system jamming. These systems where particles expand could be used to create passive smart material systems that respond to external stimuli, such as moisture or heat.

Looking at the fabrication aspects of jamming, the developed casting worked proved successful and could be implemented on a larger scale. The casting method functions by creating a mould, but another interesting possibility could involve the jammed material itself becoming the produced object. By adding a mechanism to permanently solidify the jammed material, jammed structures could be moulded into shape using an external pressure and then solidified to create the final product. For example, if metallic particles were used as the jammed media, an applied heat or electric current through the particles could sinter the metallic grains together, creating a permanent structure. Other mechanisms for solidification could include adhesive binders, malleable particles (like wax beads), and mechanical connectors.

Conclusion

In summary, the applications and possibilities for jammable granular systems are exciting and vast. Jamming, which results from an external pressure applied to a system comprised of granular media, is a natural phenomenon that allows system strength and stiffness to be dynamically controlled. The use of jamming in design is a recent development that holds significant promise for new applications. The design space for jammable materials is only beginning to be investigated and the prototypes developed in this work speak to the wide scope and potential. From robotics, to structural applications, to fabrication methods, the range of applications is immense. In the future, the materials and mechanics of robotic arms will likely dictate new modalities of control – such as system stiffness, fluid geometry, and soft compliance. Jammable granular systems offer an interesting potential for such future devices.

In this work, the materials characterization found that different types of granular media significantly affect the properties of the jammed system. The shape, size, and type of material all affect the mechanical response. In addition, the external jamming pressure controls the stiffness and strength of the structure. A number of materials were tested and coffee grains were found to offer the best strength-weight ratio. Composite granular media, comprised of several different grain types, can be mixed to achieve desired properties as well. More work into materials characterization is needed to investigate and optimum the grain shape and size for a given application.

To use jammable materials in an application, a jamming pressure can be applied using vacuum pressure and an elastomeric bladder. By manipulating the applied vacuum pressure, the granular media can be jammed to achieve different mechanical properties. The jammable system can be viewed as a material with bulk properties that are controllable. Various applications were explored in a number of fields including structural uses, manufacturing, and interactive devices. The success and range of the developed prototypes demonstrate the flexibility and potential for jammable materials in mechanical, architectural, and product design scales. The future for jammable materials is bright; it is a growing field both in terms of science and design that has yet to be defined.

Chapter 10: Immaterial and Informed Fabrication

"It is one of the commonest of mistakes to consider that the limits of our power of perception is also the limit of all there is to perceive."

– C.W. Leadbeater

Introduction

As the significance of digital fabrication continues to grow in digital design and fabrication, the definition of fabrication becomes increasingly useful as a both an organizational and generative tool. Fabrication is classically defined as a process of "construction from parts," and is traditionally broken down into categories based on how the "parts", or raw materials, are mechanically manipulated to construct an object. The three widely accepted fabrication categories include additive, subtractive, and formative processes (Cua, Leong, & Lim, 2010).

Additive processes are construction methods that add material to produce an object. Most 3D printing technologies (such as fused-deposition, stereolithography, and laser sintering processes) are included in this category. In contrast, subtractive fabrication techniques remove material to produce the manufactured object. Most machining processes are subtractive fabrication methods, and include milling, turning, and grinding. Finally, fabrication methods that mechanically shape a set amount of material are known as formative processes, such as bending, forging, and forming. Manufacturing methods that combine additive, subtractive and formative techniques are referred to as composite or hybrid processes.

With these definitions in mind, two new classes of fabrication were explored using robotic arms: *immaterial fabrication* and *informed fabrication*. Robotic arms have the benefits of speed, agility, and flexibility, and can be used as both inputs (sensing) and

outputs (modifying the physical environment). In addition to mechanical outputs, elements of an environment can be transformed as an output without the movement of physical material. Instead of physical matter, properties and fields can be made into spatial outputs of the system, such as light, sound, heat, radiation, and radio waves. Heat, for example, can be applied to a metallic object in varying quantities to impart an annealing pattern. While a digital fabrication method is implemented here, the medium has altered from relocating physical matter in a specific design to repositioning a heat source in an intended design. The design process is still a process constructed from parts – in this case it is the alteration of altering crystal structure – but not by manipulating material with direct mechanical force, as is characteristic of additive, subtractive, and formative processes. To facilitates the characterization of this type of environmental fabrication and distinguish it from physical construction, the term immaterial fabrication is used. In this chapter, this definition is explored and different examples of immaterial robotic fabrication distinct from conventional additive, subtractive, and formative processes are demonstrated.

Robotic arms are considered advanced compared with traditional fabrication methods (Pires J. N., 2006). As mentioned, robotic arms can be used as input or output devices. When implemented as an input device, sensors are coupled with the arm to allow spatial measurements of the environment. For example, an optical scanning system can be combined with the robotic arm to automatically generate 3D data of objects in an environment (Callieri, 2004). As an output device, end effectors are coupled with the arm allowing the robot to modify its environment. Such environmental modification can be made useful for a variety of digital and physical automation purposes such as fabrication, entertainment, or organization. For example, the multipurpose fabrication platform developed in Chapter 4 demonstrated various construction techniques such as milling.

The coupling of input and output fabrication capabilities of a robotic arm allows for a system capable of producing objects that incorporate environmental data. This use of environmental feedback to directly inform and influence fabrication holds many potential new avenues for design and manufacturing which will be discussed in this paper. The

term *informed fabrication* is used to refer to combinations of environmental sensing and fabrication.

Immaterial Fabrication

The conventional fabrication categories are defined by the interaction of mechanical forces with the raw stock material; additive processes build structures up, subtractive processes carve structures out, and formative processes reshape material into the final structure. Such categorization is sufficient when dealing with homogenous physical matter, however these definitions become problematic when fabricated parts cease to be only based on mass and physical matter. What happens when designs are fabricated out of material properties rather than mass, such as crystal structure, elasticity, and density? How should designs that are fabricated with fields other than mass be regarded, such as designs that are informed by electromagnetic and thermal fields? Can the definition of fabrication be extended beyond purely mechanical movements of mass?

Driven by the necessity to design and deliver highly complex material parts, new technologies and applications are increasingly focused on material properties and behavior. Materials with gradient properties are an ideal example. Functionally graded materials – materials designed with spatially varying properties – offer many advantages over conventional homogenous structures. The ability to tailor structural and materials properties spatially can improve functionality and material efficiency. For example, annealed metals often are designed with heat treatments that impart gradient material properties suitable for structure applications. By imparting heat, the crystalline features of a metal structure can be changed to produce and control various properties, such as hardness. The application of heat in a pre-designed spatial pattern to produce a desired structure, postulates a new class or category of digital fabrication termed *immaterial fabrication* in this thesis.

Immaterial fabrication processes are based on non-mechanical forces and fields, such as electromagnetic, thermal, radioactive, and acoustic fields. In the case of annealing, as previously discussed, both thermal (conductive and convective energy transfer) and electromagnetic forces (radiative energy transfer) are used to affect the material and create the designed structure. This definition is still based on the formal definition of fabrication proposing the construction of parts, yet it allows for controlled designed manipulation of non-physical parts, such as photons.

Many possibilities for immaterial fabrication exist considering media such as light, sound, heat, and material properties. Light was selected and explored as an example medium and several methods of light design fabrication were executed.

Light painting is a photographic technique where a long-exposure image is used to show motion paths of lights within the image. Light painting has been used for decades by artists and recently explored in several robotic installations including *Outrace* and *Halo: Remember Reach* (Kram & Weisshaar, 2010; Halo, 2010). Light painting is classified as a type of immaterial fabrication since the designed structure is defined through a manipulation of the electromagnetic field (i.e. light generation).

Light painting was initially explored by moving a controlled light source in a designated spatial design from a CAD file. 2D colour images were generated using this method and were captured using long exposure photography (Figures 127 and 128). 3D structures and animations were also generated, where the robotic arm rendered each frame of the animation in real space (Figure 129).

Figure 127. Using an LED mounted to the robotic arm, a light painting is created by moving the light source in a directed path. This long exposure photograph shows the light painting.

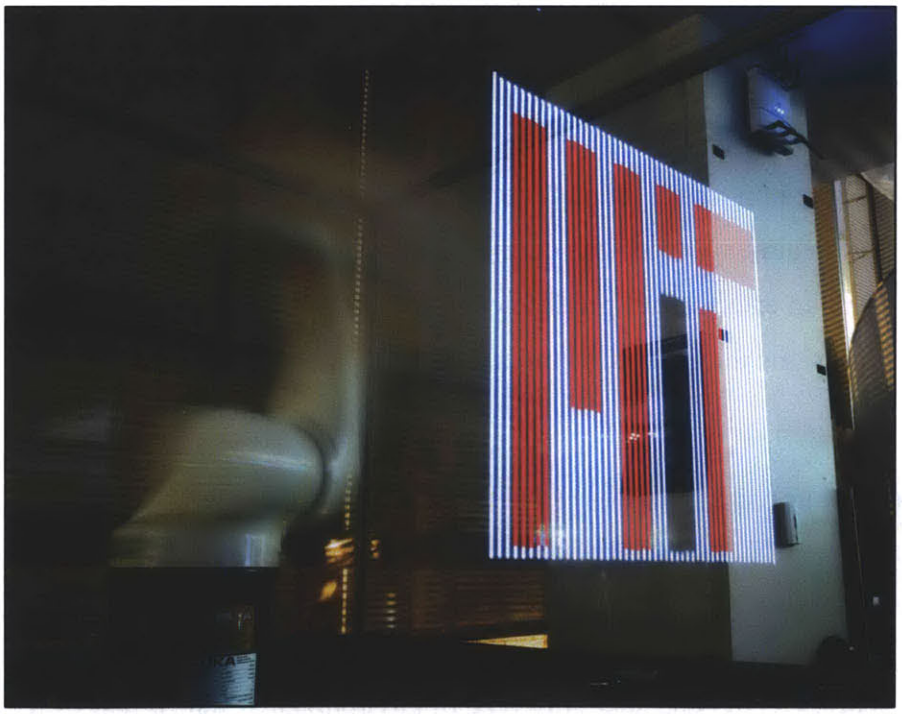

Figure 128. A light painting using a raster technique allows any digital image to be displayed.

Figure 129. Video sequences and animations can be created by successive long-exposure images. Here, frames from an animation of a growing cube are seen.

The light painting examples explored in this paper constitute a slow volumetric display. Combining this technique with a static camera to visualize the designs, a new form of digitally controlled animation is made possible where each frame of the animation is rendered in the real environment. While this application is primarily artistic, the use of immaterial fabrication may promote and contribute to industrial purposes such as localized heat treatments, specific curing designs, or magnetic patterning. Instead of outputting light, an effector can produce complex heat treatments, electromagnetic fields, and magnetic designs for target structures.

Environmental Sensing

The opposite effect, where data is captured instead of being exported, is achieved through the use of sensors. By applying a sensor as an end effector, volumetric sensor arrays can be simulated quickly and cheaply. Any type of environmental sensor that can be mounted to a robotic arm may be used to simulate a sensor array. This sensor array can have a

programmable scanning structure to allow for custom spatial resolution. The simulated array has a reduction in temporal resolution due to the serial nature of scanning and this temporal resolution is dictated by the scanning speed, distance of the scanning paths, and the total volume scanned.

As a first example, the opposing setup to the light painting experiments was explored. Instead of moving the light source and keeping the camera static, the camera's location is dynamically controlled by the robotic arm and static environmental light was used (Figure 130). Termed *inverse light painting*, a controlled light source was placed in the environment and the camera was moved in designed paths to generate an arbitrary image in the form of a long-exposure. This is seen in Figure 131, where the desired image is centered and the background is a blurred combination of the light from the rest of the environment.

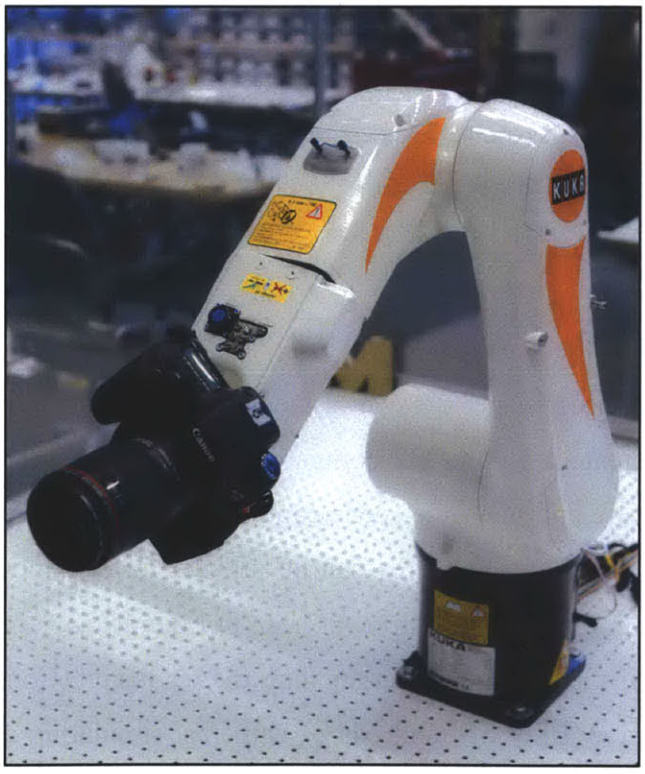

Figure 130. The robotic arm with a mounted Canon 7D camera was used to explore different computational photography possibilities.

Figure 131. By moving the camera in specific paths according to a CAD file, this long-exposure photograph displays an image painted using environmental light. The background is a result of the blurred environment.

This setup can be taken one step further to create a camera with a synthetic aperture of any given size within the reach of the robotic arm. By translating a camera with the shutter open in the desired shape and size of the synthetic aperture, an effective synthetic aperture camera is created. Figure 132 compares the result of a scene captured with the regular camera aperture and the same scene captured with a very large synthetic aperture with a robotic arm. Synthetic apertures can be utilized for a number of applications in computational photography. For example, as seen in Figure 132, larger apertures can see through occlusions if the aperture is larger than the occlusion. Compared to building a complex and expensive array of hundreds of cameras, simulating a large camera array with a robotic arm offers the benefits of simplicity, costs, and flexibility at the cost of temporal resolution. For steady-state environments, the reduced temporal resolution does not affect the data.

Figure 132. An environment (top) and the resulting inverse light painting from the same scene (bottom) shows the effects of a large synthetic aperture. Note that occlusions smaller than the synthetic aperture, like the windows on the right of the scene, can be imaged through if the focal plane is tuned past the occlusions.

Volumetric measurements can be taken as well, where a sensor is moved through a 3D space to collect spatial measurements. Based on the previous light exploration, a volumetric reading was obtained by moving a photodiode through a 500 mm cube. The measurements were taken in the dark with a single light emitting diode positioned at the bottom of the robotic arm to provide an example light field. By sampling the light intensity, a 3D map can be generated showing the spatial light intensity corresponding to the scene (Figure 133).

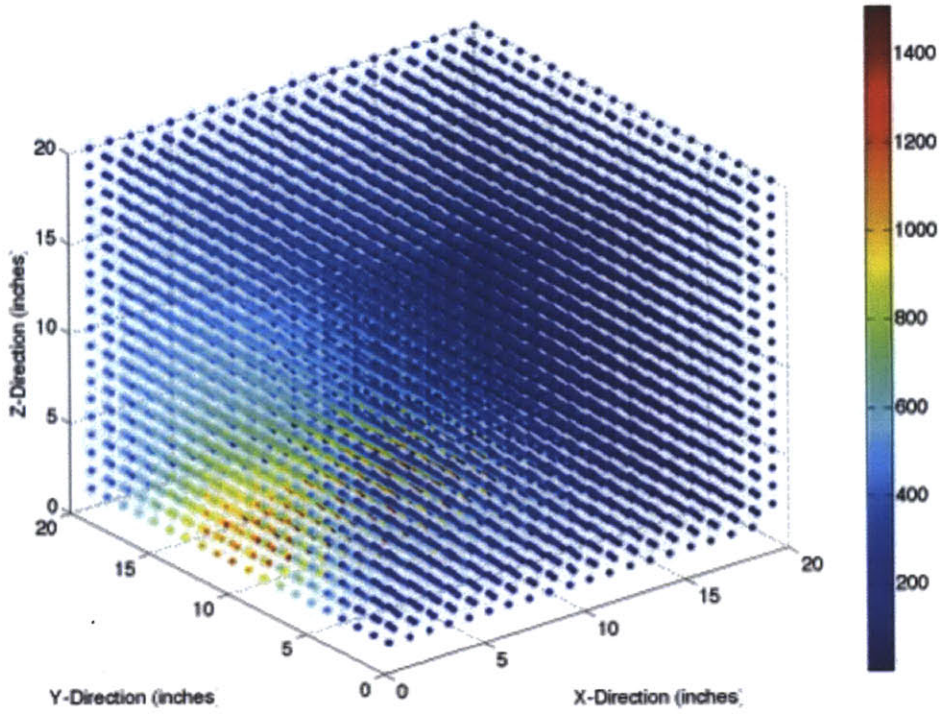

Figure 133. Volumetric light intensity measurements using the robotic arm show a single light source near the bottom left.

The potential applications for robotic sensing are vast, ranging from pure scientific applications to applied analytical ones. Examples include optical scanning, acoustical mapping for sound reduction, spatial chemical analysis, heat transfer data acquisition, structural inspections, x-ray analysis, tomography, and much more. The inherent flexibility of robotic arms is ideal for such scanning applications, as arms can unobtrusively explore spaces, be easily reconfigured, and have a small physical footprint.

Informed Fabrication

The combination of immaterial sensing and physical fabrication is here referred to as *informed fabrication*, where environmental feedback contributes to the finished design product. Using sensing equipment as an effector, the robotic platform can map out an environmental field or material property and use such information to control the fabrication process. For example, using an x-ray imaging system as a scanning sensor for crack detection on an aircraft part (Xu, Liu, Yin, Wong, & Hassan, 2010). Using the information from the sensor effector, a welding effector can then be used to apply a repair weld to the precise area required. This method is made fast and efficient by combining operations and it facilitates a secondary x-ray scan to evaluate the repaired weld seam. Informed fabrication can involve real-time feedback to enable process control. This allows for subtle corrections to ensure proper fabrication, such as correcting for observed thermal warping in 3D printing or chip removal in milling. Informed fabrication can be applied to any CNC manufacturing method, but is especially suited for robotic arm systems that have the required flexibility, internal space freedom, and agility.

Using the previous examples of light painting as immaterial fabrication, adding a sensing input to light painting creates an informed process. Several different sensors were set up on the robotic arm to inform the light painting process including microwave and magnetic fields (Figures 134 and 135).

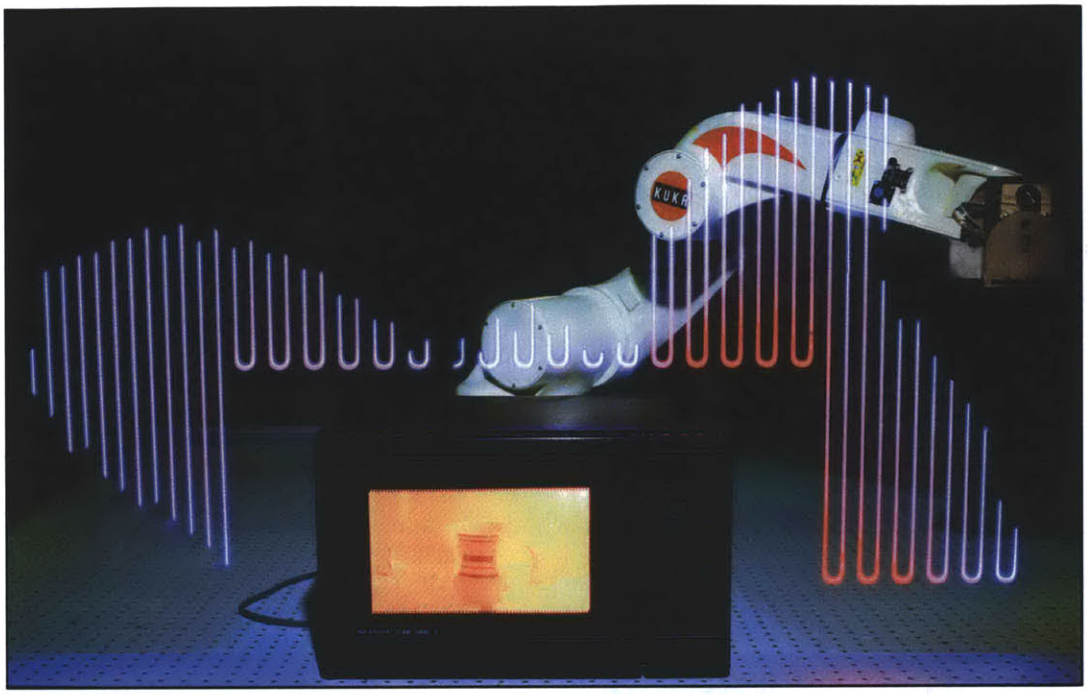

Figure 134. The microwave field around a microwave oven is seen using a scanning probe sensor and real-time light output. Note the higher field strength in the right corner indicates the location of the magnetron. As well, the sharp corners leak higher amounts of radiation.

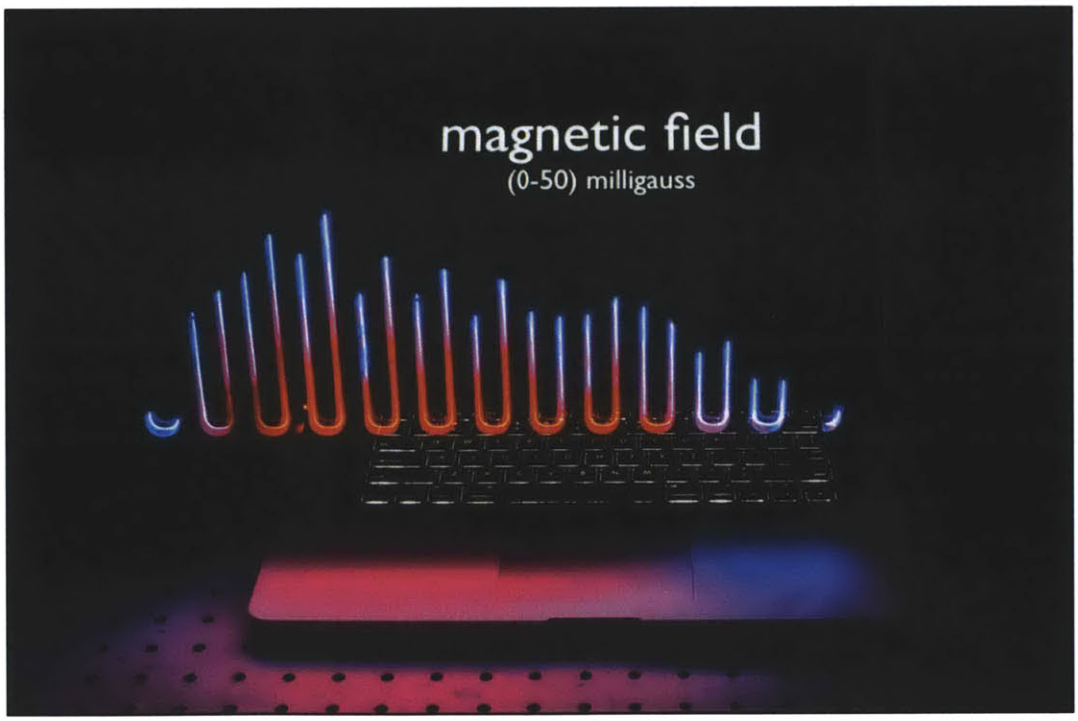

Figure 135. The magnetic field around a laptop is seen using a scanning probe and real-time light output. Note the higher field strength on the left side indicates the location of the hard drive.

Using a scanning pattern, hidden fields were visualized using the light painting technique. The intensity and colour of light was informed in real-time by the spatial field strength, producing images captured in long-exposure photographs. This was accomplished using a tri-colour light emitting diode driven by a microcontroller attached to various sensors. By setting a threshold sensor value to turn on the light and mapping sensor values higher than the threshold to a colour chart, the environmental data is represented in the light painting. As seen in Figure 134, a microwave oven produces microwave radiation that leaks outside of the oven. The magnetic field strength around a laptop is seen in Figure 135, indicating the location of the hard drive. This method of field visualization is very useful for analysis as it allows data to be directly matched to an environment. For example, a house could be scanned with a thermal sensor and any problem areas found (air leaks or insulation gaps) could be automatically identified and repaired.

Conclusion

The research work presented in this chapter proposes the term *immaterial fabrication* as a novel category of digital fabrication and construction. By altering the design medium (or substrate) from physical matter to physical properties or force fields, it promotes design processes informed by invisible forces such as heat, light and load. Though fabrication is traditionally defined as the process of constructing wholes from parts, such "parts" need not be limited to homogeneous physical solids. The photons used to fabricate designs implementing the light painting method serve than as the fabrication medium used to construct immaterial designs. Other immaterial properties can be utilized to embody a design, such as magnetic or thermal radiation. Based on this definition, the multi-fabrication platform can be utilized in a range of interesting applications that are vastly unexplored.

Extending the use of robotic arms from fabrication to sensing allows valuable sensor arrays to be simulated using single sensors and scanning motion paths. This facilitates

volumetric environmental data acquisition that can then be used for a variety of applied applications.

Informed fabrication combines fabrication and environmental sensing. With sensor data informing the fabrication process, the manufacturing process can start to take on roles both for process control and for design itself.

Finally, this chapter demonstrates the potential of immaterial and informed fabrication to transcend the utilitarian automation-centric role of robotic fabrication by proposing novel research and artistic areas where such platforms may not only execute but also inform the design process from its earliest stages to its complete and fully integrated physical manifestation.

Chapter 11: Conclusions and Contributions

"You do not see there a wireless torpedo, you see the first of a race of robots, mechanical men, which will do the laborious work of the human race."

—Nikola Tesla

This work explored fabrication, design, and artistic dimensions of industrial robotic arms outside of the traditional repetitive tasks typically assigned to robotic arms. Far more than a single-purpose machine, current industrial arms are capable of a near unlimited assortment of fabrication capabilities. However, the vast majority of industrial robots are used for simple, repetitive tasks that do not take advantage of the flexibility, reconfigurability, and multimodality of robotic arms. Most industrial robots perform a small, specific task as part of a large manufacturing process. This differentiation of processes between various robots forms the basis for many assembly lines and is analogous to different machine tools in a shop. In this thesis, a multifunctional fabrication platform was developed and explored to take a new approach; instead of having multiple differentiated machines for specific single techniques, a single robotic arm system performs compound operations. Akin to the concept of the Renaissance man, a single industrial robotic arm platform was enabled to function in multiple different capacities. The premise is based around the deconstruction of most fabrication techniques into an effector and a positioning system. By using a single positioning system and multiple end effectors, the functionality of many machines can be incorporated into a single platform.

Starting with conventional fabrication techniques, the prototype platform was successfully used to perform additive, subtractive, and formative processes. This was accomplished through the use of multiple end effectors, either mounted on the arm or as an external fixed tool with the work piece mounted on the arm. The benefits of the developed flexible system include reductions in physical footprint and cost, improvements in efficiency and speed, and new functionalities over existing machines. In addition, novel compound operations, such as combining 3D printing and milling, were

developed. As the platform requires only a single fixturing setup, many operations can be conducted in series to allow new possibilities for manufacturing. Finally, the range and geometry of an arm allows a unique clearance for large work pieces and complex undercuts. Compared to a gantry system with the same footprint, the reach of a robotic arm is far longer, more dexterous, and able to conform to a much wider range of paths. In contrast to the benefits, the use of a single robotic arm platform as a jack-of-all-trades fabrication system does have inherent limitations. Primarily, the limitations are due to the arm geometry, which results in lower system stiffness compared to a traditional gantry setup. It is a trade-off between the flexibility and reach of an arm versus the stability and stiffness of a gantry. While there are methods to reduce the effects of the lower stiffness, the robotic arm milling setup was still limited to softer materials such as wood and plastic.

Moving beyond conventional fabrication techniques, a series of projects exploring novel fabrication techniques and applications using the robotic arm were conducted. This investigation highlighted the true flexibility of robotic arm systems for applications outside the assembly line. The projects covered a broad scope including functionally graded 3D printing of concrete, construction-scale 3D printing, 3D printing with recycled materials, jammable granular systems, and immaterial robotic fabrication.

Concrete foams were mechanically characterized to evaluate the concept of functional density gradients for structural applications. The use of radial density gradients in concrete columns, similar to those found in natural structures like bone and palm trees, reduce overall weight and material usage compared to an equivalent standard homogenous column. Equations based on the experimental results were developed to calculate the optimum density gradients for a given application. To fabricate these graded concrete structures, segmented moulds with diffusion gradients were found to be the most effective. 3D printing tests using cement extrusion and the robotic arm platform found difficulties due to the varying material properties of different cement foam densities and the thixotropic nature of cement. In order to 3D print concrete with direct extrusion, a very controlled and specific concrete chemistry is required, along with a mechanism for

achieving plug flow in the extruder and feed lines. Printing concrete with varying material properties, such as different foam densities, was found to be challenging due to the fine balance in the required concrete properties suitable for 3D printing.

As opposed to direct concrete extrusion, a novel method of mould printing for structural materials, like concrete, was developed using the robotic arm platform. Fine resolution objects were fabricated using 3D printed dissolvable moulds made from PLA. Larger components were fabricated using 3D printed polyurethane foam moulds. Both small-scale and construction-scale objects were successfully printed and the results are very promising for future work into the area. The large-scale printing method, termed Print-in-Place construction, offers a potential technique for additive manufacture of buildings that could have significant impact on architectural fields. As well, the translation of industrial robotic arms to construction-scales and external environments was proposed using large delivery systems with mounted robotic arms to compensate for accuracy and vibrations.

A 3D printing system which utilizes recycled plastic feedstock was developed to explore the concept of direct recycling. Instead of the current centralized model of recycling, where scrap plastic is transported to a main recycling site and then transported back to shops as finished goods, a decentralized model was proposed and investigated. A direct recycling machine was prototyped to illustrate the concept. The robotic arm system accepts discarded HDPE beverage containers and uses the waste plastic as feedstock for an additive manufacturing process. By transforming scrap plastic into designed objects through 3D printing, the integrated system offers an example of direct, decentralized recycling. Large energy and efficiency benefits exist in decentralized recycling compared to the traditional model of recycling due to savings in transport costs and production speed. In the future, such systems could incentivize consumers to increase their recycling habits and take an active role in the customized fabrication of their own end products.

Jammable granular systems were explored for use in fabrication, robotics, and design. Granular media, such as sand or coffee, display a range of controllable mechanical properties when an external pressure is applied. This effect, commonly seen in vacuum-

packed coffee bags, is known as granular jamming. Taking advantage of this effect for mechanical design is a very recent development and the field is ripe with potential innovations and applications. The material system acts as a bulk material with a controllable stiffness and strength. The exploration into jammed system comprised of a materials characterization and a suite of novel prototypes for various design and fabrication applications. From the materials testing, the relationship between jamming pressure and mechanical properties was determined. As well, various granular materials were tested to evaluate their use for different design applications. Coffee grains were found to be well suited for applications where a high stiffness to weight ratio was desired. Composite material systems, where different grain types are mixed, offer new possibilities for designing a specific mechanical response from jammed media. The material characterization results serve as a design reference for different applications.

Using jammable materials, a number of applications were explored including structural, fabrication, and interactive uses. The produced prototypes included furniture, universal joints, fixturing tools, casting devices, desktop toys, and a robotic arm made from jammed materials. The exciting potential and versatility for jammable granular systems was demonstrated through these novel prototypes and can be combined with robotic arms in novel applications.

Finally, the use of a robotic arm for immaterial sensing and fabrication was explored. When acting as a volumetric scanner, robotic arm systems offer a flexible scanning capacity capable of spatial measurements of immaterial fields. Several test systems were developed including measurements of light intensity, electromagnetic fields, and thermal fields. Robotic arms as volumetric scanning systems can emulate an expensive sensor array with a single sensor. This capability holds vast potential for many scientific fields due to the low-cost and high spatial resolution. As an example, a large synthetic aperture camera array was emulated using a robotic arm with a single camera for various computational photography experiments.

Complementary to immaterial sensing, immaterial fabrication techniques modify material properties to construct a design. As opposed to conventional fabrication techniques that manipulate mass, immaterial fabrication techniques produce designs without mechanical forces. For example, annealing processes and light painting techniques create designs without moving physical mass or using mechanical forces. Immaterial fabrication techniques were developed with the robotic arm through light painting. New forms of rendering digital animations in the physical space were introduced and artistic light paintings informed by environmental sensors were used to reveal hidden immaterial fields.

Overall, this exploration into robotic digital fabrication techniques details the broad scope and flexibility of industrial robotic arms. Far more than repetitive, singular purpose assemblers, industrial robotic arms hold immense potential as truly multipurpose fabrication, utility, and artistic platforms. By enabling robotic arms to serve as multipurpose platforms, the applications for industrial robotics can be expanded far beyond current factories and into realms of design, architecture, personal manufacturing, and science. A robotic arm is the ultimate mechanical expression of industrial robotic capability and its potential for fabrication is just starting to be realized. The future of the robotic Renaissance man awaits.

Contributions

The main contributions from this work, listed in the order presented in the thesis chapters:

- Designed and developed the first single robotic arm platform capable of all three major fabrication categories (additive, subtractive, formative), based on a KUKA robotic arm.

- Developed and implemented a novel multi-axis 3D printing technique where the build platform is manipulated to print overhang structures without requiring support material.

- Conceptualized, designed, and demonstrated novel compound processes such as 3D printing and milling, where a single robotic arm platform performs different operations on the same work piece.

- Developed and evaluated a variable density concrete printing process. Concrete foam, both chemically foamed and mechanically foamed, was mechanically tested and the benefits of radial density gradients in columnar structures were shown through calculations.

- Developed and evaluated 3D printed dissolvable moulds for concrete objects. The mould printing technique was shown to be an effective method for additively producing complex concrete objects and segmented moulds were successively used to produce density gradients.

- Designed, developed, and evaluated the *Print-in-Place* construction process, where a robotic arm uses an insulative mould printing technique to produce building-scale structures.

- Developed, prototyped, and coined *Direct (Robotic) Recycling*, a process where decentralized 3D printers uses recycled plastic feedstock to produce new products from discarded bottles at distributed locations.

- Explored and characterized jammable granular systems for design and fabrication applications including novel structure, manufacturing, and interactive purposes.

- Coined and introduced the concept of *Immaterial Fabrication*, where designs are produced by changing material and environmental properties without mechanical forces.

- Developed and demonstrated processes of robotic light painting and novel animating techniques, where images and videos are rendered in the physical world.

- Demonstrated volumetric sensor applications for robotic arms considering a range of purposes including computation photography and electromagnetic field detection.

- Demonstrated the use of a single multi-functional robotic arm system in the context of a diverse range of applications beyond the traditional repetitive confines of assembly lines.

Future Work

The various projects and prototypes produced are only initial investigations into the new possibilities for digital fabrication using robotic arms. The broad scope of the thesis offers many potential areas for future work.

First and most importantly, in order to increase the use of robotics arms in flexible fabrication applications, the barrier of software complexity must be addressed. The current software limitations and the proprietary programming languages used for most commercial robotic arms significantly impede the development of research and broader use. While the commercial evolution of the industry has created these proprietary languages, they have also significantly restricted their use to large assembly lines and isolate technical users to a single arm manufacturer. The development of a universal,

open-source, real-time industrial robotic arm programming interface would provide enormous aid to moving towards new growth fields in robotic fabrication.

In addition to interfacing with robot arms, future work on software development could allow for integration and optimization of multiple machining processes. Currently, the there are no software options for integrating processes like 3D printing and milling. By taking advantage of these compound processes, a whole new field of integrated manufacturing processes becomes possible and the current main limitation is the software with which to do so. A user-friendly program for creating complex tool paths for robotic arms specifically for digital fabrication processes like 3D printing, multi-axis milling, and other techniques would allow a multi-functional platform to be useful to designers and engineers alike.

Aside from software, more experimentation with compound processes is warranted to quantitatively evaluate the possibilities, benefits, and drawbacks of a multi-functional fabrication platform. The work presented here proved it is possible to use a single robotic arm system for additive, subtractive, and formative techniques, but the surface has only been scratched. A whole host of techniques can be put in series using a single system to compound the methods, for example combining laser cutting with an automated bending operation. Entire new methods of production techniques could result from exploring different combinations of processes on a single multi-axis system.

In addition to exploring different compound fabrication techniques, optimizing a multi-fabrication platform is an interesting future endeavor. As detailed in this work, two setup schemes exist for fabrication with a robotic arm: mounted effectors or externally fixed effectors. This is highlighted by the 3D printing example where objects can be printed by moving the extruder relative to a fixed build platform, or by manipulating the build platform around a fixed extruder. With multiple effectors, either an automated tool changer is required or a number of fixed tool need to be mounted within reach of the arm. Determining which method is more effective and efficient depends on the complexity of the compound fabrication operation and the time required for tool changes.

Future work should also focus on a quantitative comparison to current single purpose machine tools and traditionally assemble lines. While this work has proved the possibility of a multipurpose fabrication platform, the economics and quality must be rigorously justified against conventional machines for industry to adapt these techniques.

References

Aitcin, P.C. (2000). Cements of yesterday and today: Concrete of tomorrow. *Cement and Concrete Research , 30* (9), 1349-1359.

American Heritage. (1980). Thomas Alva Edison and the Concrete Piano. *31* (5).

Arduino. (2012). *Arduino*. Retrieved July 8, 2012, from http://www.arduino.cc/

Baechler, C., & Pearce, J. (2011). *Appropedia.* Retrieved July 6, 2012, from Recyclebot.

Bechthold, M. (2010). The Return of the Future: A Second Go at Robotic Construction. *Architectural Design , 80* (4), 116-121.

Bechthold, M. (2010, July). The Return of the Future: A Second Go at Robotic Construction. *Architectural Design , 80* (4), pp. 116-121.

Brooks, H., & Aitchison, D. (2010). A review of state-of-the-art large-sized foam cutting rapid prototyping and manufacturing technologies. *Rapid Prototyping Journal , 16* (5), 318-327.

Brown, E., Rodenberg, N., J. A., Mozeikac, A., Steltzc, E., Zakind, M. R., et al. (2010). *Proceedings of the National Academy of Sciences of the United States of America , 107* (44), 18743-19132.

Callieri, M. (2004). RoboScan: an automatic system for accurate and unattended 3D scanning. *Proceedings of 2nd International Symposium on 3D Data Processing, Visualization and Transmission*, (pp. 805-812).

Chen, Y., Zhou, C., & Lao, J. (2011). A layerless additive manufacturing process based on CNC accumulation. *Rapid Prototyping Journal , 17* (3), 218-227.

Cheng, N., Lobovsky, M., Keating, S., Setapen, A., Gero, K., Hosoi, A., et al. (2012). Design and Analysis of a Robust, Low-cost, Highly Articulated Manipulator Enabled by Jamming of Granular Media. *Proceedings of the IEEE International Conference on Robotics and Automation.*

Corwin, E., Jaeger, H. M., & Nagel, S. R. (2005). Structural signature of jamming in granular media. *Nature , 435*, 1075-1078.

Cua, C., Leong, K., & Lim, C. (2010). *Rapid Prototyping: Principles and Applications.* World Scientific.

da Vinci Surgery. (2012). Retrieved July 12, 2012, from da Vinci Surgery - Minimally Invasive Robotic Surgery: http://www.davincisurgery.com/

Dini, E. (2009). *D-Shape*. Retrieved July 11, 2012, from http://d-shape.com/

Dow Chemical Company. (2012). *Froth-Pak Foam Insulation Product Information.*

Durian, D. (1995). Foam mechanics at the bubble scale. *Physical Review E , 75* (26).

Edison, T. (1917). *Patent No. 1326854.*

Elastizell. (1998). *Elastizell.* Retrieved July 7, 2012, from http://www.elastizell.com/products.html#techdata

Gibson, L. J., Ashby, M. F., & Harley, B. A. (2010). *Cellular Materials in Nature and Medicine.* Cambridge University Press.

Gibson, L., & Ashby, M. (1988). *Cellular Solids, Structures and Properties.* Oxford, England: Pergamon Press.

Gramazio, F., & Kohler, M. (2008). *Digital Materiality in Architecture.* Lars Müller Publishers.

Halo. (2010). *Halo: Remember Reach.* Retrieved July 27, 2012, from http://www.rememberreach.com

Hoeken, Z., Kintel, M., Mayer, A., & Mets, M. (2012). *ReplicatorG.* Retrieved March 8, 2011, from http://replicat.org/

Hudson, S. W. (2012). *Mechanical Characterization of Jammable Granular Systems.* Thesis, Massachusetts Institute of Technology, Cambridge.

Huijben, F., & Herwijnen, F. v. (2007). Vacuumatics; Shaping Space by "Freezing" the Geometry of Structures. *International Conference on Tectonics.*

Industries, M. (2012). *MakerBot.* Retrieved July 8, 2012, from http://www.makerbot.com/

International Federation of Robotics. (2011). *World Robotics 2011.* Retrieved from http://www.worldrobotics.org/

Kataria, A., & Rosen, D. W. (2001). Building around inserts: methods for fabricating complex devices in stereolithography. *Rapid Prototyping Journal , 7* (5), 253-262.

Khoshnevis, B. (2004). Automated Construction by Contour Crafting - Related Robotics and Information Technology. *Journal of Automation in Construction , 13* (1), 5-19.

Khullar, S., Joshi, C., Lawson, E., Keating, S., & Raskar, R. (2012). Retrieved July 8, 2012, from Infra-Red Cricket: Analysis of the HotSpot technology in Cricket and "how to hide the heat": http://cameraculture.media.mit.edu/cricket

Kohler, M., Gramzio, F., Oesterle, S., & Vansteenkiste, A. (2011). *High-efficiency concrete formwork technology.* Retrieved July 8, 2012, from Holcim Awards: http://www.holcimfoundation.org/T1332/A11EUacCH.htm

Kram, R., & Weisshaar, C. (2010). *Outrace: The Paper.* Retrieved July 28, 2012, from http://www.outrace.com

KUKA Robot Group. (2007). *KR 5 sixx R650, R850 Specification.* KUKA Roboter GmbH.

KUKA Robot Group. (2012). *KUKA Industrial Robots - Products.* Retrieved July 18, 2012, from http://www.kuka-robotics.com/en/products/

Lim, S., Buswell, R., Le, T., Austin, S., Gibb, A., & Thorpe, A. (2012). Development in construction-scale additive manufacturing processes. *Automation in Construction , 21* (1), 262-268.

Liu, A. J., & Nagel, S. R. (1998). Nonlinear dynamics: Jamming is not just cool any more. *Nature , 396*, 21-22.

Loeve, A. J., Ven, O. S., Vogel, J. G., Breedveld, P., & Dankelman, J. (2010). Vacuum packed particles as flexible endoscope guides with controllable rigidity. *Granular Matter* (12), 543-554.

Lu, K., Brodsky, E., & Kavehpour, H. (2008). A thermodynamic unification of jamming. *Nature Physics , 4*, 404-407.

Ludewig, F., Vandewalle, N., & Dorbolo, S. (2006). Compaction of granular mixtures. *Granular Matter , 8*, 87-91.

Moriwaki, T. (2008). Multi-functional machine tool. *CIRO Annals - Manufacturing Technology , 57* (2), 736-749.

NAHB Research Center. (2001). *Cost and Benefits of Insulating Concrete Forms for Residential Construction.*

National Concrete Masonry Association. (2012). *Concrete Masonry Units.* Retrieved July 28, 2012, from http://www.ncma.org/

Objet. (2012). *Connex 3D Printers.* Retrieved July 20, 2012, from http://www.objet.com/3d-printers/connex

Ochsendorf, J. (2010). *Life Cycle Assessment of Buildings.* Massachusetts Institute of Technology, MIT Concrete Sustainability Hub.

OpenKinect. (2012). *OpenKinect.* Retrieved July 8, 2012, from http://openkinect.org/wiki/Main_Page

Oxford Dictionaries. (2010, April). *"Robot"*. Retrieved July 10, 2012, from Oxford Dictionaries: http://oxforddictionaries.com/definition/american_english/robot

Oxman, N. (2010). *Material-Based Design Computation.* Thesis, Massachusetts Institute of Technology, Cambridge, MA.

Oxman, N. (2011). Variable property rapid prototyping. *Virtual and Physical Prototyping , 6* (1), 3-31.

Pandremenos, J., Doukas, C., Stavropoulos, P., & Chryssolouris, G. (2011). Machining with Robots: A Critical Review. *7th International Conference on Digital Enterprise Technology.* Athens, Greece.

Panushey, I. S., & VanderWerf, P. A. (2004). *Insulating Concrete Forms Construction: Demand, Evaluation, and Technical Practice.* New York: McGraw-Hill.

Pires, J. (2007). *Industrial Robot Programming: Building Applications for the Factories of the Future.* Springer.

Pires, J. N. (2006). *Industrial Robots Programming: Building Applications for the Factories of the Future.* Springer.

Rasband, W. (2011). *ImageJ.* (U. N. Health, Producer) Retrieved July 6, 2012, from http://imagej.hih.gov/ij/

Research Center for Advanced Manufacturing. (2012). *MultiFab.* Retrieved 7 14, 2012, from http://www.smu.edu/Lyle/Departments/ME/Research/RCAM/Laboratories/Rapid_Manufacturing/MultiFab

Rice, R. (1976). Microstructural Dependence of Mechanical Properties of Ceramics. In R. McCrone, *Treatise on Material Science and Technology.* New York: Academic Press.

Robocoaster. (2012). Retrieved July 10, 2012, from Robocoaster: http://www.robocoaster.com/

RoboFold. (2012). *RoboFold.* Retrieved May 5, 2012, from http://www.robofold.com/

Robotic Solutions Inc. (2012). *Robotic Solutions.* Retrieved July 10, 2012, from http://www.roboticmachining.com/

Robots in Architecture. (2012). *KUKA prc - parametric robot control for Grasshopper.* Retrieved July 7, 2012, from www.robotsinarchitecture.org/kuka-prc

Roy, D., & Gouda, G. (1973). Porosity-Strength Relation in Cementitious Materials with Very High Strengths. *Journal of the American Ceramic Society , 56* (10).

Short, A., & Kinniburgh, W. (1978). *Lightweight Concrete* (3rd ed.). London, England: Applied Science Publisher.

Siena Robotics and Systems Lab. (2011). *SIRSLAB - KUKA Control Toolbox.* Retrieved July 7, 2012, from http://sirslab.dii.unisi.it/software/kct/

SkyCam. (2012). *SkyCam.* Retrieved July 7, 2012, from http://www.skycam.tv/

Somfai, E., Hecke, M. v., Ellenbroek, W. G., Shundyak, K., & Saarloos, W. v. (2007). Critical and noncritical jamming of frictional grains. *Physical Review E , 75* (2).

Steltz, E., Mozeika, A., Rembisz, J., Corson, N., & Jaeger, H. (2010). Jamming as an Enabling Technology for Soft Robotics. *Conference on Electroactive Polymer Actuators and Devices*, (p. San Diego).

Tang, J., & Behringer, R. (2011). How granular materials jam in a hopper. *Chaos , 21* (4).

Taylor, M., Wamuziri, S., & Smith, I. (2003, February). Automated construction in Japan. *Proceedings of ICE .*

Taylor, W. H. (1974, February). The Production, Properties, and Uses of Foamed Concrete. *Precast Concrete* , 83-96.

Tonyan, T. (1991). *Mechanical Behaviour of Cementitious Foams.* Thesis, Massachusetts Insitute of Technology, Cambridge.

Tse, W., & Chen, Y. (1997). A robotic system for rapid prototyping. *International Conference on Robotics and Automation.* IEEE.

Vander Kooij, D. (2011). *The Endless Process.* Retrieved January 11, 2012, from http://www.dirkvanderkooij.nl/en/content/endless-process

VanderWerf, P. A. (2001). *Energy Comparisons of Concrete Homes Versus Wood Frame Homes.* Portland Cement Association.

VanderWerf, P. A. (2007). *The Concrete House: Building Solid, Safe and Efficient with Insulating Concrete Forms.* New York: Sterling.

Vosniakos, G.-C., & Matsas, E. (2010). Improving feasibility of robotic milling through robot placement optimisation. *Robotics and Computer-Integrated Manufacturing , 26* (5), 517-525.

Walker, A. (2012, April 26). *A Chevy Sonic Turned Graffiti Robot Creates Awesome Street ArT.* Retrieved July 5, 2012, from PSFK: http://www.psfk.com/2012/04/chevy-sonic-graffiti.html

Wetzstein, G., Lanman, D., Hirsch, M., & Raskar, R. (2012). Tensor Displays: Compressive Light Field Synthesis using Multilayer Displays with Directional Backlighting. *SIGGRAPH 2012 .*

Worrell, E., Price, L., Martin, N., Hendriks, C., & Meida, L. O. (2001). Carbon Dioxide Emissions from the Global Cement Industry. *Annual Review of Energy and the Environment , 26*, 303-329.

Xu, J., Liu, T., Yin, X., Wong, B., & Hassan, S. (2010). Automatic X-ray Crack Inspection of Aircraft Wing Fastener Holes. *4th Internation Symposium on NDT in Aerospace, 5.*

Figures References

Figures and photographs from outside sources are listed below with online references current at time of publication. The computer renderings of the construction-scale 3D printing process in Chapter 7 were produced by Atif Javed and Timothy Robertson under the supervision of the author. All other figures and photographs were produced by the author.

Figure 8. University of Colorado, Correll Lab. Available online: http://correll.cs.colorado.edu/?attachment_id=792

Figure 9. International Federation of Robotics, *World Robotics 2011*. Available online: http://www.worldrobotics.org/

Figure 10. KUKA Robotics. Available online: http://www.kuka.com/

Figure 42. Food and Agriculture Organization of the United Nations. Available online: http://www.fao.org/docrep/009/ag335e/AG335E02.htm

Figure 51. STX International. Available online: http://www.stxinternational.com/Grinders/STX%20Turbo%20Force%201800W.html

Figure 61. Wikimedia Commons. Available online: http://en.wikipedia.org/wiki/File:Thomas_Edison_concrete_house.jpg

Figure 62. Khoshnevis, Behrokh. *Contour Crafting*. Available online: http://www.contourcrafting.org

Figure 63. Loughborough University. *Freeform Construction*. Available online: http://www.buildfreeform.com/index.php

Figures 64 and 65. Dini, Enrico. D-Shape. Available online: http://d-shape.com

Figure 85. New Home Construction. *Alaska in Pictures*. Available online: http://www.alaska-in-pictures.com/new-home-construction-4488-pictures.htm

Figure 86. Obsit. *Home Designs and Furniture Gallery*. Available online: http://obsit.com/everything-you-should-to-know-about-concrete-block-walls.html

Figure 87. Denver Infill Blog. *One Lincoln Park Construction*. Available online: http://denverinfill.com/blog/2008/01/one-lincoln-park-construction-update.html

Figure 88. Concrete Works. Available online: http://www.concreteworksnh.com/

Figure 95. Tang, J., & Behringer, R. (2011). How granular materials jam in a hopper. *Chaos , 21* (4).

Figure 122 and 123. Cheng, N., Lobovsky, M., Keating, S., Setapen, A., Gero, K., Hosoi, A., et al. (2012). Design and Analysis of a Robust, Low-cost, Highly Articulated Manipulator Enabled by Jamming of Granular Media. *Proceedings of the IEEE International Conference on Robotics and Automation.*

Appendix A – Code

Examples of code used for some of the different projects are listed below. Coding was done by the author with the help of several undergraduate research assistants including Julian Merrick, Ali AlShehab, Louis DeScioli, Keren Gu, and Banks Hunter.

Typical KRL Program Structure

The typical header structure used for different KRL programs is shown below. For many of the less complex programs, such as print tests for simple walls and raster scanning, this header was used in combination with hand coding to achieve the desired paths. For more complicated programs, this header structure was still used but with automated code generation.

Code

```
DEF codestructure() //Name of program
FOLD INI
;FOLD BASISTECH INI
GLOBAL INTERRUPT DECL 3 WHEN $STOPMESS==TRUE DO IR_STOPM ( )
INTERRUPT ON 3
BAS (#INITMOV,0 )
;ENDFOLD (BASISTECH INI)
;FOLD USER INI
;ENDFOLD (USER INI)
;ENDFOLD (INI)

;FOLD PTP HOME  Vel= 100 % DEFAULT;%{PE}%MKUKATPBASIS,%CMOVE,%VPTP,%P 1:PTP,
2:HOME, 3:, 5:100, 7:DEFAULT
$BWDSTART = FALSE
PDAT_ACT=PDEFAULT
FDAT_ACT=FHOME
BAS (#PTP_PARAMS,100 )
$H_POS=XHOME
PTP  XHOME  // Start at home position
;ENDFOLD

// Define tool and coordinate system here

// Axis velocities
```

```
$VEL_AXIS[1]=20
$VEL_AXIS[2]=20
$VEL_AXIS[3]=20
$VEL_AXIS[4]=20
$VEL_AXIS[5]=20
$VEL_AXIS[6]=20

$vel.cp= 1    // Speed
$apo.cvel= 95  // Approximate motion control

LIN(X 500, Y 600, Z 500, A 0, B 90, C 0) //Insert coordinates here (EG. LIN PTP CIRC)

END
```

Example of Parametric KRL for Printing Wall Test

```
DEF arc_form_gen()

;-- My declarations
decl int counter, counter2, layers
decl real hHeight, hWidth, track, capHeight, highX, lowX, zed, stHt

;FOLD INI
  ;FOLD BASISTECH INI
    GLOBAL INTERRUPT DECL 3 WHEN $STOPMESS==TRUE DO IR_STOPM ( )
    INTERRUPT ON 3
    BAS (#INITMOV,0 )
  ;ENDFOLD (BASISTECH INI)
  ;FOLD USER INI

  ;ENDFOLD (USER INI)
;ENDFOLD (INI)

;FOLD PTP HOME  Vel= 100 %DEFAULT;%{PE}%MKUKATPBASIS,%CMOVE,%VPTP,%P 1:PTP,
2:HOME, 3:, 5:100, 7:DEFAULT
$BWDSTART = FALSE
;-- No foam
$out[2] = FALSE
PDAT_ACT=PDEFAULT
FDAT_ACT=FHOME
BAS (#PTP_PARAMS,100 )
$H_POS=XHOME
PTP  XHOME
;ENDFOLD

;------ Actual code -------
highX = 845.59
lowX = 456.58
hWidth = 600
hHeight = (highX-lowX)/2 ;-- Relative to start pt
capHeight = 50.0
zed = 50
```

```
layers = 5
track = 190.0
stHt = 270
$vel.cp= .6

;-- Going to shifted start pt
ptp {pos: x 660, y -595, z 275, s 110}

;-- Goes aux pt then end pt
for counter = 1 to layers

;-- Move over a little, turn on, move to start
lin_rel {x -100} c_vel
$out[2] = TRUE
wait sec 0.3
lin_rel {x -100} c_vel

circ_rel {x 50, y 250},{x 90, y 550} c_vel
circ_rel {x 40, y 300},{x 90, y 550} c_vel
circ_rel {x -95, y 70},{x -190, y 0} c_vel
circ_rel {x -50, y -250}, {x -90, y -550} c_vel
circ_rel {x -40, y -300}, {x -90, y -550} c_vel
circ_rel {x 95, y -70}, {x 190, y 0} c_vel

;FOLD Generalized
;circ_rel {x capHeight, y (track/2)},{x 0, y track} c_vel
;circ_rel {x ((-1*(hHeight-track)), y ((hWidth-track)/2)},{x 0, y (hWidth-track)} c_vel
;circ_rel {x hHeight, y (hWidth/2)},{x 0, y hWidth} c_vel
;circ_rel {x (-1*capHeight), y (-1*track/2)},{x 0, y (-1*track)} c_vel
;circ_rel {x (hHeight-track), y (-1*(hWidth-2*track)/2)},{x 0, y (-1*(hWidth-2*track))} c_vel
;circ_rel {x (-1*hHeight), y (-1*hWidth/2)},{x 0, y (-1*hWidth)} c_vel
;ENDFOLD

;-- Move over turn off, move more, move up, wait
lin_rel {x 100} c_vel
$out[2] = FALSE
lin_rel {x 100} c_vel
lin_rel {frame: z 19}
WAIT SEC 3.0

endfor
;---------------------------

;FOLD PTP HOME  Vel= 100 % DEFAULT;%{PE}%MKUKATPBASIS,%CMOVE,%VPTP,%P 1:PTP,
2:HOME, 3:, 5:100, 7:DEFAULT
$BWDSTART = FALSE
PDAT_ACT=PDEFAULT
FDAT_ACT=FHOME
BAS (#PTP_PARAMS,100 )
$H_POS=XHOME
PTP  XHOME
;ENDFOLd
END
```

Milling Code Generation

The milling program HSMWorks is a plug-in for the CAD program SolidWorks and facilitates tool path generation. A custom post-processing script was written using the HSMWorks Editor to facilitate direct output of KRL code from within SolidWorks.

Code

```
/**
  Mediated Matter - KUKA Milling Script
  $Revision: 24282 $
  $Date: 2011-03-07 17:35:20 +0100 (ma, 07 mar 2011) $
*/

description = "KUKA KRL Output - Robot Arm";
vendor = "HSMWorks ApS";
vendorUrl = "www.media.mit.edu/research/groups/mediated-matter";
legal = "Copyright (C) 2007-2011 HSMWorks ApS";
certificationLevel = 2;

extension = "tp.xml";
setCodePage("utf-8");

allowHelicalMoves = false;
allowedCircularPlanes = 0; // allow any circular motion
maximumCircularSweep = toRad(100 * 360); // 100 revolutions

var mapRCTable = new Table(
  [" compensation='off'", " compensation='left'", "", " compensation='right'"],
  {initial:RADIUS_COMPENSATION_OFF},
  "Invalid radius compensation"
);

function toPos(x, y, z) {
  return x + " " + y + " " + z;
}

var x_old = 0;
var y_old = 0;
var z_old = 0;
var c_vel = 0.2;
var previousFeed;

function toFeed(feed) {
  if (feed != previousFeed) {
    previousFeed = feed;
    return " feed='" + feed + "'";
  }
  return "";
}
```

```
function toRC(radiusCompensation) {
 return mapRCTable.lookup(radiusCompensation);
/*
 switch (radiusCompensation) {
 case RADIUS_COMPENSATION_OFF:
  return " compensation='off'";
 case RADIUS_COMPENSATION_LEFT:
  return " compensation='left'";
 case RADIUS_COMPENSATION_RIGHT:
  return " compensation='right'";
 }
 return "";
*/
}

function toString(value) {
 if (typeof(value) == 'string') {
  return "\"" + value + "\"";
 } else {
  return value;
 }
}

function onOpen() {

writeln ("DEF ()");
writeln ("");
writeln(";Mediated Matter KUKA Robot Milling");
writeln(";www.media.mit.edu/research/groups/mediated-matter");
var d = new Date();
writeln(";date timestamp='" + (d.getTime() * 1000));
writeln ("");
writeln (";FOLD INI");
writeln (";FOLD BASISTECH INI");
writeln ("GLOBAL INTERRUPT DECL 3 WHEN $STOPMESS==TRUE DO IR_STOPM ( )");
writeln ("INTERRUPT ON 3");
writeln ("BAS (#INITMOV,0 )");
writeln (";ENDFOLD (BASISTECH INI)");
writeln (";ENDFOLD (INI)");
writeln (";FOLD PTP HOME Vel= 100 %
DEFAULT;%{PE}%MKUKATPBASIS,%CMOVE,%VPTP,%P 1:PTP, 2:HOME, 3:, 5:100,
7:DEFAULT");
writeln ("$BWDSTART = FALSE");
writeln ("PDAT_ACT=PDEFAULT");
writeln ("FDAT_ACT=FHOME");
writeln ("BAS (#PTP_PARAMS,100 )");
writeln ("$H_POS=XHOME");
writeln ("PTP  XHOME");
writeln (";ENDFOLD");
writeln ("$VEL_AXIS[1]=20");
writeln ("$VEL_AXIS[2]=20");
writeln ("$VEL_AXIS[3]=20");
writeln ("$VEL_AXIS[4]=20");
writeln ("$VEL_AXIS[5]=20");
```

```
writeln ("$VEL_AXIS[6]=20");
writeln ("$vel.cp= 0.2");
writeln ("$apo.cvel= 99");
writeln ("PTP {Z 200, S 110}");
writeln ("");
}

function onComment(text) {
 // TAG: escape
 writeln("<comment>" + text + "</comment>");
}

function onSection() {
 var u = (unit == IN) ? "inches" : "millimeters";
 var o = toPos(600, 0, 189);
 writeln(";<context unit='" + u + "' origin='" + o + "'/>");

 var type = "unspecified"; // TAG: fixme
 var n = tool.number;
 var d = tool.diameter;
 var cr = tool.cornerRadius;
 var ta = tool.taperAngle;
 var fl = tool.fluteLength;
 var sl = tool.shoulderLength;
 var sd = tool.shaftDiameter;
 var bl = tool.bodyLength;
 var tp = tool.threadPitch;
 var _do = tool.diameterOffset;
 var lo = tool.lengthOffset;
 var sr = tool.spindleRPM;
 var COOLANT_NAMES = ["disabled", "flood", "mist", "tool", "air", "air through tool"];
 var coolant = COOLANT_NAMES[tool.coolant];

 writeln(";<tool type='" + type + "' number='" + n + "' diameter='" + d + "' corner-radius='" + cr + "' taper-angle='" + ta + "' flute-length='" + fl + "' shoulder-length='" + sl + "' body-length='" + bl + "' shaft-diameter='" + sd + "' thread-pitch='" + tp + "' diameter-offset='" + _do + "' length-offset='" + lo + "' spindle-rpm='" + sr + "' coolant='" + coolant + "'>");

 var holder = tool.holder;
 if (holder) {

  writeln("<holder>");

  for (var i = 0; i < holder.getNumberOfSections(); ++i) {
   var section = holder.getSection(i);
   var d = section.getDiameter();
   var l = section.getLength();
   writeln("<section diameter='" + d + "' length='" + l + "'/>");
  }
  writeln("</holder>");
 }
 writeln(";</tool>");
previousFeed = undefined;
}
```

```
function onParameter(name, value) {
 // TAG: escape
 var type = "float";

 if (typeof(value) == 'string') {
  type = "string";
 } else if ((value % 1) == 0) {
  type = "integer";
 }
 //writeln("<parameter name='" + name + "' value='" + toString(value) + "' type='" + type + '/>");

function onDwell(seconds) {
 writeln("<dwell seconds='" + secFormat.format(seconds) + "'/>");
}
function onCycle() {
 writeln("<group id='" + cycleType + "'");
 for (var name in cycle) {
  //writeln("<parameter name='" + name + "' value='" + toString(cycle[name]) + "'/>");
 }
}

function onCyclePoint(x, y, z) {
 writeln("lin_rel{x " + (x - x_old)  + ", y " + (y - y_old) + ", z " + (z - z_old) + "} c_vel");
 x_old = x;
y_old = y;
z_old = z;
}

function onCycleEnd() {
 writeln("</group>");
}

function onRapid(x, y, z) {
 writeln("lin_rel{x " + (x - x_old)  + ", y " + (y - y_old) + ", z " + (z - z_old) + "} c_vel");

previousFeed = undefined;
x_old = x;
y_old = y;
z_old = z;
}
function onLinear(x, y, z, feed) {
writeln("lin_rel{x " + (x - x_old)  + ", y " + (y - y_old) + ", z " + (z - z_old) + "} c_vel");
x_old = x;
y_old = y;
z_old = z;
}

function onRapid5D(x, y, z, dx, dy, dz) {
 writeln("<rapid to='" + toPos(x, y, z) + "' axis='" + toPos(dx, dy, dz) + "'/>");
 previousFeed = undefined;
}

function onLinear5D(x, y, z, dx, dy, dz, feed) {
writeln("<linear to='" + toPos(x, y, z) + "' axis='" + toPos(dx, dy, dz) + "'" + toFeed(feed) + "/>")
}
```

```
function onCircular(clockwise, cx, cy, cz, x, y, z, feed) {
  var n = getCircularNormal();
  var block = "";
  var big = getCircularSweep() > Math.PI;
  if (big) {
    block += "circular";
  } else {
    block += isClockwise() ? "arc-cw" : "arc-ccw";
  }
  block += " to='" + toPos(x, y, z) + "'";
  block += " center='" + toPos(cx, cy, cz) + "'";
  if ((n.x != 0) || (n.y != 0) || (n.z != 1)) {
    block += " normal='" + toPos(n.x, n.y, n.z) + "'";
  }
  if (big) {
    block += " sweep='" + getCircularSweep() + "'";
  }
  block += toFeed(feed);
  block += toRC(radiusCompensation);
  writeln("<" + block + "/>");
}

function onCommand() {
  writeln("<command/>");
}

function onSectionEnd() {
  writeln(";</section>");
}

function onClose() {
  writeln("PTP XHOME");
  writeln("END");
}
```

Python KRL Generator Codes

To generate KRL from external inputs, such as 3D printing programs and image files, a number of Python scripts were written. These scripts output KRL .SRC files that were loaded directly onto the KUKA controller.

Subprogram Generation

Due to a software limitation in the KUKA controller, KRL .SRC files for a program can only have up to 32,000 lines of KRL. This limitation seems to be a relic of the evolution of KUKA and its arms and KUKA sells an add-on program to allow users to reference comma separated values in a separate text file to avoid this problem for complex tool paths. Instead of purchasing this add-on, a Python script was written to split programs larger than 32,000 lines into different subprograms which were linked by calls at the end of each subprogram.

Code

```
##Input the name of the file after Running the Program and the number of lines per subprogram
##The program will split the file into subprograms
##ex: Subprogramer('canadaflag',30000)

def Subprogramer(FileName,NumberOfLines):
    filename=Filename
    f = open(filename+'.src', 'r')
    numberOfLines = NumberOfLines
    lines=f.readlines()
    lines=lines[12:len(lines)-2]
    numberOfFiles= len(lines)/numberOfLines
    linesLeft = len(lines)%numberOfLines
    numberOfFilesList= range(1,numberOfFiles+1)
    x=0
    SubList=[]
    if linesLeft>0:
        numberOfFilesList= range(1,numberOfFiles+2)
    for i in numberOfFilesList:
##      print 'File# '+str(i)
        outFile= open('GLOBAL_'+filename+str(i)+'.src', 'w')
        outFile.write('DEF GLOBAL_'+filename+str(i)+'()')
        outFile.write('\n')
        outFile.write('    GLOBAL INTERRUPT DECL 3 WHEN $STOPMESS==TRUE DO IR_STOPM (
)')
        outFile.write('\n')
        outFile.write('    BAS (#INITMOV,0 )')
        outFile.write('\n')
        for j in range(numberOfLines):
##          print 'j+x= '+str(j+x)
            if j+x==len(lines):
                break
            outFile.write(lines[j+x])
        x=i*numberOfLines
```

```
        outFile.write('\n')
        outFile.write('END')
        outFile.write('\n')
        SubList= SubList+['GLOBAL_'+filename+str(i)+'()']
        outFile.close
##      print SubList
    f2 = open('MAIN_'+filename+'.src', 'w')
    f2.write('DEF MAIN_'+filename+'()')
    f2.write('\n')
    for member in SubList:
        f2.write('ext '+member)
        f2.write('\n')
    f2.write('EXT BAS (BAS_COMMAND :In,REAL :In )')
    f2.write('\n')
    f2.write('INT I')
    f2.write('\n')
    f2.write('BAS (#INITMOV,0 )')
    f2.write('\n')
    f2.write('For I=1 To 6')
    f2.write('\n')
    f2.write('$VEL_AXIS[I]=30')
    f2.write('\n')
    f2.write('$ACC_AXIS[I]=20')
    f2.write('\n')
    f2.write('ENDFOR')
    f2.write('\n')
    f2.write('$vel.cp = 1')
    f2.write('\n')
    f2.write('$apo.cvel = 95')
    f2.write('\n')
    f2.write('$apo.cdis = 1')
    f2.write('\n')
    f2.write('PTP  XHOME')
    f2.write('\n')
    for member in SubList:
        f2.write(member)
        f2.write('\n')
    f2.write('PTP  XHOME')
    f2.write('\n')
    f2.write('END')
    f2.close

    print 'Done!'
```

G-Code to KRL Convertor

A Python script was developed to convert between machine G-Code and KUKA KRL to facilitate 3D printing projects. ReplicatorG, an open source 3D printing tool path generation program, was used to create tool paths for 3D printing from an input .STL file.

The G-Code output from ReplicatorG was used as an input file for a Python script to convert to KRL.

Main Convertor Program

```
#Konverter v0.1 Gcode to Kuka Robot Language converter
#uses the replicatorg reprap gcodes and mcodes

import command_library

gcode_filename = raw_input('enter file: ')
src_file = gcode_filename[:-5] + 'src'
filename=gcode_filename[:-6]
gcode_file = open(gcode_filename, 'r')
gcode=gcode_file.readlines()
command_library.krl = open(src_file, 'w')

#this header sets axis velocities and defaults for the file
command_library.krl.write('DEF ' + filename+ '() ' +"""
;FOLD INI
  ;FOLD BASISTECH INI
    GLOBAL INTERRUPT DECL 3 WHEN $STOPMESS==TRUE DO IR_STOPM ( )
    INTERRUPT ON 3
    BAS (#INITMOV,0 )
  ;ENDFOLD (BASISTECH INI)
  ;FOLD USER INI
    ;Make your modifications here

  ;ENDFOLD (USER INI)
;ENDFOLD (INI)

;FOLD PTP HOME  Vel= 100 % DEFAULT;%{PE}%MKUKATPBASIS,%CMOVE,%VPTP,%P 1:PTP,
2:HOME, 3:, 5:100, 7:DEFAULT
$BWDSTART = FALSE
PDAT_ACT=PDEFAULT
FDAT_ACT=FHOME
BAS (#PTP_PARAMS,100 )
$H_POS=XHOME
PTP  XHOME
;ENDFOLD

$VEL_AXIS[1]=20
$VEL_AXIS[2]=20
$VEL_AXIS[3]=20
$VEL_AXIS[4]=20
$VEL_AXIS[5]=20
$VEL_AXIS[6]=20

$vel.cp= 1
$apo.cvel= 95
```

```
PTP {Z 200, S 110}
""")

for command_library.line in gcode:
   command_letter=command_library.line[0:1]
   if command_letter == 'M':
      command_library.mcommand()
   elif command_letter == 'G':
      command_library.gcommand()
   elif command_letter == '(':
      command_library.comment()
   elif command_letter == ';':
      command_library.krl.write(';skipped')
   command_library.krl.write ('\n')
command_library.krl.write('$OUT[6]=FALSE \nPTP XHOME\nEND')
command_library.krl.close()
print 'conversion completed'
```

Command Library for G-Code to KRL Convertor

```
#This file stores the various commands and functions that the main file references import

global line, krl, gcode
line=krl=gcode='default value'

def comment():
   global krl
   global line
   begin_comment= line.find('(')+1
   end_comment= line.find(')')
   if end_comment <> -1:
      krl.write(';' + line[begin_comment:end_comment])


def extract_num():
   #extracts the command number
   global end_num
   global command_num
   end_num=int(line.find(' '))
   command_num=line[1:end_num]

def extract_coordinates():
   global xstart, ystart, zstart
   global xend, yend, zend
   global xval, yval, zval

   xstart=line.find('X')+1
   ystart=line.find('Y')+1
   zstart=line.find('Z')+1

   xend=line.find(' ',xstart)
   yend=line.find(' ',ystart)
   zend=line.find(' ',zstart)
```

```
    if xstart<> 0:
        xval = line[xstart:xend]

    if ystart<> 0:
        yval = line[ystart:yend]

    if zstart<> 0:
        zval = line[zstart:zend]

def gcommand():
    extract_num()
    global xval, yval, zval
    if command_num =='0':
        #ptp motion
        extract_coordinates()

        krl.write('PTP {')
        if xstart <> 0:
            krl.write('X '+ xval)
            if ystart <> 0 or zstart <> 0:
                krl.write(', ')
        else: xval='noval'


        if ystart <> 0:
            krl.write('Y '+yval)
            if zstart <> 0:
                krl.write(', ')
        else: yval='noval'

        if zstart <> 0:
            krl.write('Z '+zval)
        else: zval='noval'

        krl.write('}')
        comment()

    elif command_num == '1':
        #linear movement command
        #begin by extracting coordinates
        extract_coordinates()

        #print the linear command data (speed not included)
        krl.write('lin {')
        if xstart <> 0:
            krl.write('X '+ xval)
            if ystart <> 0 or zstart <> 0:
                krl.write(', ')
        else: xval='noval'


        if ystart <> 0:
            krl.write('Y '+yval)
            if zstart <> 0:
                krl.write(', ')
```

```
        else: yval='noval'

        if zstart <> 0:
          krl.write('Z '+zval)
        else: zval='noval'

        krl.write('} C_VEL')
        comment()

    elif command_num == '2':
        #arc clockwise
        krl.write(';circ')

    elif command_num == '3':
        #arc counter clockwise
        krl.write(';countercirc')
    elif command_num == '04':
        #dwell
        time_start=line.find('P') + 1
        time_end=line.find(' ',time_start)
        iscomment=line.find('(')

        time= float(line[time_start:time_end]) / 1000

        krl.write('WAIT SEC ' + str(time))
        #print time
        if iscomment <>-1:
          comment()

    elif command_num == '21':
        #changes units to mm
        krl.write('; G21 redundant, changes units to mm')

    elif command_num == '92' or '90':
        extract_coordinates()
        #set absolute coordinates by setting the base to the current position
        #yaw, pitch, roll are all set to 0
        #NEED TO GET DIFFERENCE BETWEEN G90 AND G92
        krl.write('BASE_FRAME=$POS_ACT\n')
        krl.write('BASE_FRAME.A=0\nBASE_FRAME.B=0\nBASE_FRAME.C=0\n')
        krl.write('$BASE= BASE_FRAME')

    else: krl.write(';G' + command_num)

def mcommand():
    extract_num()
    if command_num == '101':
        #extruder on forward
        krl.write('$OUT[6]=TRUE')

    elif command_num == '102':
        #extruder on backwards
        #no backwards extruder needed at the moment
        krl.write(';no reverse extruder support')
```

```
elif command_num == '103':
   #extruder stop
   krl.write('$OUT[6]=FALSE')

elif command_num == '104':
   #set temperature
   krl.write(';cannot set temperature in krl at this time')

elif command_num == '105':
   #reads extruder temperature
   krl.write(';cannot read temperature in krl')
elif command_num == '106':
   #fan on
   krl.write(';fan on, no fan support')
elif command_num == '107':
   #fan off
   krl.write(';fan off, no fan support')
elif command_num == '108':
   #extruder speed pwm or rpm
   krl.write(';no extruder speed support at this time')
elif command_num == '109':
   #get heater platform up to temp
   krl.write(';no heater platform support at this time')
else: krl.write(';M' + command_num)
```

Appendix B – Compressive Cement Foam Test Data

Table 5. Summary of the raw data collected from density measurements and compression testing of the chemically foamed cement foam samples.

Sample	Height (cm)	Diameter (cm)	Weight (kg)	Density (kg/m^3)	Average Density (kg/m^3)	Max Compressive Load (kN)	Compressive Strength (MPa)	Average compressive strength (MPa)
a-1	20.3	10.1	3.08	1890.88	1905.45	181.80	22.69	21.17
a-2	20.1	10.1	3.10	1926.60		150.09	18.73	
a-3	20.2	10.1	3.08	1900.24		189.11	23.60	
a-4	20.1	10.1	3.07	1904.06		157.45	19.65	
b-1	20.2	10.1	2.22	1373.33	1367.34	28.66	3.58	3.49
b-2	20.1	10.1	2.20	1363.26		27.57	3.44	
b-3	20.4	10.1	2.23	1365.42		27.55	3.44	
b-4	Sample dropped, initial data collection problem.							
c-1	Sample dropped, computer data collection failure.				1220.14	N/A		2.66
c-2	20.1	10.1	2.00	1244.96		19.24	2.40	
c-3	20.4	10.1	1.99	1215.56		19.89	2.48	
c-4	20.1	10.1	1.93	1199.90		24.86	3.10	
d-1	20.1	10.1	1.80	1115.40	1133.84	14.88	1.86	2.36
d-2	20	10.1	1.91	1188.91		23.53	2.94	
d-3	20.2	10.1	1.77	1093.06		22.82	2.85	
d-4	19.9	10.1	1.81	1137.99		14.40	1.80	
e-1	15.7	10.1	1.55	1233.27	1208.34	24.96	3.12	2.78
e-2	14.3	10.1	1.37	1195.64		24.17	3.02	
e-3	15.2	10.1	1.44	1184.44		19.96	2.49	
e-4	14.2	10.1	1.39	1220.01		19.90	2.48	

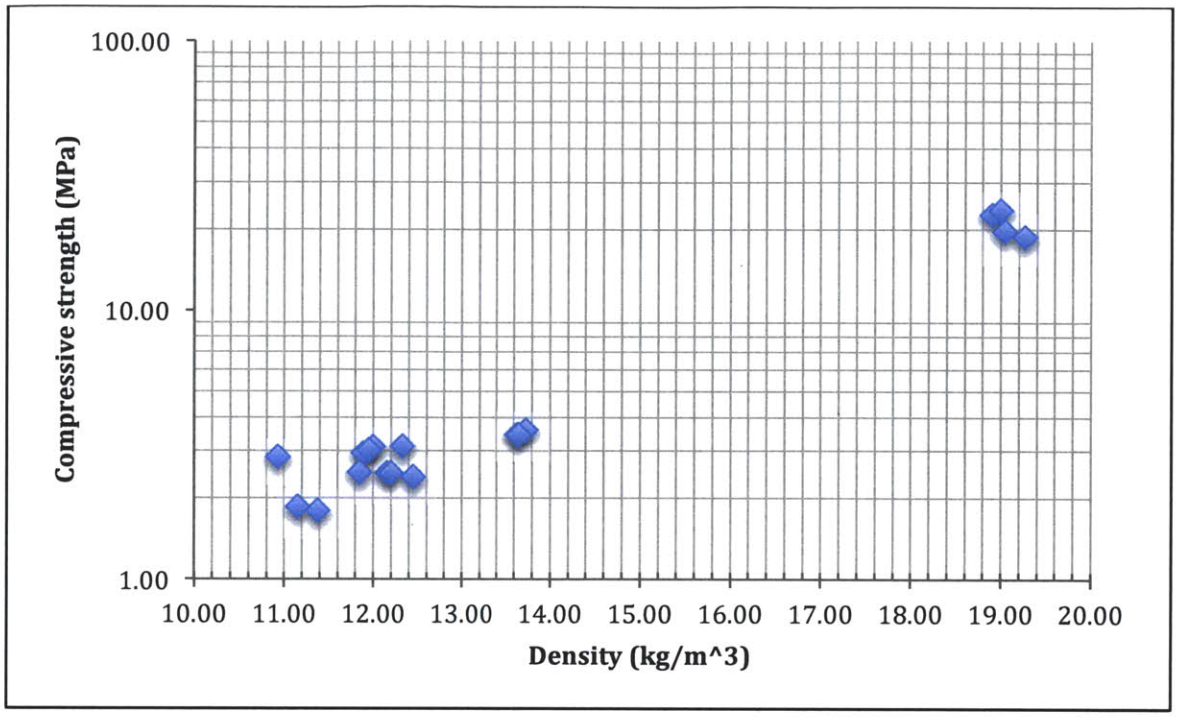

Figure 136. Compression strength vs density for all of the samples tested in the experiment.

Appendix C – Materials and Suppliers

The following equipment and materials were used and can be found at these suppliers:

Robotic Arm Equipment and Materials

KUKA robot arm and controller: KUKA Robotics (http://www.kuka.com/)
Spray urethane foam: Dow Chemical Company
(http://building.dow.com/na/en/applications/building/walls/spray.htm)
ABS extruder, feedstock: MakerBot (http://www.makerbot.com/)
PLA feedstock: MakerBot (http://www.makerbot.com/)
Heated build platform: MakerBot (http://www.makerbot.com/)
Nichrome wire and thermocouples: Ultimaker (http://www.ultimaker.com/)
Aluminum framing: 80/20 (http://www.8020.net/)
Dremel rotary tool: Dremel (http://www.dremel.com/)
Electric router: Porter-Cable (http://www.portercable.com/)
Extruder servos: Hitec, ServoCity (http://www.servocity.com/)
External microcontrollers and sensors: Sparkfun (https://www.sparkfun.com/)
Electric meat grinder: STX International (http://www.stxinternational.com/)

Materials for Concrete Testing

Slaked lime: Home Depot (http://www.homedepot.com/)
Type III Portland cement: Home Depot (http://www.homedepot.com/)
Fine aluminum powder: Schenk (www.schlenk.com)
Fly Ash: Headwaters, Inc (http://www.flyash.com/contactus.asp)
Foaming agent: Elastizell (http://www.elastizell.com/)
Foam generator pump: Elastizell (http://www.elastizell.com/)

Materials for Jammable Granular System Testing

Ecoflex silicone: Smooth-On (http://www.smooth-on.com/)
EZ-Brush Vac Bag silicone: Smooth-On (http://www.smooth-on.com/)
Vacuum lines, connectors, and gauges: McMaster-Carr (http://www.mcmaster.com/#)
Soft polyurethane foam: McMaster-Carr (http://www.mcmaster.com/#)
Vacuum pump: Robinair (http://www.robinair.com/)
Small vacuum pump (from food sealing machine): FoodSaver
(http://www.foodsaver.com/)
Glass media: MoSci Corporation and Kramer Industries
Latex condoms: Trojan Condoms (http://www.trojancondoms.com/)
Sand media: Home Depot, Quickcrete Product (http://www.homedepot.com/)
Ground coffee: Shopper's Value, Shaw's Supermarket (http://www.shaws.com/)